

**CHARACTERIZATION OF BAST FIBER OF
STERCULIA VILLOSA (ROXB.) AND *BAUHINIA VAHLII*
AND FABRICATION OF BIOMASS-BASED NANO-
COMPOSITE MEMBRANE**



**A THESIS SUBMITTED TO THE
CENTRAL DEPARTMENT OF CHEMISTRY
INSTITUTE OF SCIENCE AND TECHNOLOGY
TRIBHUVAN UNIVERSITY
NEPAL**

**FOR THE AWARD OF
DOCTOR OF PHILOSOPHY
IN CHEMISTRY**

**BY
KRISHNA PRASAD KANDEL
AUGUST 2023**

**CHARACTERIZATION OF BAST FIBER OF
STERCULIA VILLOSA (ROXB.) AND *BAUHINIA VAHLII*
AND FABRICATION OF BIOMASS-BASED NANO-
COMPOSITE MEMBRANE**



**A THESIS SUBMITTED TO THE
CENTRAL DEPARTMENT OF CHEMISTRY
INSTITUTE OF SCIENCE AND TECHNOLOGY
TRIBHUVAN UNIVERSITY
NEPAL**

**FOR THE AWARD OF
DOCTOR OF PHILOSOPHY
IN CHEMISTRY**

**BY
KRISHNA PRASAD KANDEL
AUGUST 2023**



Reference No.:

TRIBHUVAN UNIVERSITY
Institute of Science and Technology

DEAN'S OFFICE

Kirtipur, Kathmandu, Nepal



EXTERNAL EXAMINERS

The Title of Ph.D. Thesis: " Characterization of Bast Fiber of *Sterculia Villosa* (ROXB.) and *Bauhinia Vahlii* and Fabrication of Biomass-Based Nano-Composite Membrane "

Name of Candidate: Krishna Prasad Kandel

External Examiners:

- (1) Prof. Dr. Hem Raj Pant
Institute of Engineering
Tribhuvan University, NEPAL
- (2) Prof. Dr. M.G.H. Zaidi
G.B. Pant University of Agriculture and Technology
Uttarakhand, INDIA
- (3) Prof. Dr. Hak Yong Kim
Jeonju National University
Jeonju, SOUTH KOREA

August 01, 2023

(Dr. Surendra Kumar Gautam)
Asst. Dean

DECLARATION

This thesis entitled “**Characterization of Bast Fiber of *Sterculia villosa* (Roxb.) and *Bauhinia vahlii* and Fabrication of Biomass-based Nano-composite Membrane**” which is being submitted to the Central Department of Chemistry, Institute of Science and Technology (IOST), Tribhuvan University, Nepal for the award of the degree of Doctor of Philosophy (Ph.D.), is a research work carried out by me under the supervision of Dr. Bhanu Bhakta Neupane of Central Department of Chemistry, Tribhuvan University and co-supervised by Dr. Mahesh Kumar Joshi of Central Department of Chemistry, Tribhuvan University, Kirtipur, Kathmandu, Nepal and Dr. Soma Dhakal of Virginia Commonwealth University, USA.

This research is original and has not been submitted earlier in part or full in this or any other forms to any university or institute, here or elsewhere, for the award of any degree.



Krishna Prasad Kandel

RECOMMENDATION

This is to recommend that **Krishna Prasad Kandel** has carried out research entitled “**Characterization of Bast Fiber of *Sterculia villosa* (Roxb.) and *Bauhinia vahlii* and Fabrication of Biomass-based Nano-composite Membrane**” for the award of Doctor of Philosophy (Ph.D.) in **Chemistry** under our supervision. To our knowledge, this work has not been submitted for any other degree.

He has fulfilled all the requirements laid down by the Institute of Science and Technology (IOST), Tribhuvan University, Kirtipur for the submission of the thesis for the award of Ph.D. degree.



.....
Supervisor

Dr. Bhanu Bhakta Neupane

(Assistant Professor)

Central Department of Chemistry
Tribhuvan University, Kirtipur,
Kathmandu, Nepal

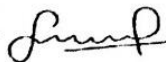


.....
Dr. Mahesh Kumar Joshi

Co-Supervisor

(Associate Professor)

Central Department of Chemistry
Tribhuvan University, Kirtipur,
Kathmandu, Nepal



.....
Dr. Soma Dhakal

Co-Supervisor

(Associate Professor)

Virginia Commonwealth University, USA

1st August 2023



त्रिभुवन विश्वविद्यालय
TRIBHUVAN UNIVERSITY
विज्ञान तथा प्रविधि अध्ययन संस्थान
Institute of Science and Technology
रसायन शास्त्र केन्द्रीय विभाग
CENTRAL DEPARTMENT OF CHEMISTRY
कीर्तिपुर, काठमाडौं, नेपाल
Kirtipur, Kathmandu, NEPAL

पत्र संख्या:
Ref. No.:



Date: August 01, 2023

On the recommendation of **Dr. Bhanu Bhakta Neupane, Dr. Mahesh Kumar Joshi, and Dr. Soma Dhakal**, this Ph.D. thesis submitted by **Krishna Prasad Kandel** entitled "**Characterization of Bast Fiber of *Sterculia Villosa* (Roxb.) and *Bauhinia Vahlia* and Fabrication of Biomass-based Nano-Composite Membrane**" is forwarded by Central Department Research Committee (CDRC) to the Dean, IOST, T.U.

Prof. Dr. Jagadeesh Bhattarai
Head
Central Department of Chemistry
Tribhuvan University
Kirtipur, Kathmandu
Nepal

ACKNOWLEDGEMENTS

I am grateful to my supervisor Dr. Bhanu Bhakta Neupane, Asst. Professor, Central Department of Chemistry, Institute of Science and Technology, Tribhuvan University and Co-Supervisor Dr. Mahesh Kumar Joshi, Associate Professor, Tri Chandra Campus, Tribhuvan University and Dr. Soma Nath Dhakal, Assistant Professor of Chemistry at Virginia Commonwealth University, USA for their support, keen supervision and guidance throughout my study. They are always willing to discuss methods validation and research ideas for the study and data collection.

I like to extend my special thanks to Asst. Prof. Dr Bhoj Raj Gautam, Department of Chemistry, Physics and Materials Science, Fayetteville State University, Fayetteville, North Carolina, USA and Asst. Prof. Dr. Bipeen Dahal, Tribhuvan University, for supporting in SEM, XRD and TGA/DTA analysis. I like to extend my special thanks to Prof. Dr. Hem Raj Pant, IOE, Pulchowk Campus, Tribhuvan University, Kathmandu, Nepal for UV-Visible measurement and Mr. Bhawani Prasad Adhikari, officer, Nepal bureau of standards and metrology, for helping in measurements of paper properties, and Dr. Laxmi Thapa for helping in microbial measurement. I am also thankful to Prof. Dr. Rameshwar Adhikari and Assoc. Prof. Khaga Raj Sharma, Central Department of Chemistry for supporting in FTIR measurement.

I am grateful to the University Grants Commission, Nepal, for providing Ph.D. research grants (PhD-76/77-S&T-10).

My sincere thanks go to Prof. Dr. Binil Aryal, Dean of Institute of Science and Technology, and Assoc. Prof. Dr. Surendra Kumar Gautam, Assistant Dean, Tribhuvan University for all the academic and administrative support. I am grateful to Prof. Dr. Kedar Ghimire, Prof. Dr. Megh Raj Pokhrel, Dr. Surya Kant Kalauni, Dr. Santosh Khanal, Dr. Hari Paudyal, Dr. Jagan Nath Adhikari for inspiration and suggestion on my Ph.D. research. Their valuable comments help to improve the quality of my work. I am thankful to all of the faculty members and staff of the Central Department of Chemistry for their encouragement and administrative support. My thanks go to all my friends, colleagues along with Ph.D. scholars for valuable discussion, inspiration, and support. Technical support from the Kathmandu Institute of Applied Sciences (KIAS) and insightful discussion with Dr.

Basant Giri, are valued for me. My special thanks go to Prof. Dayaram Poudel, Campus Chief, and Mr. Govinda Sapkota, former Campus Chief of Birendra Multiple Campus, Bharatpur Tribhuvan University for encouraging and providing study leave. I am thankful to Neupane family from Digam for providing me knowledge about traditional importance of Plant samples and assistance for sample collection.

Finally, my special thanks go to all of my family members for their love and support. My deepest inspiration lies with my wife Ashmita Sharma, who has supported me throughout this study with great patience and understanding. The exhausting emotion that by my wife and our offspring, Krishma and Krishal faced during my abstinence for the purpose of my study were definitely immeasurable, however, I am deeply indebted to them for their inspiration and support. This work is only possible with so many aspirations of my family, friends, colleagues, and blessings from my seniors.



Krishna Prasad Kandel

August 1, 2023

ABSTRACT

Lignocellulose biomass performs an important role in both traditional and next-generation composite materials. Different stages of chemo-mechanical processing are required to achieve the desired properties from the biomass. Commercial alkali is used extensively in the pulp, paper, and related industries for the purpose of bleaching raw fiber and/or recycling waste. It would be beneficial to have a low-cost substitute for commercial alkali in order to lower manufacturing and recycling costs and lower global alkali consumption. The performance of composites may be better understood by knowing the material characteristics of lignocellulose fiber. Cellulose nanocomposite materials have interesting uses in antimicrobial packaging and photocatalytic activity.

In this study, material properties of comparatively fewer investigated and traditionally significant wild plant species *Sterculia villosa* (Roxb.) (Local name Murgilo or Mudilo) and *Bauhinia vahlii* fibers (local name Bharlo) were explored. Water sorption kinetics was one of the material characteristics investigated in its various forms; including untreated, commercial, and wood ash alkali retted. In addition, alkali-treated fibers were compared in terms of sorption data. Fibers treated with alkali were examined for their mechanical strength in both their sorbed and dry states. Specific focus is given to the material properties of fiber mats made from these plant species. Additionally, the antimicrobial and photocatalytic activity of the Ag-ZnO/cellulose nanocomposite prepared were studied.

In the water retting study, many properties of raw *Sterculia villosa* (Roxb.) and *Bauhinia vahlii* fiber samples ($n = 8$) were thoroughly evaluated after they were retted for 0, 20, 30, and 55 days. After water retting, both lignin and extractive levels dropped significantly ($p < 0.05$), but cellulose levels increased. Fiber bundle strength increased significantly ($R^2 = 0.7$) with retting time in *Sterculia villosa* (Roxb.), but not in *Bauhinia vahlii* ($p > 0.05$).

The *Sterculia villosa* (Roxb.) fiber treated with 5% sodium hydroxide and the fiber processed with wood-ash alkali (WAA) were evaluated in terms of their material properties. A net weight loss of $29.1 \pm 2.6\%$ was seen after WAA treatment, whereas a net weight loss of $41 \pm 3.3\%$ was observed after sodium hydroxide treatment. The elimination of hemicellulose and lignin may be responsible for the weight loss in both procedures.

Cellulose fiber produced by the two processes was thoroughly compared with regard to their crystallinity, surface morphology, and thermal stability. The average diffusion coefficient, sorption coefficient, water permeability, and diffusion coefficients at the early and late sorption phases were calculated after the Fickian model was fitted to the experimental kinetic data. For *Sterculia villosa* (Roxb.) average diffusion coefficient (D) for untreated, wood ash alkali and commercial alkali treated was found to be 10.6×10^{-13} m²/sec, 3.08×10^{-12} m²/sec, and 2.35×10^{-12} m²/sec; respectively. *Bauhinia vahlii* had the corresponding values of 6.8×10^{-13} m²/sec, 3.80×10^{-12} m²/sec, and 3.46×10^{-12} m²/sec.

Finally, the physico-mechanical, and optical properties of the cellulose mat prepared were examined. Ag-ZnO nanoparticles were doped in the mat using a single-pot hydrothermal synthesis procedure. The materials' properties were investigated by FE-SEM, EDS, XRD, FTIR, and UV-Vis spectroscopy. Images taken with a FE-SEM demonstrated that the nanoparticles were distributed uniformly throughout the mat. The paper disc diffusion method was used to evaluate the antimicrobial efficacy against *Escherichia coli*, *Bacillus subtilis*, and *Candida albicans*. Methylene blue was utilized to evaluate photocatalytic performance in an ultraviolet light environment.

It is interesting to note that water retting improved the stability of both kinds of fibers at high temperatures and increased their resistance to water. Fibers made by alkali and WAA retting methods have very comparable mechanical strengths. These findings suggested that WAA treatment of lignocellulosic biomass might be a low-cost alternative. The elimination of cementing components and the subsequent rise in crystallinity both contributed to a significant reduction in the equilibrium water sorption of the alkali-treated fiber. Sorbed fibers lose mechanical strength. The produced nanocomposite showed promising photocatalytic and antibacterial activity. These outcomes point out that the nanocomposite mat is suitable for antibacterial and photodegradation in water resources.

Keywords: Lignocellulose biomass, Diffusion coefficient, Paper and pulp, Water retting, Photodegradation, Nanocomposite

LIST OF ACRONYMS AND ABBREVIATIONS

AGU	: Anhydroglucose
ASTM	: American Society for Testing and Materials
ATR	: Attenuated Total Reflection
BV	: <i>Bauhinia vahlii</i>
CI	: Confidence Interval
DP	: Degree of Polymerization
DTG	: Derivative Thermogravimetry
EDX	: Energy-dispersive X-ray Spectroscopy
Eq.	: Equation
FTIR	: Fourier Transform Infrared Spectroscopy
GaM	: <i>d</i> -galacto- <i>d</i> -mannan
GSM	: Grams Per Square Meter
HP	: Handmade Paper
ISO	: International Organization for Standardization
masl	: Meters Above Mean Sea Level
MB	: Methyl Blue
NPs	: Nanoparticles
RBA	: Relative Bonding Area
RH	: Relative Humidity
SEM	: Scanning Electron Microscopy
Sp.	: Species
SV	: <i>Sterculia villosa</i> (Roxb.)
TGA	: Thermogravimetric Analysis

UV : Ultra-violet
UV-Vis : Ultraviolet-visible Spectroscopy
WAA : Wood-ash Alkali
XG : *d*-xylo-*d*-glucan
XRD : X-ray Diffraction

LIST OF SYMBOLS

Å	: Ångström
β	: Beta
λ	: Lambda
θ	: Theta
ε	: Epsilon
ρ	: Rho
E	: Elongation
h	: Hours
°C	: Degrees Celsius
%	: percentage
μg	: Microgram
μS	: Microsiemens
kV	: Kilovolt
v/v	: Volume/volume
w/v	: Weight/volume
w/w	: Weight/weight

LIST OF TABLES

	Page No.
Table 1: Chemical characterization of fiber samples	43
Table 2: Elemental composition of ash	44
Table 3: Crystalline properties of the fiber samples	49
Table 4: A summary of weight loss data for the fiber samples	51
Table 5: Mechanical properties of fiber samples	52
Table 6: Chemical composition of lignocellulose biomass	60
Table 7: Diffusion parameters for untreated fiber	63
Table 8: Diffusion parameters for alkali-treated fiber	64
Table 9: Physical properties of Paper sheet	75
Table 10: Density of <i>Bauhinia vahlii</i> and <i>Sterculia villosa</i> (Roxb.)	76
Table 11: Zone of inhibition microbial test	87

LISTS OF FIGURES

	Page No.
Figure 1: Structure of cellulose, hemicellulose, and lignin in plant cell wall	2
Figure 2: Structure of fiber showing cellulose micro fibrils and cellulose chain	3
Figure 3: Amorphous and crystalline regions of cellulose micro fibrils in plant fibers	3
Figure 4: Representation of cellulose molecule	4
Figure 5: Structure of Hemicellulose; A) Equatorial β -1-4 linkage, B) β -1-4 Xylan, C) β -1-4, mannan, D) β -1-4, glucomannan, E) β -1-4, glucan, F) β -1-4, galactan	6
Figure 6: Primary structure of 4-O-methyl-d-glucurono-d-xylan (MGX)	6
Figure 7: Primary structure of a) β -(1 \rightarrow 3)-D-xylan type X3 and b) β -(1 \rightarrow 3, 1 \rightarrow 4)-D- xylan type Xm.....	7
Figure 8: Primary structure of d-galacto-d-mannan (GaM)	7
Figure 9: Cereal β - glucan	8
Figure 10: Primary structure of d-xylo-d-glucan (XG)	8
Figure 11: Chemical structure of lignin	9
Figure 12: Typical lignin and carbohydrate reactions in alkaline conditions	15
Figure 13: Different parts of plants of studies; A, B, and C are tree, Steam and bark of <i>Sterculia villosa</i> , D, E, and f represent Plant, Climbing nature and steam of <i>Bauhinia vahlii</i>	20
Figure 14: Schematic outline of the experimental design used in this work.	26
Figure 15: Analysis of major chemical components in the fiber samples. (A) Extractive. (B) Lignin. (C) Hemicellulose. (D) Cellulose.	30
Figure 16: Mechanical strength of the fiber samples.....	31
Figure 17: XRD data for the fiber samples. (A) XRD data of <i>Sterculia villosa</i> (Roxb.) samples retted for 0 (S0), 30 (S30) and 55 (S55) days. (B) XRD data of <i>Bauhinia vahlii</i> samples retted for 0 (B0), 30 (B30) and 55 (B55) days....	33
Figure 18: TGA and DTG data for the fiber samples. (A), (B) TGA and DTG for <i>Sterculia villosa</i> (Roxb.) water retted for 0 (S0), 30 (S30), and 55 (S55) days.	

(C), (D) TGA and DTG for <i>Bauhinia vahlii</i> water retted for 0 (B0), 30 (B30), and 55 (B55) days.....	35
Figure 19: SEM images. A, B, and C are the images of <i>Sterculia villosa</i> (Roxb.) fiber retted for 0 (S0), 30 (S30), and 55 (S55) days; respectively. D, E, and F are the corresponding images for <i>Bauhinia vahlii</i> fiber.....	36
Figure 20: A simple schematic of WAA treatment method.	39
Figure 21: SEM-EDX spectrum of the ash powder.....	43
Figure 22: XRD profile of the ash powder.....	44
Figure 23: FTIR spectra of untreated and NaOH and WAA-treated fibers.	45
Figure 24: SEM images of A) untreated, B) WAA-treated, and C) NaOH-treated fibers.....	46
Figure 25: XRD data of untreated, WAA-treated, and NaOH-treated fibers. For easy comparison, data are overlaid vertically. The inset shows six components that fit the XRD data of WAA-treated fiber.	48
Figure 26: Thermogravimetric analysis. The main frame and inset show the TGA and DTG data of three fiber samples;	50
Figure 27: Tensile strength of the fiber samples. For easy comparison, range, mean, and median values along with a few outliers are shown in a box plot	52
Figure 28: Sorption kinetic data for untreated <i>Sterculia villosa</i> (Roxb.) and <i>Bauhinia vahlii</i> fibers. Fickian fit to the experimental data points is plotted as solid curves	62
Figure 29: (A) Plot of $(M_t/M_{eq})^2$ versus t and linear regression $(M_t/M_{eq})^2 = f(t)$ derived from the experimental data in the $M_t/M_{eq} < 0.5$ regime (inset). (B) A plot of $\ln(1-M_t/M_{eq})$ versus t and the linear regression $\ln(1-M_t/M_{eq}) = f(t)$ derived from the experimental data in the longer time regime ($0.7 < M_t/M_{eq} < 1$)	63
Figure 30: Water sorption kinetic data for alkali-treated <i>Sterculia villosa</i> (Roxb.) (A) and <i>Bauhinia vahlii</i> fibers (B). The Fickian fit to the experimental data is plotted as solid curves.....	65
Figure 31: Equilibrium weight gain for untreated and alkali-treated fibers.	66
Figure 32: Mechanical strength of different samples.	67

Figure 33: Schematic figure for the conceptual framework used in this work.....	71
Figure 34: Diameter of fiber distribution A) <i>Sterculia villosa</i> (Roxb.) B) <i>Bauhinia vahlii</i>	79
Figure 35: SEM image of <i>Bauhinia Vahlii</i>: A) Cellulose paper mat, B) Cellulose-ZnO/Ag, C) 10 min sonicated Cellulose-ZnO/Ag, D) 20 min sonicated cellulose-ZnO/Ag; and E, F, G, H represent the corresponding data for <i>Sterculia villosa</i> (Roxb.).....	80
Figure 36: SEMEDX, B1) Cellulose Paper), B2) Cellulose-ZnO/Ag, B3) B2 sonicated for 10 min, B6) B2 sonicated for 20 min	81
Figure 37: SEM EDX <i>Sterculia villosa</i> (Roxb.), S1) Cellulose Paper (CP), S2) CP-ZnO/Ag, S3) CP-Ag-ZnO sonicated for 10 min, S4) CP-Ag-ZnO sonicated for 20 min.....	82
Figure 38: XRD data of cellulose paper (B1), cellulose-ZnO (B2), Ag-ZnO/cellulose (B3 and B4), and Sonicated Ag-ZnO/cellulose mat.....	83
Figure 39: FTIR of paper, and nanocomposite made from <i>Bauhinia vahlii</i> fibers...	84
Figure 40: UV-vis spectra of the Ag-ZnO/Cellulose nanocomposites. The spectra are normalized to the peak around 450 nm	85
Figure 41: UV-vis absorption spectra of Methyl Blue measured at different time interval of UV- interaction where 0 to 150 refers time in minutes. Inset shows absorbance versus time plot.....	86
Figure 42: Antimicrobial Acitivity of Nanocomposite Paper-mat of <i>Bauhinia</i> A) <i>Bacillus subtilis</i> B) <i>Candida Albicans</i> C) <i>Escherichia coli</i> and <i>Sterculia</i> D) <i>Bacillus subtilis</i> E) <i>Candida Albicans</i> F) <i>Escherichia coli</i>	88

TABLE OF CONTENTS

Page No.

Declaration.....	iv
Recommendation	Error! Bookmark not defined.v
Letter of Approval.....	Error! Bookmark not defined.vi
Acknowledgements.....	vii
Abstract	ix
List of Acronyms and Abbreviations	xi
List of Symbols	xiii
List of Tables.....	xiv
Lists of figures	xv
Table of Contents	xviii
CHAPTER 1	1
1. INTRODUCTION.....	1
1.1. Background	1
1.1.1. Molecular Structure of Lignocellulosic biomass.....	1
1.1.2. Retting of natural fiber	9
1.1.3. Pulping.....	16
1.1.4. Water absorption by lignocellulose biomass	18
1.1.5. Nanocomposite.....	19
1.1.6. Description of plant studied	20
1.1.7. Rationale.....	21
1.1.8. Objectives.....	21
1.1.9. Research questions	22

1.1.10. Organization of the thesis.....	23
CHAPTER 2	24
2. A SYSTEMATIC STUDY ON MATERIAL PROPERTIES OF WATER- RETTEED <i>STERCULIA VILLOSA</i> (ROXB.) AND <i>BAUHINIA VAHLII</i> FIBER	24
2.1. Introduction	24
2.2. Materials and methods	25
2.2.1. Materials.....	25
2.2.2. Water retting.....	26
2.2.3. Chemical analysis.....	27
2.2.4. Mechanical strength of fiber.....	27
2.2.5. XRD, TGA, and SEM measurements.....	28
2.2.6. Statistical analysis	28
2.3. Results and discussion.....	28
2.3.1. Gravimetric analysis.....	28
2.3.2. Mechanical strength	31
2.3.3. XRD data.....	31
2.3.4. Thermal properties	33
2.3.5. SEM imaging.....	35
2.4. Conclusions	36
CHAPTER 3	37
3. COMPARATIVE STUDY ON MATERIAL PROPERTIES OF WOOD-ASH ALKALI AND COMMERCIAL ALKALI-TREATED <i>STERCULIA VILLOSA</i> (ROXB.) FIBER.....	37
3.1. Introduction	37
3.2. Materials and methods	38

3.2.1.	Fiber treatment with commercial alkali.....	38
3.2.2.	Wood ash alkali extraction and fiber treatment.....	39
3.2.3.	Estimation of cellulose, hemicellulose, and lignin.....	39
3.2.4.	Measurement of fiber width.....	40
3.2.5.	FTIR, XRD, DTA, and SEM measurements.....	41
3.2.6.	Mechanical strength of fiber.....	41
3.2.7.	Statistical analysis.....	42
3.3.	Results and discussion.....	42
3.3.1.	Weight loss, chemical characterization, and fiber width.....	42
3.3.2.	SEM, SEM-EDX, and XRD.....	43
3.3.3.	Further implications of the research.....	53
3.3.4.	Conclusions.....	53
CHAPTER 4	54
4. KINETICS OF WATER SORPTION IN SINGLE <i>STERCULIA VILLOSA</i> (ROXB.) AND <i>BAUHINIA VAHLII</i> FIBERS AT AMBIENT TEMPERATURE	54
4.1.	Introduction.....	54
4.2.	Materials and methods.....	55
4.2.1.	Chemical characterization.....	55
4.2.2.	Alkali treatment.....	57
4.2.3.	Measurement of fiber width.....	57
4.2.4.	Sorption kinetics study.....	57
4.2.5.	Fickian diffusion model and data analysis.....	58
4.2.6.	Measurement of mechanical strength.....	59
4.2.7.	Statistical analysis.....	59

4.3.	Results and discussion.....	60
4.3.1.	Fiber characterization	60
4.3.2.	Sorption kinetics in untreated fiber	61
4.3.3.	Sorption kinetics in alkali-treated fiber	64
4.3.4.	Mechanical strength of fiber.....	66
4.4.	Conclusions	67
CHAPTER 5	68
5.	FABRICATION OF Ag-ZnO/CELLULOSE NANOCOMPOSITE MAT FOR DYE DEGRADATION AND ANTIMICROBIAL PACKAGING	68
5.1.	Introduction	68
5.2.	Materials and methods	70
5.2.1.	Materials.....	70
5.2.2.	Extraction of Fibers	70
5.2.3.	Pulping.....	70
5.2.4.	Making paper sheet	70
5.2.5.	Characterization.....	71
5.2.6.	Preparation of ZnO-Ag/cellulose sheet	71
5.2.7.	Antimicrobial test preparation.....	72
5.2.8.	Determination of antibacterial efficiency.....	72
5.2.9.	Measurement of fiber width	73
5.2.10.	FTIR, XRD, and SEM measurements	73
5.2.11.	Measurement of Physical Properties	73
5.3.	Results and discussion.....	74
5.3.1.	Physical Properties of paper mat	74
5.3.2.	Cobb 60	76

5.3.3.	Optical Properties	77
5.3.4.	Opacity	77
5.3.5.	Mechanical Properties	78
5.3.6.	SEM Imaging of the Paper Samples.....	79
5.3.7.	XRD Study	82
5.3.8.	FTIR and UV-vis Study.....	83
5.3.9.	Photocatalysis of Methylene blue.....	85
5.3.10.	Determination of antimicrobial efficiency	86
5.4.	Conclusions	88
CHAPTER 6		89
6. SUMMARY AND CONCLUSIONS.....		89
6.1.	Summary	89
6.2.	Conclusions	91
6.3.	Recommendations for Further work	92
6.3.1.	Research recommendations.....	92
6.3.2.	Policy recommendations	93
REFERENCES		94
APPENDIX		113
Appendix I: Permission letter from Department of Plant Resources, MoFE, Government of Nepal, for collection of plant samples.....		113
Appendix II: Identification of Plants from National Herbarium and Plant Laboratories (KATH), Department of Plant Resources, Government of Nepal.		114
Appendix III: Deposition of Plant to the National Herbarium and Plant Laboratories (KATH), Department of Plant Resources, Government of Nepal. “Voucher specimen: Gulmi district, C Nepal, Chhatrakot-4, BB Neupane & KP Kandel 03, 26.04.2023, KATH”		116

Appendix IV: Publications	118
Appendix V: Conference.....	126
Appendix VI: Laboratory equipment used during research	133

CHAPTER 1

1. INTRODUCTION

1.1. Background

Lignocellulosic biomass is one of the most widespread, inexpensive, and ecologically favorable forms of terrestrial biomass. Lignocellulose fiber obtained from plants is a crucial component of the paper, pulp, and cardboard manufacturing processes. After undergoing chemical and/or mechanical processing, the fiber can be separated from a different plant part, including bark, leaf, root, and others (Reddy and Yang, 2007; Bajpai, 2018b; Tanpichai *et al.*, 2019a). Hemp, sisal, coir, kenaf, and jute are all different forms of lignocellulose fibers that may be processed into materials with low density, high specific strength, and minimal environmental impact. Bast fibers are a kind of soft, woody fiber is derived from phloem tissues of plant stems. The fibers are often long and strong, and shape a crucial component of the future generation, composite materials with implications in waste water treatment, biomedical applications, agribusiness, and the automobile industry (Camargo *et al.*, 2009; Sharma, *et al.*, 2019; Jaspal and Malviya, 2020; Amara *et al.*, 2021; Veerasimman *et al.*, 2021). Fabricating textiles with self-cleaning, antibacterial, and UV protection qualities using cellulose nano-composite fibers is also being investigated (Zhang *et al.*, 2013; Aladpoosh *et al.*, 2014; Haslinger *et al.*, 2019). In their natural form, the sticky or non-cellulosic substances such as wax, pectin, and lignin bind bast fibers to the surrounding tissues. Cellulose, hemicellulose, lignin, (Figure 1), and extractives are the primary chemical components of raw cellulosic fiber.

1.1.1. Molecular Structure of Lignocellulosic biomass

1.1.1.1. Molecular Structure of Cellulose

Cellulose is the most widely distributed renewable polymer source (Du *et al.*, 2019; Hu *et al.*, 2019). It is extensively distributed in the cell walls of higher plants and marine organisms and is also produced by algae, fungi, and bacteria (Liu, K. *et al.*, 2021). There is a wide range of cellulose content across plant fibers; some examples are cotton (95%), henequen (78%), sisal (73%), jute (71%), hemp (70%), North American hard wood (66–67%), flax (63%), rice straw (45–55%), sugarcane bagasse (43%), kenaf (36%), and wheat straw (30%) (Heinze *et al.*, 2018). These cellulose contents may vary

according to harvesting periods (Keller *et al.* 2001), method of processing (Nykter *et al.*, 2008).

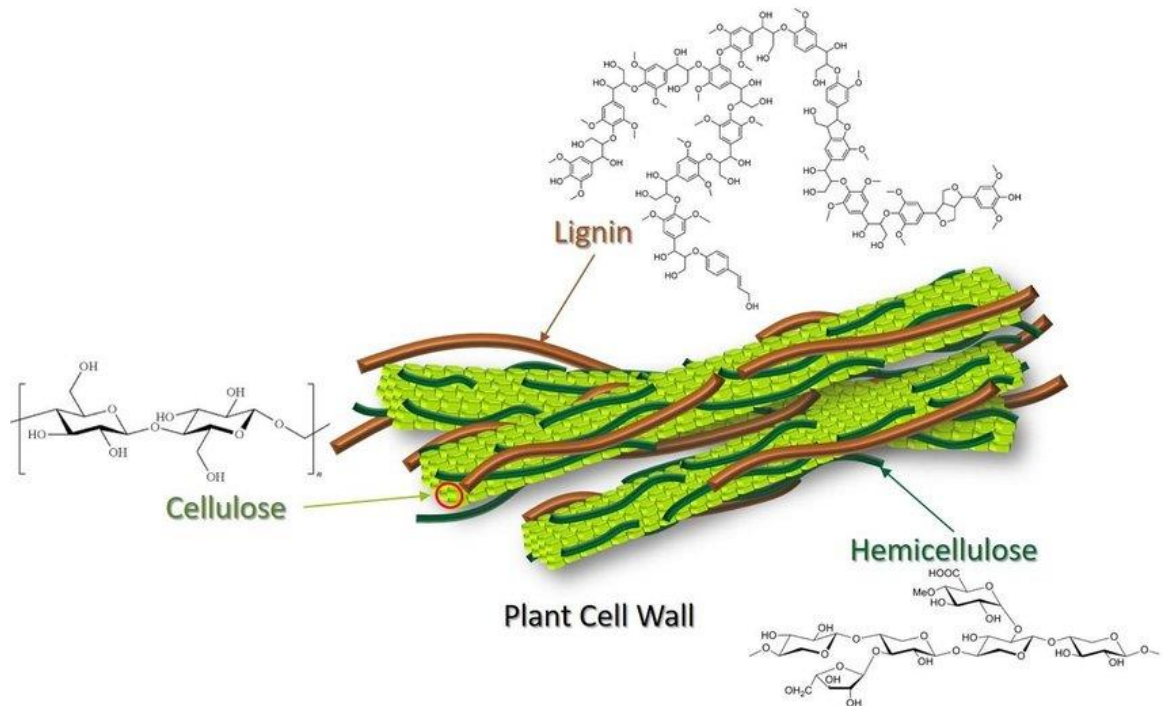


Figure 1: Structure of cellulose, hemicellulose, and lignin in plant cell wall (reproduced from the permission from reference Jensen *et al.* (2017). Copyright 2017 by Springer)

Both eucalyptus and rice straw have been discovered to have different chemical compositions depending on where they are grown. Wheat straw from various regions has chemically and morphologically similar tendencies. The reported variations in carbohydrate content are about 5%. The origin of these variances may be linked to genetics or growing circumstances (Beadle *et al.*, 1996; Mckean and Jacobs, 1997).

Cellulose, no matter its origin, is mainly comprised of the identical polymer chain linked by D-glucopyranosyl units via β -1,4-glycosidic bonds (Rao *et al.*, 1967). Each glucose unit contains hydroxyl groups on C2, C3, and C6 that are capable of forming hydrogen bonds within and among cellulose macromolecules. Therefore, it is evident that these hydroxyl groups and their capacity to create hydrogen bonds are helpful in interpretation of the crystal arrangement and regulating the physicochemical features of cellulose (Moon *et al.*, 2011; Heinze *et al.*, 2018; Wang *et al.*, 2020).

Cellulose, in its natural state, is not a single molecule but rather a fiber made up of several cellulosic molecular chains. The cellulose source affects the polymer chain length. Natural lignocellulose typically has a high degree of polymerization, up to

10,000 glucose units (Klemm *et al.*, 2005). Through hydrogen bonding, 18–36 distinct cellulose chains come together to form elementary fibrils, which are larger entities. Microfibrils and microfibril bundles (macro fibrils) are constructed from the smaller elementary fibrils (Figure 2) (Moon *et al.*, 2011; Liu *et al.*, 2021).

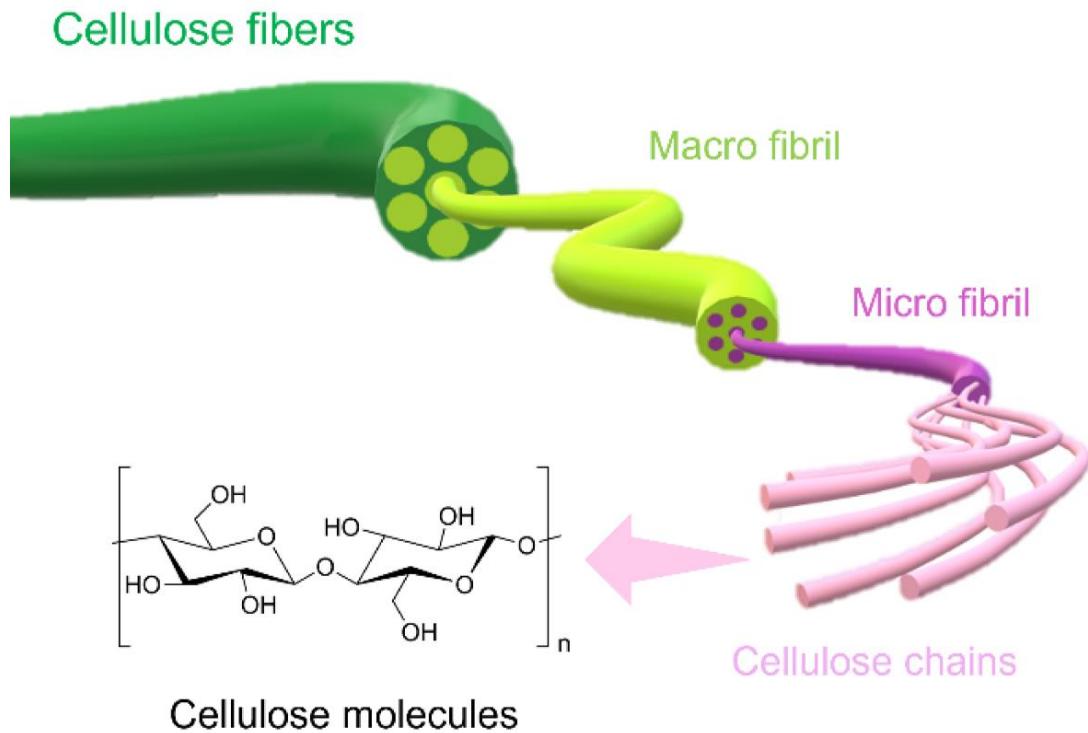


Figure 2: Structure of fiber showing cellulose micro fibrils and cellulose chain (Reproduced with permission from reference Fornari *et al.* (2022). Copyright 2022 by the authors)

The cellulose molecular chain in a single cellulose microfibril is separated into well-organized structural sections (crystalline regions) and disarranged regions (amorphous regions) (Figure 3), where the cellulose chains are compactly packed and form a solid structure in the crystalline fields and are arbitrarily intertwined in the disordered sections (Lee *et al.*, 2014; Yang *et al.*, 2019).

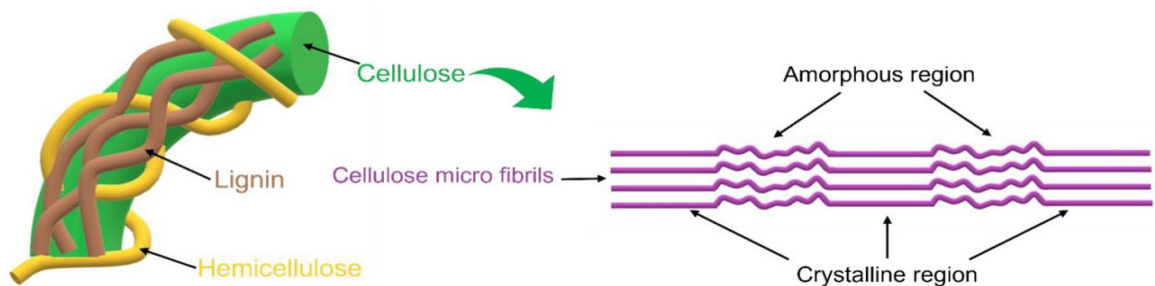


Figure 3: Amorphous and crystalline regions of cellulose micro fibrils in plant fibers (Reproduced with permission from reference Fornari *et al.* (2022). Copyright 2022 by the authors)

In cellulose (Figure 4), the two ends of the chain are chemically distinct, as is usual for polymers generated by polycondensation (Pérez and Mazeau, 2005). The nonreducing end has an anomeric C atom interconnected by glycosidic bonds. Similarly, the reducing end has a D-glucopyranose unit in equilibrium with the aldehyde functional group (Heinze, 2016).

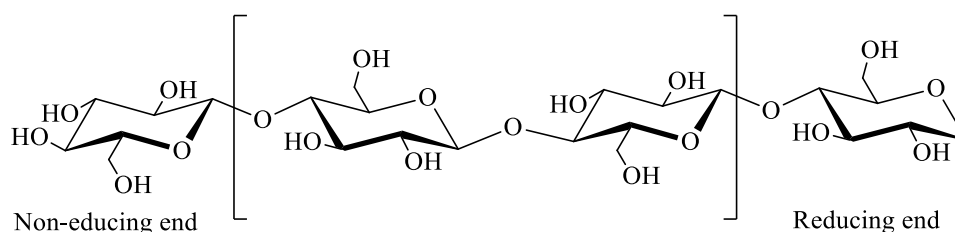


Figure 4: Representation of cellulose molecule

Hydrolysis or oxidation of the cellulose chain is the process that causes structural modifications. These reactions mostly take place in amorphous or fibril surface areas. Native cellulose from a variety of sources has a degree of polymerization (DP) between 1,000 and 30,000, which maps to chain lengths between 500 and 15,000 nm. When using separation techniques, cellulose samples have DP values around 800 and 3,000 (Krässig, 1993).

Hydrogen bonding networks in cellulose are very diverse and have a role in determining its characteristics (Kondo, 1997). Strong hydrogen bonding systems are responsible for several properties of cellulose, including its crystallinity, its low solubility in various solvents, and the reactivity of its hydroxyl groups. Hydrophobic regions (around C atoms) in cellulose may also affect its overall characteristics, particularly its solubility. Hydrogen bonds, both intramolecular and intermolecular, are formed between the three hydroxyl groups of the AGU. During this process, the oxygen atoms of the D-glucopyranose ring and the glycosidic linkage connect with one another and with another cellulose chain. As a result of hydrogen bonding, many different configurations in three dimensions might arise (Heinze, 2016).

1.1.1.2. Molecular Structure of Hemicellulose

Hemicellulose is a complex carbohydrate that shapes the significant proportion of plant cell wall. Hemicelluloses are a valuable resource for the production of a variety of products, including biofuels, animal feed, and paper. During the papermaking process, hemicelluloses remain bound with cellulose fibers, thereby enhancing the final

material's properties (Gandini and Belgacem, 2012). They are also being investigated for their potential use in the development of new medical treatments. It is a heteropolymer with branch consisting of pentoses (xylans), interchanging mannose and glucose units (mannans or glucomannans), or galactose units (galactan). Hemicellulose, in contrast to cellulose, has 50–3000 carbohydrate units per polymer as compared to 7000–10,000 glucose molecules in cellulose. Based on the hydration of the fibers, these various subtypes may be classified into two broad groups. Hydrogen bonding interactions with cellulose and covalent interactions with lignin are the primary roles of low-hydration polysaccharides (xylans) in cell wall stabilization. Because of their branching nature, they dissolve easily in hot water. The second kind, hydrocolloid-based hemicelluloses, are found mostly in seeds and serve as water retention mechanisms (Wyman *et al.*, 2004). Hydrolysis is more effective on hemicellulose because it is amorphous and not crystalline like cellulose (Peterson *et al.*, 2008). It is made up of short, amply branched polymers of five- and six-carbon polysaccharide units, like xylan, mannan, glucans, and xyloglucans (Scheller and Ulvskov, 2010; Peng and She, 2014; Negahdar *et al.*, 2016; Luo *et al.*, 2019). Hemicelluloses are regarded as a β -(1→4)-linked backbone with an equatorial configuration at C1 and C4 and Polysaccharides such as β -(1→4)-galactan organize with axial configuration at C4 and not included with hemicelluloses (Figure 5) (Scheller and Ulvskov, 2010).

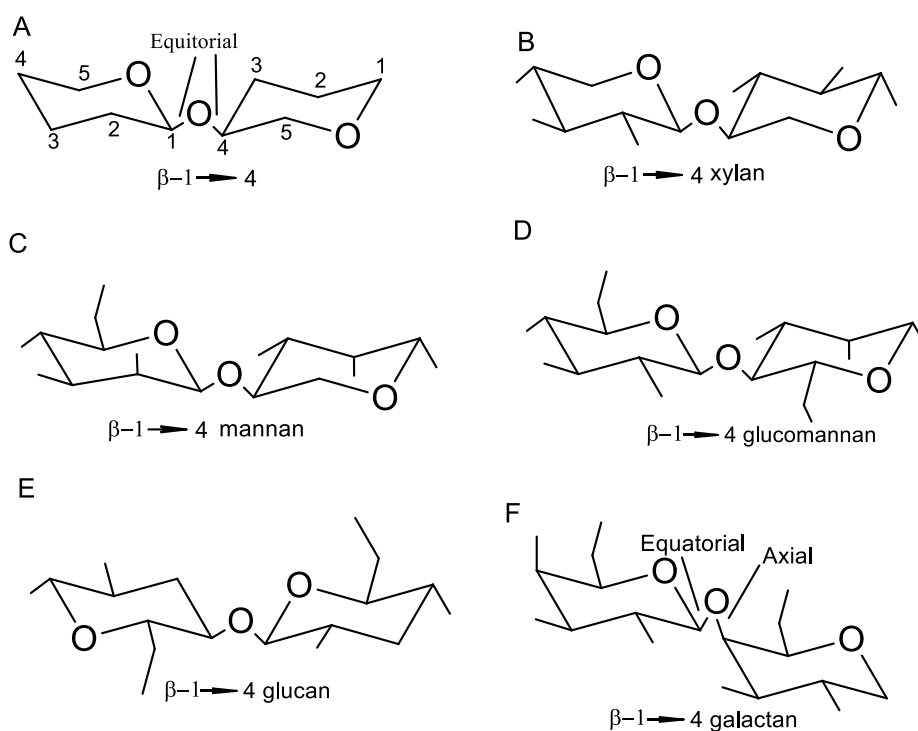


Figure 5: Structure of Hemicellulose; A) Equatorial β -1-4 linkage, B) β -1-4 Xylan, C) β -1-4, mannan, D) β -1-4, glucomannan, E) β -1-4, glucan, F) β -1-4, galactan (Scheller and Ulvskov, 2010)

1.1.1.2.1. Xylans

Around 20-30% of the biomass of plants, is made up of the xylan-type (Figures 6 and 7) polysaccharides found in secondary cell walls. Terrestrial plants produce xylans, which are heteropolymers with a β -(1 \rightarrow 4)-d-xylopyranose backbone. This is branched by short carbohydrate chains which comprised of numerous oligosaccharides made of d-xylose, L-arabinose, d- or l-galactose, and d-glucose, as well as d-glucuronic acid or its 4-O-methyl ether (Ebringerová *et al.*, 2005).

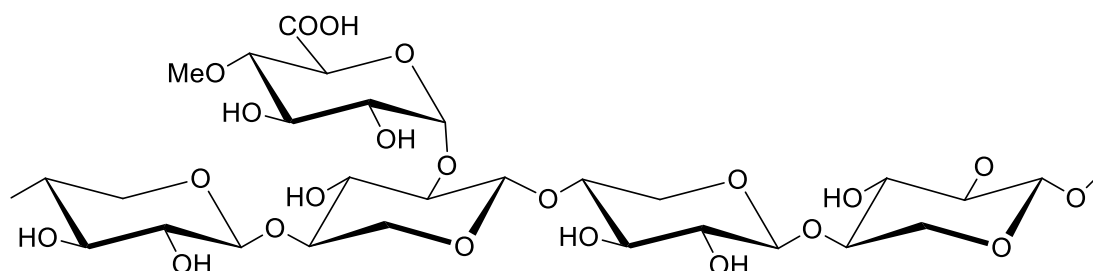


Figure 6: Primary structure of 4-O-methyl-d-glucurono-d-xylan (MGX)

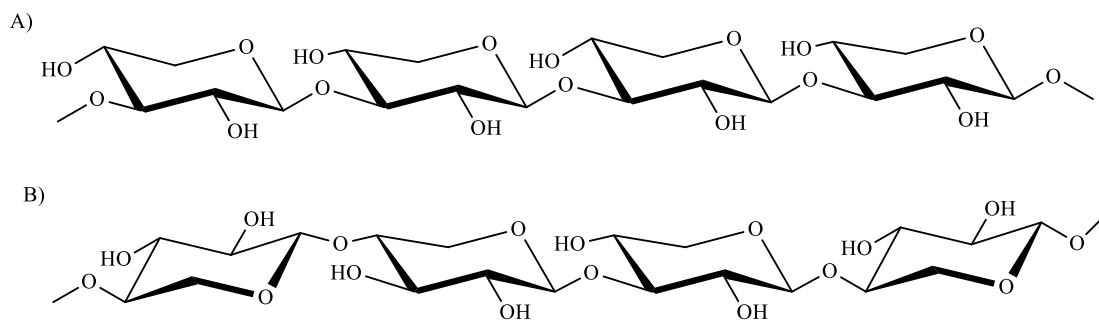


Figure 7: Primary structure of a) β -(1 \rightarrow 3)-D-xylan type X3 and b) β -(1 \rightarrow 3, 1 \rightarrow 4)-D-xylan type Xm

1.1.1.2.2. Mannans

Linear polymers best describe galactosylated mannans (Figure 8). Due to the presence of a cellulose-like (1 \rightarrow 4)- β -d-mannan structure, they have a propensity for self-association, insolubility, and crystallinity. An orthorhombic unit cell was proposed based on crystallographic analysis (Kapoor *et al.*, 1995).

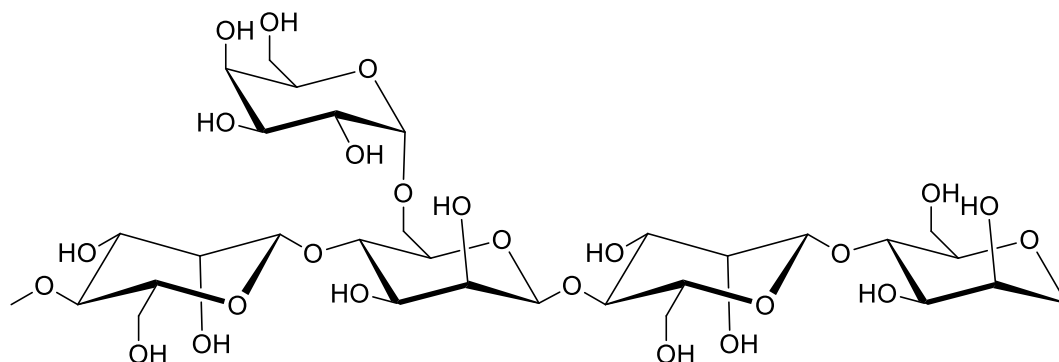


Figure 8: Primary structure of d-galacto-d-mannan (GaM) (Ebringerová *et al.*, 2005)

1.1.1.2.3. β -glucans

Cereal grains contain hemicellulose molecules called (1 \rightarrow 3,1 \rightarrow 4)-d-glucans (-glucans) (Figure 9) in the endospermic cell walls. They play a crucial role in cell development as the primary molecules linked to cellulose microfibrils (Roubroeks *et al.*, 2000).

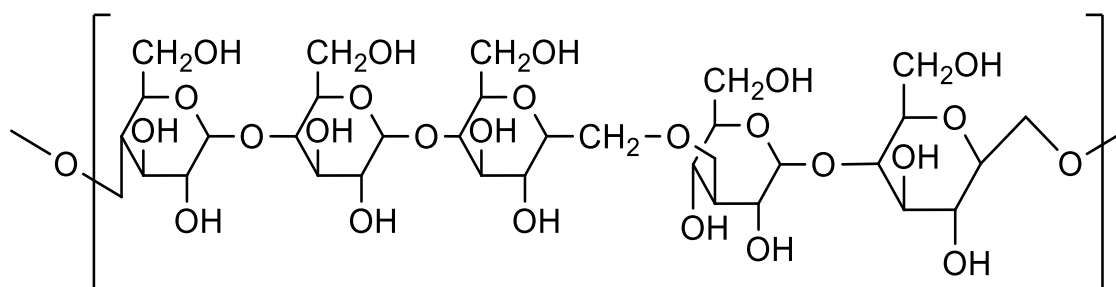


Figure 9: Cereal β -glucan

1.1.1.2.4. Xyloglucans

d-xylo-d-glucan (XG) include -d-Xylo residues at position 6 along a cellulosic backbone, specifically a (1 \rightarrow 4)- β -d-glucopyranan backbone (Figure 10). According to Pauly *et al.* (1999) majority of XG have strong hydrogen bonds with cellulose microfibrils (Figure 9) in the cell wall.

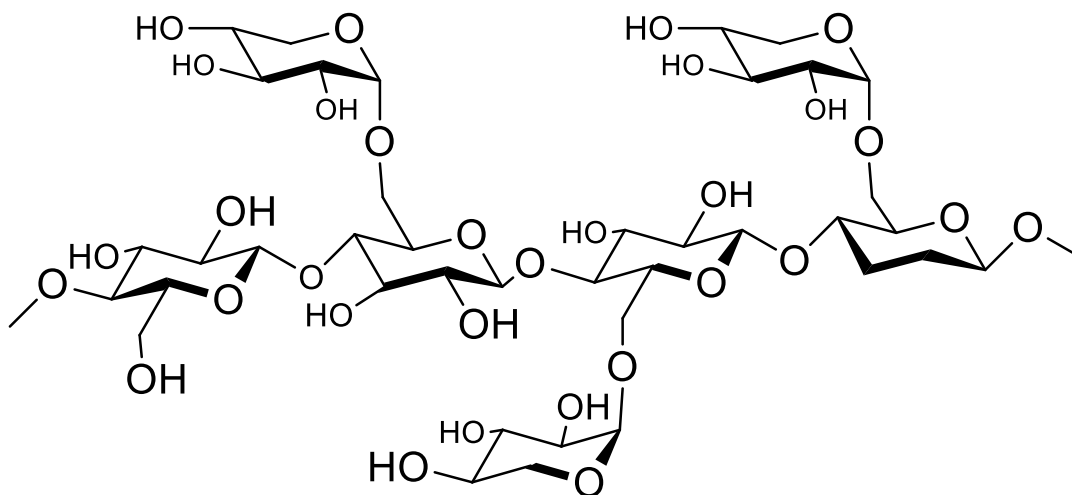


Figure 10: Primary structure of d-xylo-d-glucan (XG) (Ebringerová *et al.*, 2005)

Hemicellulose and cellulose are considered to join together in the cell walls of plants, allowing hemicellulose to create very durable networks with cellulose via hydrogen bonds and van der Waals interactions. In a study by Agger *et al.* (2014), Ferulic acid causes the development of hemicellulose-lignin connections by forming covalent feruloyl ester-ether sandwiched between hemicellulose and lignin (Luo *et al.*, 2019). Because of its highly branched and amorphous structure, hemicellulose may be readily transformed. Nevertheless, hemicellulose's DP is only around 100-200 U, which is much lesser than that of cellulose and lignin. In comparison to cellulose, hemicellulose is more prone to degradation when heated (Luo *et al.*, 2019).

1.1.1.3. Molecular structure of Lignin

Lignin is a complicated three-dimensional phenolic polymer mostly constituted of three distinct monolignols. These are p-coumaryl, coniferyl, and sinapyl (Figures 11). These phenylpropane units are mostly cross-linked via ether linkages. von Schenck *et al.* (2013) found that up to 65% of the bonds between lignin units as the α -O-4 and β -O-4

ether linkages. Subunits of lignin behave differently depending on whether or not the phenolic units have been etherified.

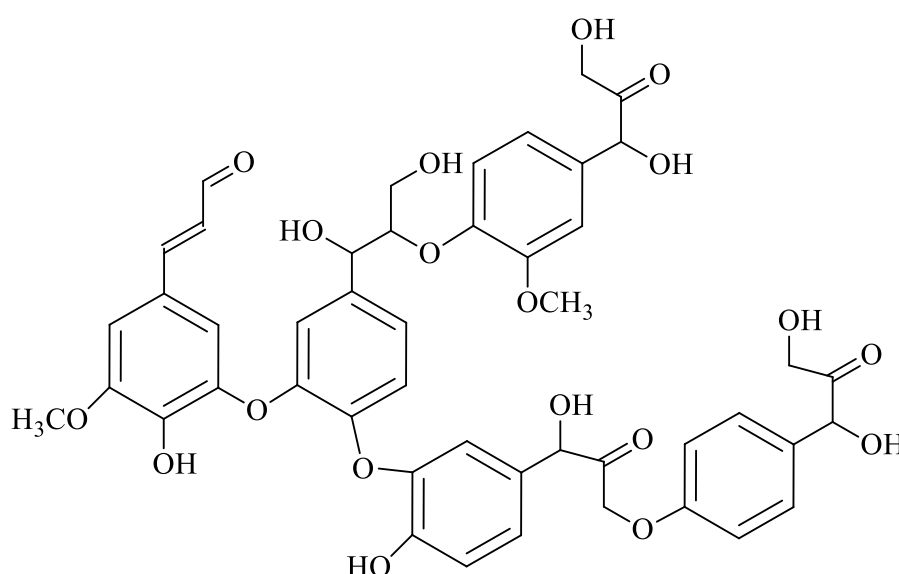
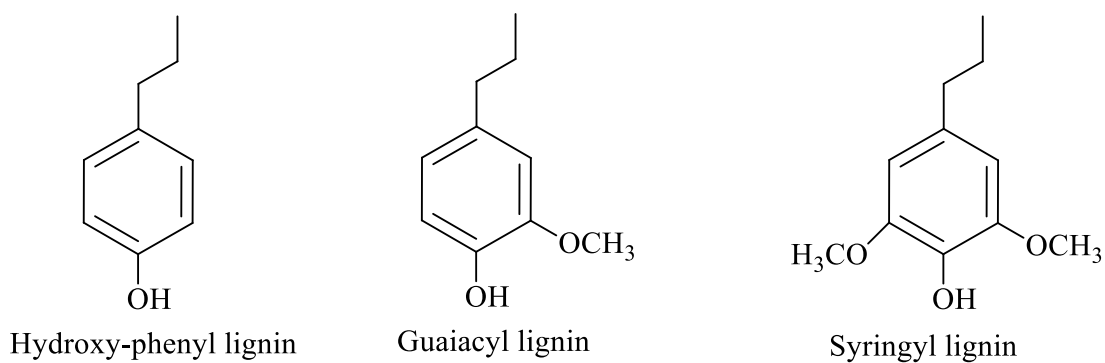


Figure 11: Chemical structure of lignin (Kock, 2006)

1.1.2. Retting of natural fiber

1.1.2.1. Water retting

Different chemo-mechanical techniques must be used to separate the gummy components and get fibers with the necessary characteristics. One of the important degumming techniques is retting. Chemical retting, enzyme retting, aqueous retting, dew retting, gel retting, ribbon retting, or various combinations (Banik *et al.*, 2003; Harwood *et al.*, 2004; Akin *et al.*, 2007) are a few of the retting types that in used. Retting often involves the removal of non-cellulosic elements, which causes fiber bundles to partly split. Retting conditions must be controlled to produce fibers with the greatest strength possible (Paridah *et al.*, 2011).

In water retting, fiber bundles are typically immersed for 2–3 weeks in slowly running or static water in a pond or tank (Banik *et al.*, 2003; Yu and Yu, 2010). The gummy or fiber-binding substances lignin and pectin may be hydrolyzed by anaerobic bacterial and/or fungal colonies in groundwater or tap water, releasing galacturonic acid and sugar as the main byproducts (Paridah *et al.*, 2011; Brindha *et al.*, 2019; chares Subash and Muthiah, 2021). Fiber bundles partly split as a consequence of the partial elimination of gummy components.

The fiber quality is determined by the retting circumstances, including retting duration, microbial variety and concentration, and fiber type. Foul-smelling water and a variety of contaminants are produced by water retting. But this is one of the most affordable techniques, and the fibers it produces have great length uniformity and strength (Hurren *et al.*, 2002; Banik *et al.*, 2003).

Retting may also be accomplished under controlled conditions utilizing an enzyme like pectinase or xylanases. Enzymatic retting produces low-strength fiber even though it is quicker (12–24 hours) and produces no unwanted pollutants (Yu and Yu, 2010; Paridah *et al.*, 2011). Retting may also be carried out mechanically by employing a decorticator to separate the bonds between the fibers. Although mechanical retting is quick, the fiber produced is of poor quality. Furthermore, its high cost restricts its use in resource-constrained contexts. As a consequence, classical water retting is still being investigated as potential method for producing fibers with great strength and a range of lengths (Ganan *et al.*, 2004).

1.1.2.2. Dew retting

Dew retting involves gathering the stems, spreading the stems out across the ground. The quality of flax straw is affected by weather conditions in the field (Jankauskiene *et al.*, 2007; Chabbert *et al.*, 2020). In dew retting, also called field-retting, stem surface becomes colonized by microorganisms, which eventually spread throughout the plant. Pectinase enzymes produced by microorganisms target these binding sites such as plant's cortical section and the pectic interstitial lamellae interconnecting the fibers (Ribeiro *et al.*, 2015; Djemiel *et al.*, 2017). Due to the constant moisture provided by rain-fall and dew, several fungi, such as *C. herbarum*, *Mucor sp.*, *Rhizopus sp.*, and *Epicoccum nigrum*, invade the stems of the flax plant during dew-retting. Dew-retting

is still widely used by flax growers (Kozłowski *et al.*, 2006; Kozłowski and Różańska, 2020).

1.1.2.3. Enzyme retting

The enzyme retting process targets the pectin and lignin components of various plant fibers, most notably flax, and hemp, and separate the fiber bundle from the stem. Bio retting, also known as enzymatic retting, is the substitution of industrially manufactured enzymes, mostly pectinases, for the microbial enzymes synthesized by the retting agents in dew retting or in water retting (Chauhan *et al.*, 2013). Enzymes are added to the water during retting to speed up the breakdown of the pectin and lignin. The enzymes used in this method are typically purified from microbial sources like fungi and bacteria.

The use of enzymes for retting has several advantages. Using the method, better fiber can be extracted more efficiently and reliably. It leaves less of an environmental impact since it uses less water and produces less waste. Enzyme retting is often used in the textile industry to produce high-quality fibers for garments and other applications.

1.1.2.4. Chemical retting

A variety of chemical and mechanical processes must be applied to raw fiber before it can be used in a particular application (Bajpai, 2018b). The different variants of chemical retting are (a) Kraft pulping (combination of sodium hydroxide and sodium sulfide) or (b) an alkali or intermixture of alkalis pulping, or (c) sulfite pulping (a mixture of sulfurous acid and bisulfite ion).

1.1.2.4.1. Kraft pulping:

Kraft pulping is one of the most familiar methods for creating chemical pulp. The pulping process comprises heating wood pieces in an aqueous solution of sodium hydroxide and sodium sulfide from about 70°C to boiling temperature (around 170°C) and then allowing them to heat for 1-2 h. During this process, lignin is thoroughly broken down, and the breakdown byproducts are dissolved. Hemicelluloses, in specific, removed by incomplete degradation and dissolution during Kraft pulping. Extractives are also eliminated to a significant degree (Gierer, 1980).

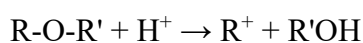
1.1.2.4.2. Alkaline Pulping

Alkaline Pulping is the process of treating fiber with alkali or a mixture of alkalis such as NaOH, Ca(OH)₂. The separation of cellulose fibers from wood or other plant-based materials is often accomplished using this method in the paper and pulp industry. Alkali is absorbed at the contact point to the lignin complex's acidic phenolic groups. The separation of the alkali-lignin complex from the lignin surface and its solubility in the liquid occurs as a result of chemical hydrolysis (Larocque and Maass, 1941). This results in the partial separation of fiber bundles.

1.1.2.4.3. Sulfite pulping

During the sulfite process, bio-mass is treated with solution containing sulfite and bisulfite ions. The treatment degrades lignocellulose biomass into its basic building blocks, cellulose, and lignin. This result, wood pulp being almost completely changed into cellulose fibers. The treatment solution contains appropriate amount of sodium carbonate, sodium sulphite, and water mixed to get a sulphite concentration of 12.5% and a liquid and solid ratio of 6:1. The mixture is baked at 165°C for around 120 minutes after adding 0.5% anthraquinone (López *et al.*, 2000). Hydrolysis of lignin to soluble lignosulfonates allows for further extraction of lignin from the cellulose.

During sulfite pulping, many of the lignin components are separated by hydronation of carbon-carbon double bonds or acidic breakage of ethereal bonds, which generate resonance-stabilized carbocations (R⁺). In the sulfite process, the latter reaction is the main mechanism by which lignin is broken down. Electrophilic carbocations interact with bisulfite ions to form sulfonates (HSO₃⁻).



The lignosulfonates produced during the sulfite process may be put to good use, and the method itself doesn't destroy lignin to the identical amount as the Kraft process prepares.

According to Sun *et al.* (2016), the significant recalcitrance of lignocelluloses to enzymatic breakdown of carbohydrate exists. This is triggered by the intimate association of hemicellulose and lignin with cellulose by means of hydrogen and covalent bonding, or hydrophobic and ionic interactions. The chemical interactions

between alkali and lignocelluloses consist mostly of lignin reactions, cellulose, and hemicellulose reactions. In the reaction, sugar is lost as a byproduct and lignin, on the other hand, degrades and dissolves. Although the primary reaction pathway of alkali-based treatment involves rupture of ester bonds cross-linking lignin and xylan during solvation and saponification, different treatment chemicals may bring about different degradation reactions of lignocellulosic components. In general, phenolic lignin moieties are much more reactive than nonphenolic ones, and lignin degradation (through breakage of ether bond) and enhanced hydrophilicity are the key mechanisms by which lignin is dissolved from lignocellulosic biomass (Xu, H. *et al.*, 2016). The important reactions of lignin and carbohydrates in an alkaline solution are shown in brief (Figure 12).

1.1.2.4.4. The cleavage of the phenol type α -aryl ethers or α -alkyl ethers

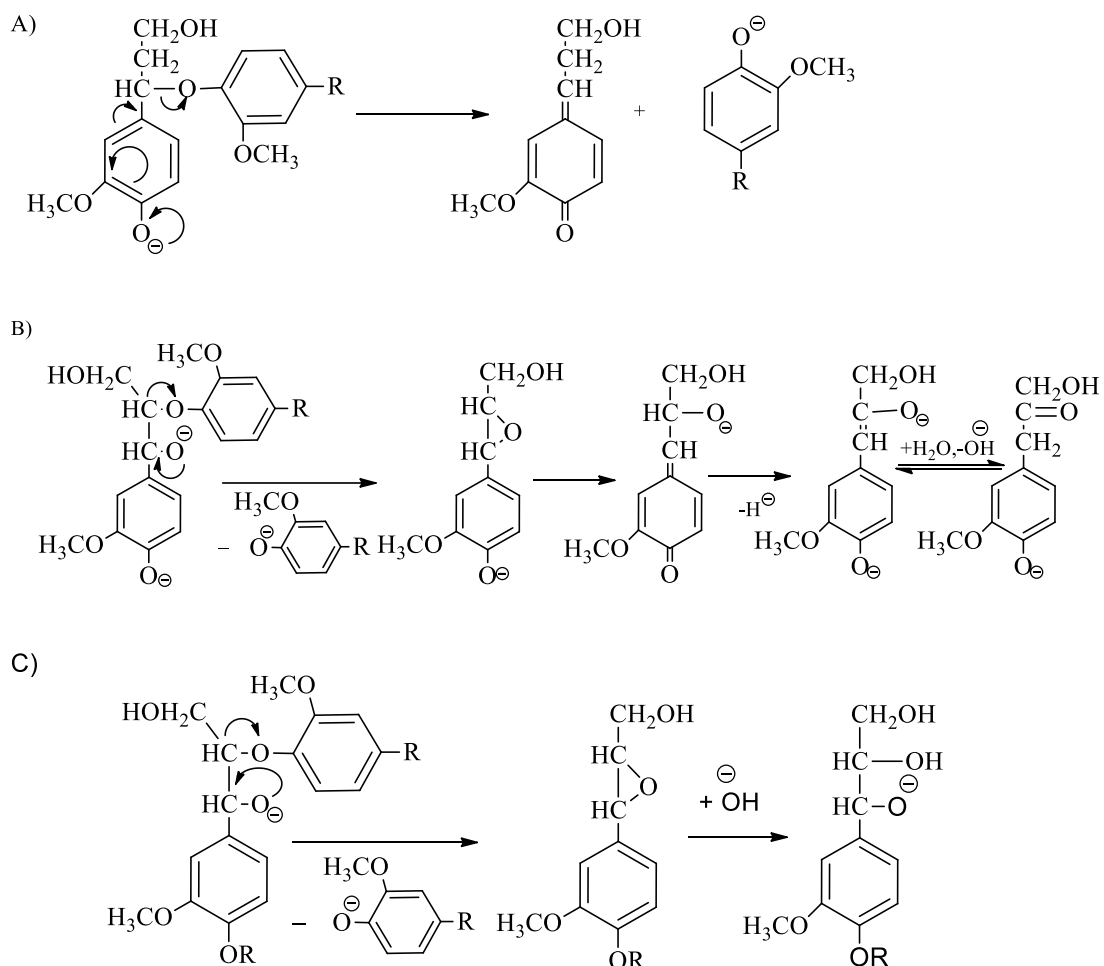
During an alkali-based treatment, the alkali (OH) initially interacts with the acidic phenolic hydroxyl to produce water-soluble phenates. After this, the quinone methide intermediates are formed by the structural rearrangement of phenate ions, which facilitates the breaking of the connection between the α -C in the phenylpropane unit and the -O- of the aryl ethers or the alkyl ethers (von Schenck *et al.*, 2013). The formation of quinone methide can lead to a variety of events, including addition, elimination, and electron transfer processes (Xu, H. *et al.*, 2016). The molecular weight of lignin will dramatically drop following the breakage of the phenol type α -aryl ether bond, as illustrated in Figure 12a, which represents a characteristic cleavage of phenol type α -aryl ether. A non-phenol α -aryl ether bond tends to be more stable than a phenol α -aryl ether bond, and the former is often simple to break (Yang, Haitao *et al.*, 2016).

1.1.2.4.5. The cleavage of the phenol type β -aryl ethers

Cleavage of phenol type β -aryl ethers is crucial reaction of delignification, especially for softwoods, due to their central involvement in the diversity of linkages within lignin macromolecule structures (Xu, H. *et al.*, 2016). Cleavage of phenol-type β -aryl ethers are facilitated by hydroxyl's nucleophilic assault on the α -C to create an epoxy compound during alkali-based pretreatment (Figure 12b). The cleavage of phenol type β -aryl ethers (by producing an episulfide molecule) may be greatly improved if there are other stronger nucleophiles (like HS⁻) in pretreatment fluid (Figure 12f) (Yang, Haitao *et al.*, 2016).

1.1.2.4.6. The cleavage of the non-phenol type β -aryl ethers

The inability to produce the quinone methide structure upon alkaline treatment is the defining feature of non-phenol type β -aryl ether as opposed to phenol type β -aryl ether. Hence, the non-phenol type β -aryl ether is extremely stable and can only be broken by the presence of α -OH (Xu, H. *et al.*, 2016). As seen in Figure 12c, α -OH is easily ionized in alkaline settings, and the resulting oxygen ion may connect to β -C to create the epoxy compound, therefore breaking the bonds of non-phenol type β -aryl ethers. Nevertheless, more extreme circumstances may break the C-C connection of aryl-alkyl or alkyl-alkyl, which might decline the molecular size of lignin (von Schenck *et al.*, 2013; Sun *et al.*, 2016).



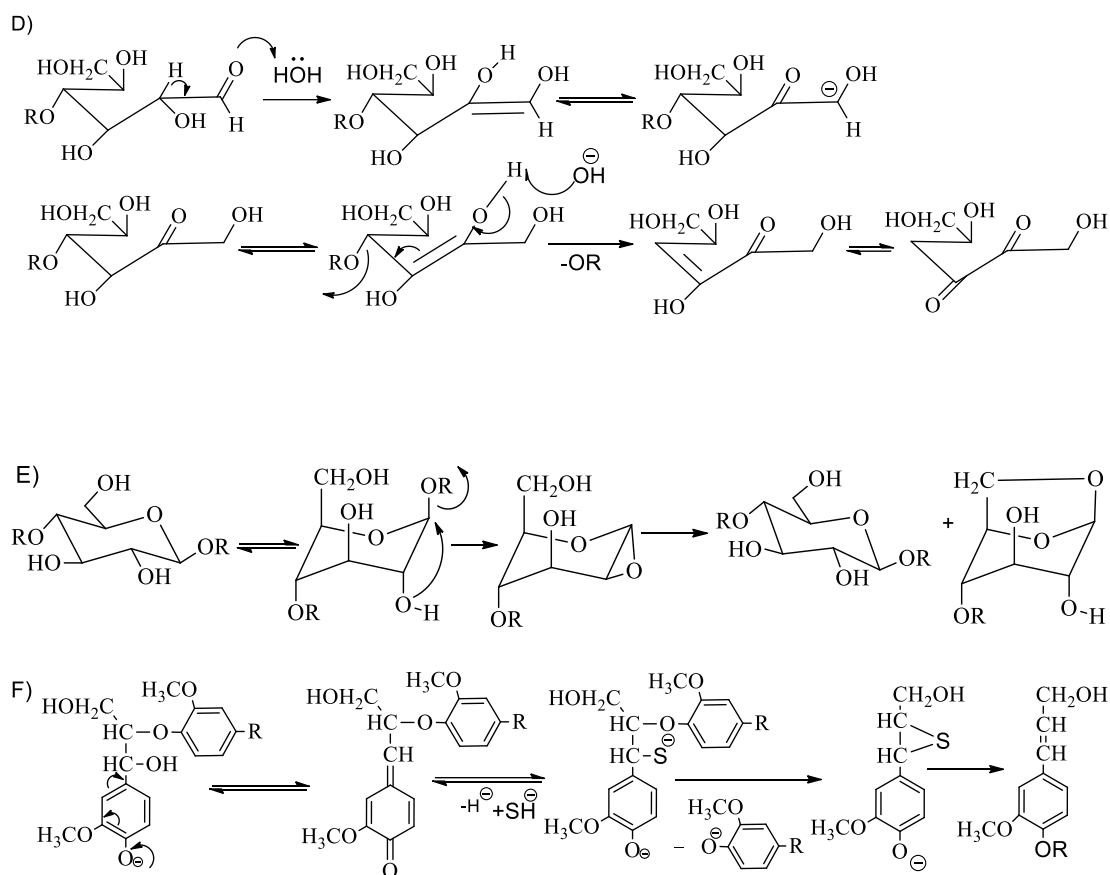


Figure 12: Typical lignin and carbohydrate reactions in alkaline conditions (a: The fracture of the phenol type α -aryl ethers; b: The cleavage of the phenol type β -aryl ethers; c: The fracture of the non-phenol type β -aryl ethers; d: cellulose peeling reaction; e: alkaline hydrolysis of cellulose; f: the sulphide fracture of the phenol type β -aryl ethers)(Xu, H. *et al.*, 2016)

1.1.2.4.7. Carbohydrates reactions

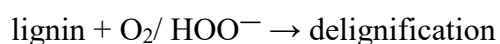
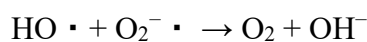
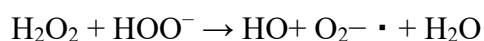
The breakdown of cellulose and hemicellulose is an inevitable side effect of alkali-based pretreatment, whose primary purpose is to eliminate lignin. Fermentable sugars are lost in carbohydrate reactions, but cellulose's extremely homogeneous and crystalline structure makes it additional resistant in alkaline settings and causes it to degrade at a slower rate than hemicelluloses do. All of the carboxyl groups in carbohydrates are neutralized in highly alkaline environments. At temperatures over 70 °C, the acetyl moieties in hemicelluloses may be de-acetylated due to the high pH at the start of pretreatment resulting in partial loss from the biomass (Xu, H. *et al.*, 2016).

1.1.2.4.8. Delignification and bleaching with H₂O₂

H₂O₂ is the simplest form of peroxide and the weakest acid. H₂O₂ is a transparent watery liquid with a viscosity a little higher than that of water. It is often used as the aqueous

solution with a concentration between 30 and 70 wt.%, which is a clear liquid similar to water used for reasons of safety (Xu, H. *et al.*, 2016). Alkaline H₂O₂ bleaching is a relatively safe process of removing remaining lignin and colorants from fiber. This may have a little influence on weight reduction. There was a noticeable increase in fiber brightness after bleaching, as predicted (Kandel *et al.*, 2022). The chemical stability of H₂O₂ is poor, and it possesses powerful oxidizing characteristics. Surface disinfectants, bleaching agents, and oxidants are common uses for hydrogen peroxide in the home, the hospital, and the lab (Gong *et al.*, 2015). H₂O₂ decomposes into HOO⁻ under alkaline circumstances (pKa = 11.6). Oxygen released on the decomposition of hydrogen peroxide is responsible for delignification (Xu, H. *et al.*, 2016). HOO⁻ promotes delignification by reacting with phenyl propanol, propiophenone, and quinone structures in lignin, as well as the double bonds and carbonyl of side chains, to fragment lignin and increase its solubility.

Hydrogen peroxide decomposes on alkaline conditions to produce O₂^{-•} and HO[•] as shown in reactions:



The fact that H₂O₂ may break down into oxygen and water makes it a particularly attractive treatment option since it ensures that the treated biomass has no residual contaminants. By adding H₂O₂, lignin removal may be improved, preparing the substrate further accessible to enzymatic digestion after treatment (Xu, H. *et al.*, 2016).

1.1.3. Pulping

The process of pulping involves employing chemical and mechanical, and/or biological methods to separate the cellulose fibers from the lignin in wood (Mboowa, 2021). Pulping reduces the effective width of fiber bundles and partially or completely separates the bundles by removing non-cellulosic fixing constituents' lignin and hemicellulose and extra residues. These changes take place on varying degrees depending on the fiber-treatment parameters. The morphology, specific strength, thermal stability, and crystallinity of fiber are all modified throughout the pulping process (Saha *et al.*, 2010; Liu *et al.*, 2013; Chandrasekar *et al.*, 2017). Approximately

75% of total pulp output and 91% of chemically produced pulp worldwide is Kraft pulping (Bajpai, 2015). Commercial alkali or a combination of alkalis is typically used in the processing of fiber in small-scale or handmade paper companies (Hubbe and Bowden, 2009; Chauhan *et al.*, 2013; Mejouyo *et al.*, 2020; Sannapamma *et al.*, 2020; Chauhan and Meena, 2021).

The contamination of water, land, and air is intensified by the waste produced by the paper, pulp, and cardboard industries (Chakraborty *et al.*, 2019; Gaur *et al.*, 2020; Sharma, P. and Singh, 2021). For this reason, today's paper and pulp mills are more equipped than ever to retrieve chemicals, renovate waste biomass into additional energy-worth stuff, or adapt the waste bio-mass for longer to stimulate more beneficial microbes (Chakraborty *et al.*, 2019). The manufacturing cost and worldwide alkali consumption may be lowered with the help of any cheap and environmentally-beneficial option that can be employed in fiber processing and waste reprocessing.

Plant-based lignocellulose fiber, such as that found in leaves, roots, and bark, is a key ingredient in many composites. In addition, they have a central role in the production of paper, pulp, and cardboard (Reddy and Yang, 2007; Bajpai, 2018b; Tanpichai *et al.*, 2019a). In an effort to find more sustainable alternatives to conventional composites made with plastic or glass fiber, lignocellulose fiber-reinforced composites are being researched. There are various uses for composite materials reinforced with natural fibers due to their many benefits, including those in the automotive and agricultural sectors, as well as in waste water treatment and structural engineering (Manimaran *et al.*, 2020; Vigneshwaran *et al.*, 2020). These materials are considered low density, high thermal stability, specific strength, and decreased abrasiveness. These materials have found increasing use in several fields in recent years, including agriculture and the automotive industry, medicine, architecture, and pollution control (Liu, W. *et al.*, 2020; Vigneshwaran *et al.*, 2020; Dasore *et al.*, 2021). Mercerization involves immersing the fibers in a dilute solution of sodium hydroxide (NaOH). By changing the alkaline solution's concentration, the temperature, and the period of the treatment, a variety of modifications may be achieved. The mercerization process creates a rough topography on the fiber's surface, which enhances its adhesive properties by reducing the presence of natural and synthetic contaminants. In addition to increasing the effectual external area in contact with the wet matrix, mercerization causes fiber fibrillation, or the breakage of the composite fiber bundle into tiny fibers (Zafeiropoulos, 2008).

Mercerization is often used to improve the quality of cotton fabrics. It can also be used to produce special effects, such as a frosted or moiré finish (creates a repeating pattern of light and dark bands). Alkaline pulping is the most common method of producing cellulose fibers from wood. It is used to create a broad range of paper goods, including as writing paper, newspaper, and printing paper.

1.1.4. Water absorption by lignocellulose biomass

Materials reinforced with natural fibers often degrade quickly in the presence of external factors like sunlight, humidity, water, and microorganisms. Natural fiber has hydrophilic properties which makes them less stable and durable than synthetic materials because of increased water absorption. (Joseph *et al.*, 2002; Lin *et al.*, 2002; Brebu, 2020). Depending on their intended usage, composites may be subjected to a broad variety of humidity and moisture conditions. Thus, knowledge of the water acceptance capability of cellulose fiber may be useful in understanding the impacts of water absorption in composites and limiting water uptake.

Three main channels for the movement of tiny permeants in polymers have been reported. Micro-gaps created by polymeric chains are critical for the diffusion of water molecules. Microcracks and capillary movement are two minor contributors. (Naylor, 1989; Espert *et al.*, 2004). The experimental kinetic data may be fitted using diffusion as a model parameter. The mobility of the polymer segments is much higher than the diffusion rate in the case of I diffusion (pseudo-Fickian and Fickian). Case II (or extreme case II) improves penetrant mobility considerably more than the other relaxation stages. Here, there is a clear demarcation between the swollen and the unswollen areas, and this boundary moves linearly over time. Anomalous or non-Fickian diffusion (case III), the mobility of the penetrant is comparable to the relaxation of polymer segments. The shape of the sorption-time curve, which is often written as (Eq. 1), may be used to deduce information about the dominant mode.

$$\frac{M_t}{M_{eq}} = kt^n$$

The moisture content at time t (M_t) and equilibrium moisture content (M_{eq}) are represented by the variables in this equation, whereas k and n are constants. The slope of the straight line formed by the relationship between $\log(M_t/M_{eq})$ and $\log t$ is equal to

the n factor. For pseudo-Fickian diffusion ($n < 1/2$), Fickian diffusion ($n = 1/2$), case II ($n = 1$), and anomalous diffusion (case III), n has an intermediate value ($1/2 < n < 1$) (Naylor, 1989; Espert *et al.*, 2004; Jasso-Gastinel, 2017; Sahu and Gupta, 2022). Several literature studies (Saikia 2010; Nosbi *et al.*, 2011; Ronald Aseer *et al.*, 2013) have reported the water sorption kinetics in natural fibers and composites under various experimental condition.

1.1.5. Nanocomposite

The term "nanocomposite" is used to describe a substance in which nanoparticles are dispersed throughout a polymer or metal matrix. Nanoparticles may be made from a widespread range of materials, including metals, ceramics, and polymers, and generally vary in size from 1 to 100 nanometers. Nanocomposites have several unique properties that are not found in traditional materials, such as increased strength, stiffness, and durability.

In recent years, cellulose based nanocomposite materials are finding applications in electronics, aircraft, and biomedical engineering, among others. Functionalized nanocomposites ZnO-Ag coated cotton fabric exhibited a synergistic antibacterial effect (El-Nahhal *et al.*, 2020). Synthesizing silver-zinc oxide nanocomposites (Ag-ZnO nanocomposites) with distinctive quantities of Ag-doped to the ZnO improved the photocatalytic degradation of methylene blue. (Rafaie *et al.*, 2017). Increased efforts to purify water and the environment have led to the widespread use of photocatalytic materials in recent years (Liu, Huifang *et al.*, 2019). Using cellulose fiber as a substrate, Ag-ZnO nanocomposites can be synthesized. The cellulose mat acts as a scaffold for the nanocomposite to grow on by providing both mechanical support and a porous, biodegradable environment. The Ag-ZnO nanocomposite is made by soaking a cellulose mat in a solution of zinc nitrate and silver nitrate. The mat with the precursor solution is heated to create Ag-ZnO nanoparticles on the cellulose fibers. The Ag-ZnO nanocomposite has a wide range of potential applications, including antimicrobial coatings, sensors, and catalysis. Silver nanoparticles in the nanocomposite may have antimicrobial properties, whereas ZnO nanoparticles may enhance photocatalytic activity. The use of a cellulose mat matrix in the synthesis of a Ag-ZnO nanocomposite provides a more sustainable, biodegradable alternative to traditional synthetic

materials. High-strength fiber from *Sterculia villosa* (Roxb.) and *Bauhinia vahlii* may be employed as a matrix in the synthesis of Ag-ZnO/cellulose nanocomposite material.

1.1.6. Description of plant studied

Sterculia villosa Roxb, is widely accessible in the East Himalaya, India, Nepal, Pakistan, and the West Himalaya (POWO, 2023). Murgilo or Mudilo are the common names used by locals in the Gulmi district of Nepal (Figure 13 A, B and C). One of the species of plants with a rapid rate of growth (Kandel *et al.*, 2023). It has properties that make it suitable for use in paper production. In addition to its traditional usage as firewood, high strength fastening fiber the plant is now widely used in the production of tea boxes and other lightweight packing containers. Seeds and stem cuttings both work for propagating this plant. When mature, a tree may reach heights of 15-18 meters, widths of 1.4-1.6 meters, and bark thicknesses of 2.5 centimeters. (Ghosh and Baruah, 1997).

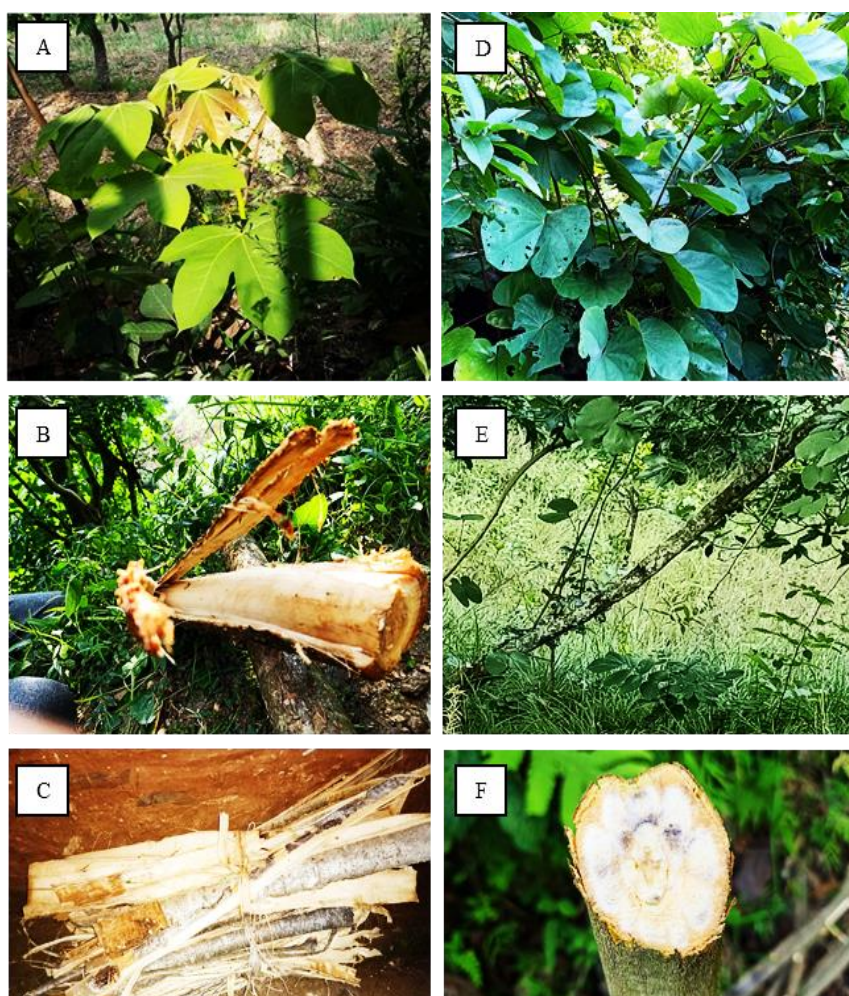


Figure 13: Different parts of plants of studies; A, B, and C are tree, Stem and bark of *Sterculia villosa*, D, E, and f represent Plant, Climbing nature and stem of *Bauhinia vahlii*

Bauhinia vahlii, a woody climber, is utilized by Nepalese rural populations as high-strength fiber. Bhorlo is the common name used by locals (Figure 13 D, E, and F). Additionally, it is used medicinally. It is distributed on the South Asian continent. Unselective taking out of the woody climber has led to decline in its distribution range (Thakur *et al.*, 2022). *Bauhinia vahlii* is an active climbing shrub that may reach the very peaks of the forest's trees. Besides being high in fiber, it also has anti-inflammatory properties. Barks, stems, leaves, and seeds are just some of the various *Bauhinia vahlii* components used in traditional medicine. It has a tough stem that may grow to be 17–20 m in height and 10–15 cm in diameter (Ray *et al.*, 2020)

1.1.7. Rationale

Synthetic plastic-based materials are extensively used in daily life. These materials degrade very slowly and persist in the environment for a longer time (*i.e.*, persistent material) thereby causing environmental pollution at different levels. In this respect, there is always a need for a novel material that is cheap, easily available, and environmentally friendly. From a material point perspective, the natural fiber pick up from *Sterculia villosa* (Roxb.) and *Bauhinia vahlii* are the least studied plant species.

Although the fabrication and application of nano-composite membranes made from traditional plastic-based material are explored in the literature (H. J. Kim, Han, Joshi, & Kim, 2017; H. J. Kim, Pant, Park, *et al.*, 2013; J. H. Kim, Joshi, Lee, Park, & Kim, 2018), the possibility of fabrication of cheaper and safer bio-mass based nanocomposite membrane is not explored. The proposed research work plays a significant role in fulfilling the research gap by characterizing the cellulosic fiber obtained from the *Sterculia villosa* (Roxb.) *Bauhinia vahlii*, fabricating the novel nano-composite membrane and exploring its: 1) photocatalytic dye degradation efficiency, and 2) antimicrobial activity.

1.1.8. Objectives

The broad/general objectives of the proposed research were to assess the Physico-mechanical properties of cellulosic fiber acquired from *Sterculia villosa* (Roxb.) and *Bauhinia vahlii* and fabricate the nano-composite membrane.

The specific objectives of the proposed academic proposal are, as listed.

- Extraction of cellulosic fiber by different chemical methods.

- Measure the chemical composition (cellulose, lignin, and hemicellulose) of fiber extracted by different methods.
- Measure and compare the morphology and degree of crystallinity, mean length, diameter, linear mass density, water absorbency, and tensile strength of fiber extracted by different methods from the two plants.
- Fabrication of the cellulose mat/paper and incorporate the ZnO and Ag nanoparticles on the cellulose membrane by Hydrothermal method (fabrication of nano-composite membrane).
- Measure the antimicrobial and photocatalytic dye degradation efficiency of the fabricated nanocomposite mat.

1.1.9. Research questions

- Do the mechanical properties of natural fiber obtained from *Sterculia villosa* (Roxb.) and *Bauhinia vahlii* compared with the other commonly studied counterparts?
- How do the physical and chemical properties of the fiber depend on processing parameters?
- Can the wood ash alkali be used in processing cellulose biomass?
- Can the cellulose biomass obtained from the plant materials be efficiently converted to cellulose mats?
- Can a nano-composite membrane having antimicrobial and photocatalytic activities be fabricated from the cellulose biomass of the selected plants?

1.1.10. Organization of the thesis

This dissertation consists of six chapters, excluding references and appendices. The first chapter of the thesis contains the introduction and discusses the context, rationale, research question, objectives, and thesis organization. The chapters 2-5 are arranged as an introduction, materials and methods, result and discussion, and conclusions. Chapter -2 deals with a “systematic study on material properties of water-retted *Sterculia villosa* (Roxb.) and *Bauhinia vahlii* fiber”. The chapter-3 describes the “Comparative study on material properties of wood-ash alkali and commercial alkali treated *Sterculia villosa* fiber”, chapter-4 evaluates “Kinetics of water sorption in single *Sterculia villosa* (Roxb.) and *Bauhinia vahlii* fibers at ambient temperature”. The chapter-5 describes “Fabrication of Ag-ZnO/cellulose nanocomposite mat for dye degradation and antimicrobial packaging”. Overall findings and suggestions for future research and the thesis is summed up and highlighted in Chapter 6.

CHAPTER 2

2. A SYSTEMATIC STUDY ON MATERIAL PROPERTIES OF WATER-RETTEDED *Sterculia villosa* (ROXB.) AND *Bauhinia vahlii* FIBER

2.1. Introduction

Lignocellulose biomass is one of the most widespread, inexpensive, and ecologically favorable forms of terrestrial biomass. Following various processing techniques, the biomass may be produced from the leaf, seed, fruit, and bast portions of various plant species or other plant-derived wastes (Beghello, 1998; Reddy and Yang, 2007; Paridah *et al.*, 2011; Bajpai, 2018b; Tanpichai *et al.*, 2019a). Bast fibers are a kind of soft, woody fiber that is derived from phloem tissues in plant stems. The fibers are often long and strong, and they are critical parts of materials for the future generation, with implications in waste water treatment, biomedical applications, agribusiness, and the automobile industry (Camargo *et al.*, 2009; Sharma, A. *et al.*, 2019; Jaspal and Malviya, 2020; Amara *et al.*, 2021; Veerasimman *et al.*, 2021). Fabricating textiles with self-cleaning, antibacterial, and UV protection qualities using cellulose nano-composite fibers is also being investigated (Zhang *et al.*, 2013; Aladpoosh *et al.*, 2014; Haslinger *et al.*, 2019).

In their natural condition, wax, pectin, and lignin are only a few examples of the sticky or non-cellulosic substances that bind bast fibers to the surrounding tissues. Different chemical and mechanical methods must be used to separate the sticky parts in order to make fibers with the right properties. Retting is a crucial degumming method. There are several different kinds of retting in use, including chemical retting, enzyme retting, aqueous retting, dew retting, gel retting, ribbon retting, and many more (Banik *et al.*, 2003; Harwood *et al.*, 2004; Akin *et al.*, 2007; Lee *et al.*, 2020). Non-cellulosic components are often removed during retting, which causes fiber bundles to partially separate. Maximum strength fibers can only be produced under carefully managed retting circumstances (Paridah *et al.*, 2011).

Fiber bundles are submerged in water for two to three weeks (Banik *et al.*, 2003; Yu and Yu, 2010) to undergo the retting process. Hydrolysis of the gummy or fiber-binding compounds lignin and pectin by anaerobic bacterial and/or fungal colonies in groundwater or tap water might release galacturonic acid and sugar as the major byproducts (Paridah *et al.*, 2011; Brindha *et al.*, 2019; chares Subash and Muthiah,

2021). The partial removal of gummy components causes fiber bundles to separate. Conditions during retting, including as retting time, microbial diversity, and microbial concentration, and fiber type, all contribute to the final fiber quality. Water retting results in contaminated, foul-smelling water. This is one of the cheapest methods, and the fibers it produces are very uniform in length and robust (Hurren *et al.*, 2002; Banik *et al.*, 2003).

Retting may also be achieved in a controlled environment using an enzyme such as pectinase or xylanases. Even though it's faster (12-24 hours) and doesn't generate any undesirable pollutants, enzymatic retting results in low-strength fiber (Yu and Yu, 2010; Paridah *et al.*, 2011). Retting may also be done mechanically by using a decorticator to remove the fiber connections. The fiber quality is low, but mechanical retting is fast. Its high price also limits its use in situations where resources are scarce. Therefore, research into classical water retting continues as a viable option for creating fibers with high strength and variable lengths (Ganan *et al.*, 2004).

The fiber bio-mass derived from *Sterculia villosa* (Roxb.) and *Bauhinia vahlii* plant species is considered to have good water firmness and is consequently traditionally employed to fasten items immersed in water or very humid environments. It would be essential to investigate the material characteristics of fibers that have been water-retted for varying durations. In this investigation, two fiber kinds were retted in container water after 0, 20, 30, and 55 days. Experimental fibers were analyzed for their retting efficiency, chemical composition after retting, strength, and thermal stability. We also connect the obtained final characteristics to the morphological and crystallinity changes. The paper concludes with a short discussion of the research's broader implications.

2.2. Materials and methods

2.2.1. Materials

The stems of the *Sterculia villosa* (Roxb.) and *Bauhinia vahlii* plants (about ~1 m long and ~3 cm broad) were gathered from Digam, Gulmi, Nepal (hilly region, 1250 masl). Following a conventional procedure, bast fiber bio-mass was extracted from the wet stem. The stalks were physically removed by gently hammering a slab of wood around one end of each one. Using a stainless-steel knife, the outer cuticular layer was peeled

off of the biomass (Figure 14). The samples were taken to the lab for further research after being sun-dried to eliminate extra moisture.

2.2.2. Water retting

Water retting was accomplished using techniques documented in the literature with minor modifications (Henriksson, G. *et al.*, 1997; Ruan *et al.*, 2015). Samples of bast fiber were separated into four 100-gram groups. The samples were thoroughly washed with tap water and then crushed lightly to separate the bundles. The samples were submerged in 4 Liter of distilled water (pH 7.2±1, conductivity 9±1 µS) in individual containers. The samples were exposed to natural circumstances (temperatures between 20 and 30 degrees Celsius and relative humidity between 50 and 70 percent) for 20, 30, and 55 days. Tank water was attenuated by one-third every ten days to avoid extreme growth of microbes and contamination. Samples were cleaned with distilled water and dried in an oven at 105±2°C after each retting period. On the basis of the beginning and end weights, the weight loss percentage or retting effectiveness was computed. *Sterculia villosa* (Roxb.) samples retted for 0, 20, 30, and 55 days are designated as S0, S20, S30, and S55, whereas *Bauhinia vahlii* samples are designated as B0, B20, B30, and B55. These samples were kept in a sealed plastic container in the dark until they could be characterized further. Figure 14 provides a simplified outline of the experimental setup employed in this study.

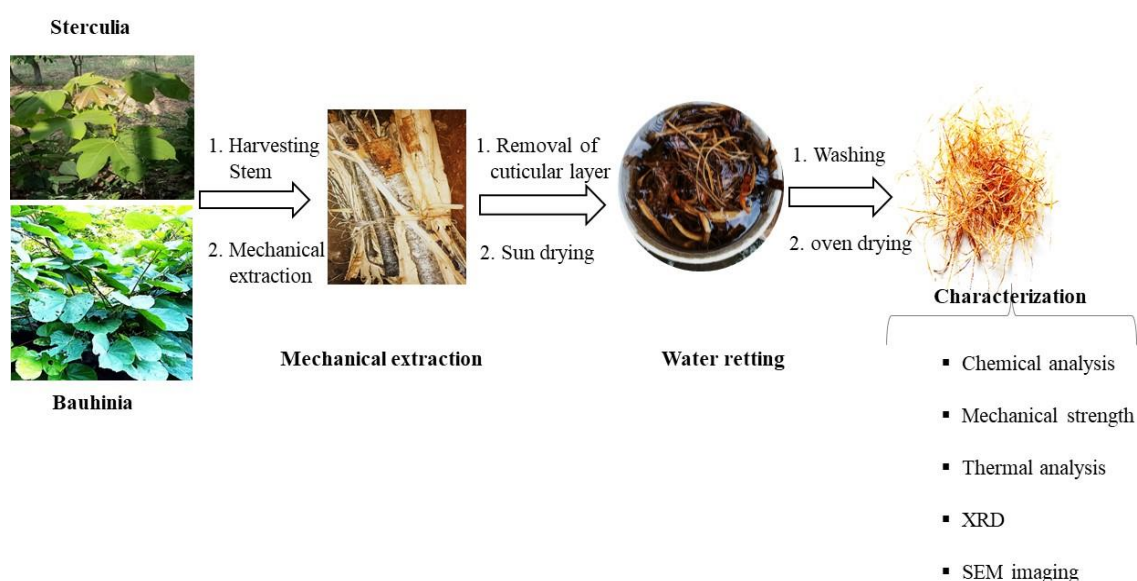


Figure 14: Schematic outline of the experimental design used in this work

2.2.3. Chemical analysis

Extractives, lignin, hemicellulose, cellulose, and ash content were gravimetrically estimated in the water-retted samples (S0, S20, S30, S55, and B0, B20, B30, and B55) using previously described methods (Boopathi *et al.*, 2012; Adeeyo *et al.*, 2015; Aryal *et al.*, 2022; Kandel *et al.*, 2022). Each chemical was measured in triplicate across all samples.

For the analysis of extractives, one gram of each sample was Soxhlet extracted for five hours in a solution of hexane and methanol (2:1), followed by five hours of boiling in water. Following this, the samples were dehydrated in a convection oven at 105 degrees Celsius till the fiber weight was uniform. Extractive matter in percent was calculated using the given starting and ending weights.

For the purpose of estimating the amount of lignin, 1.000 g of an extractive-free dry sample was treated for two hours at room temperature with 72% H₂SO₄ (1:12.5 m/v ratio). Several washes with distilled water were required to get rid of the remaining solvent at the surface. A steady weight was achieved by drying the residue at 105 degrees Celsius. Lignin content was calculated by comparing the known starting and ending weights.

1.000 g of extractive-free dry biomass was boiled for 4 hours in 150 mL of 0.5 mol/L NaOH to evaluate the hemicellulose content. Repeated washings by distilled water neutralized the treated fiber content, and then it was dried in an oven at 105 degrees Celsius till a consistent weight was achieved. The percentage of hemicellulose was calculated by comparing the biomass's starting and ending weights. The cellulose percentage was calculated by deducting the total extractive, lignin, and hemicellulose percentages from 100.

2.2.4. Mechanical strength of fiber

The samples of water-retted fibers were pre-conditioned for 24 h at 23±1 °C and 65% relative humidity (ASTM, 2004). Fiber strength in term of tenacity was measured with a fiber bundle strength tester (Stelometer, TTS India instruments, India) that could handle loads of up to 7 kg. The Pressley Jaw was used to load the tester with flat fiber bundles (gauze length 15 mm). One kilogram per second was applied continuously until

the fiber bundle split. The breaking strain of the fiber was measured. Broken fiber fragments were extracted from the Pressley Jaw and weighed with a precision of 0.0001 on an analytical balance. Known values for the breaking load, grammage, and gauge length were used to calculate breaking tenacity in g/tex. For each sample type, 25 measurements were conducted to ensure statistical significance.

2.2.5. XRD, TGA, and SEM measurements

We used an X-ray diffractometer to collect data throughout the range of 2θ , or 5-30°. (Rigaku Mini Flex600) The parameters were 40 kV, 0.02°/min, and 0.02° for the voltage, scan rate, and step size, respectively. The X-rays were generated via a monochromatic source based on the Cu-K α line ($\lambda = 1.540 \text{ \AA}$).

Fiber samples were analyzed for their thermogravimetric data using a Perkin Elmer TGA7 thermogravimetric analyzer. Using an alumina crucible and an environment of nitrogen (flow rate 80 mL/min), 7-10 mg of fiber was heated at a rate of 10°C/minute. The temperatures collected ranged from 26 to 600 degrees Celsius, and the precision and accuracy of the scales were 0.1 μg and $\pm 2 \text{ }^\circ\text{C}$, respectively.

We used a JEOL JXA-8530F field emission scanning electron microscope with an acceleration voltage of 15 kV to capture these micrographs. For further analysis, the gathered photos were processed to ImageJ (NIH, USA).

2.2.6. Statistical analysis

Origin Pro was used to compute descriptive statistics like means, medians, ranges, and confidence intervals (Origin lab, USA). When applicable, t-tests were run to conclude whether or not there was a statistically considerable difference between sets of data.

2.3. Results and discussion

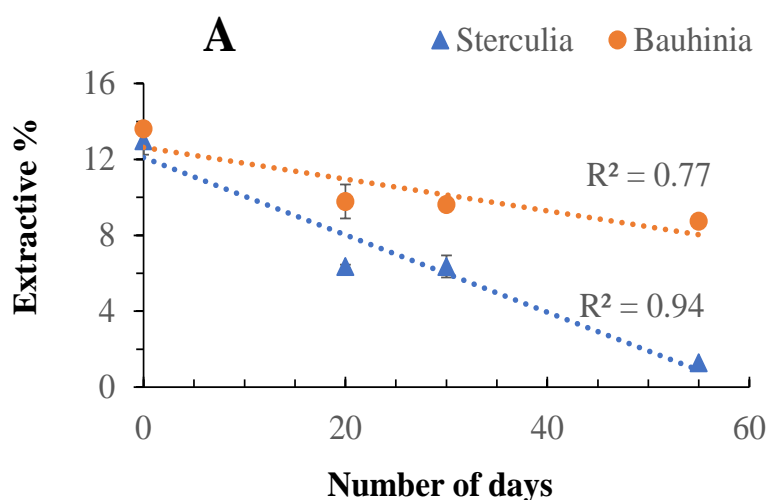
2.3.1. Gravimetric analysis

The percentage of weight lost by *Sterculia villosa* (Roxb.) fiber after being retted for 20, 30, and 55 days was 10.5, 15.2, and 17.5%, respectively. *Bauhinia vahlii* fiber had similar values of 4.1%, 5.1%, and 8.1%. According to these results, *Sterculia villosa* (Roxb.) fiber is more effective in retting than *Bauhinia vahlii* fiber. Since both kinds of fiber were subjected to identical retting settings, the variation in retting efficiency may

have resulted from inherent differences in the fibers themselves, such as their chemical make-up or their ability to bind to one another.

Figure 15 shows the extractive, lignin, hemicellulose, and cellulose contents of fiber samples from two different fiber types. Water retting led to a predictable decline in extractive content as retting duration increased (Figure 15 A). *Sterculia villosa* (Roxb.) fiber's extractive content dropped from 13% to 1.3% ($p < 0.05$) after 55 days of retting. *Bauhinia vahlii* fiber dropped by the same percentage, from 13.6% to 8.7%. Pectin and waxy components may have been removed owing to antimicrobial activity, leading to weight reduction. Lignin concentration in *Sterculia villosa* (Roxb.) decreased significantly ($p < 0.05$) from 21.9 to 15.5% during the course of 55 days (Figure 15 B). Weight loss during retting varies with the kind of microorganism used, the water composition, the duration of the retting, and the fibers used (Brindha *et al.*, 2019; Lee *et al.*, 2020). Therefore, the difference between the two kinds of fibers reported is not shocking.

There was no noticeable difference in the hemicellulose percentage of the two sample types (Figure 15 C). During the retting process, the hemicellulose content of the *Sterculia villosa* (Roxb.) fiber increased from 28.6% to 33.2%. *Bauhinia vahlii* fiber went risen from 31.2% to 33.6% throughout this time. The cellulose content of *Sterculia villosa* (Roxb.) fiber considerably increased during the same time period (Figure 15 D), rising from 36.5% to 50% ($p < 0.05$). In *Bauhinia vahlii* fiber, a minimal shift from 27 to 30% was seen.



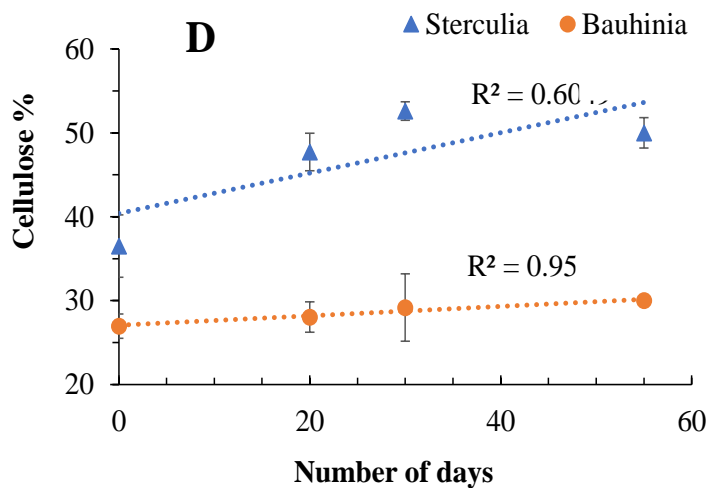
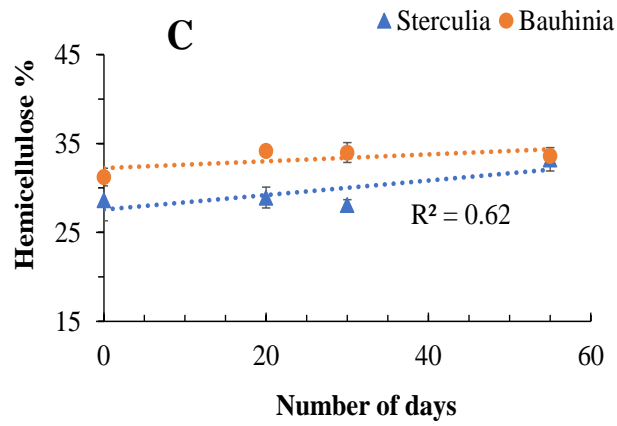
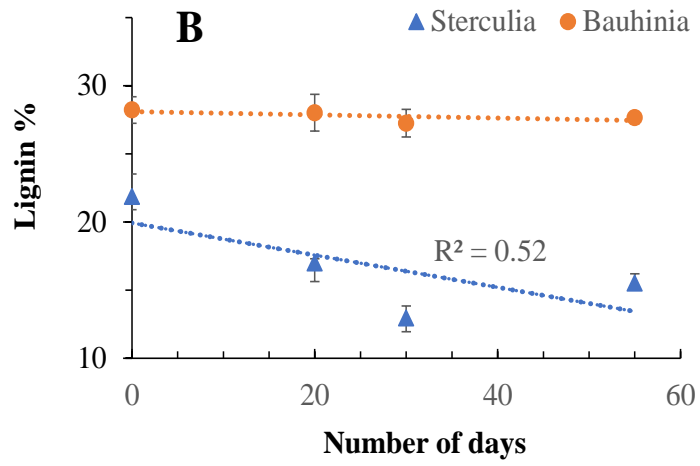


Figure 15: Analysis of major chemical components in the fiber samples. (A) Extractive. (B) Lignin. (C) Hemicellulose. (D) Cellulose. The blue and red data points correspond to *Sterculia villosa* (Roxb.) and *Bauhinia vahlii*; respectively. The dotted lines are the linear fit to the experimental data and R^2 values greater than 0.5 are only shown

For comparison, we also determined the ash concentration in fibers that had been retted for 0 and 55 days. *Sterculia villosa* (Roxb.) and *Bauhinia vahlii* were at 6.7 and 4.7% and 6.2 and 4.4%, respectively. There may have been some loss of inorganic minerals and other compounds during water retting, which would explain the lower ash level. The percentage change in ash content has significantly negative correlation to the extractive content ($r = -0.9$), as was to be predicted.

2.3.2. Mechanical strength

Tenacity values for all experimental specimens are shown in Figure 16. The breaking tenacity of *Sterculia villosa* (Roxb.) fiber went up ($p < 0.05$) during the course of 55 days, from 18.3 ± 1.6 (mean 95% CI) to 26.9 ± 2.7 g/tex ($R^2 = 0.73$). Throughout the same time setting, there was no significant change in the mechanical strength of *Bauhinia vahlii* fiber ($p > 0.05$). Increases in cellulose content (figure 16) and crystallinity may account for *Sterculia villosa*'s improved fiber strength (later section).

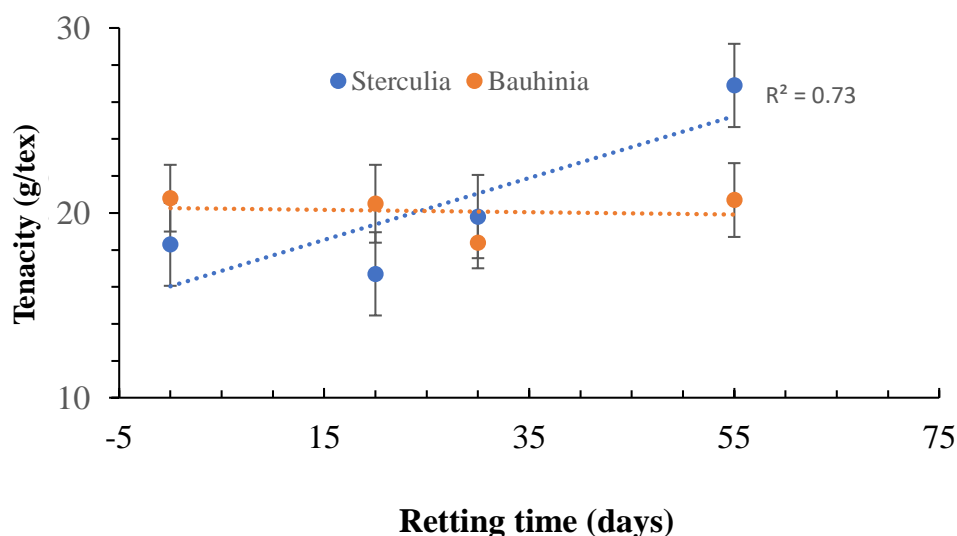


Figure 16: Mechanical strength of the fiber samples. The dotted lines are the linear fit to the experimental data points. The error bars are the 95% CI values to the mean ($n=25$)

2.3.3. XRD data

Selected *Sterculia villosa* (Roxb.) as well as *Bauhinia vahlii* samples were analyzed for XRD data (Figures 17 A and B). All of the samples have XRD patterns that are consistent with those of common cellulose. In its native state, cellulose fiber has both amorphous and crystalline components. The crystalline planes (1-10) and (110) give rise to the broad peak at a 2θ value of $\sim 15.5^\circ$, while the (200) plane is responsible for

the sharp peak at a 2θ value of $\sim 21.5^\circ$. The large contribution beneath the crystalline peaks is known to result from amorphous scattering (Yao *et al.*, 2020). The crystallinity index (CI) was determined applying the deconvolution technique in the 2θ range of $5\text{--}30^\circ$ (Park *et al.*, 2010b).

$$CI = \left(\frac{A_t - A_{am}}{A_t} \right) \times 100 \quad \dots\dots\dots\text{Eq. 1}$$

Where A_{am} is the integrated intensity of the amorphous phase and A_t is the sum of the intensities of the crystalline and amorphous phases. For crystalline and non-crystalline or amorphous contributions, respectively, Gaussian and Voigt profiles were utilized (French, 2020; Yao *et al.*, 2020). A two-point background correction was performed prior to deconvolution in order to eliminate the instrumental background. This adjustment ensures that the intensity is zero (2θ at 5° and 40°) away from the position of the crystalline peak (Yao *et al.*, 2020). The crystallinity index of *Sterculia villosa* (Roxb.) samples retted for 0, 30, and 55 days was determined to be 44%, 48%, and 50%, respectively. Crystallinity and strength were shown to have a strong positive connection ($r=+0.85$). Hemp fibers have been shown to rise in crystallinity index after being retted in water (Mazian *et al.*, 2018). When lignin is removed from the interfibrillar area, cellulose chains are more likely to pack closely together, which increases the crystallinity index (Kandel *et al.*, 2022).

Samples of *Bauhinia vahlii* retted for 0 days, 30 days, and 55 days had a crystallinity index of 55%, 54%, and 54%, respectively. The relationship between the crystallinity shifts and the strength was weakly positive ($r=+0.5$). This may be attributable to a decrease in lignin from the interfibrillar area, which is consistent with the findings presented in Figure 15 B.

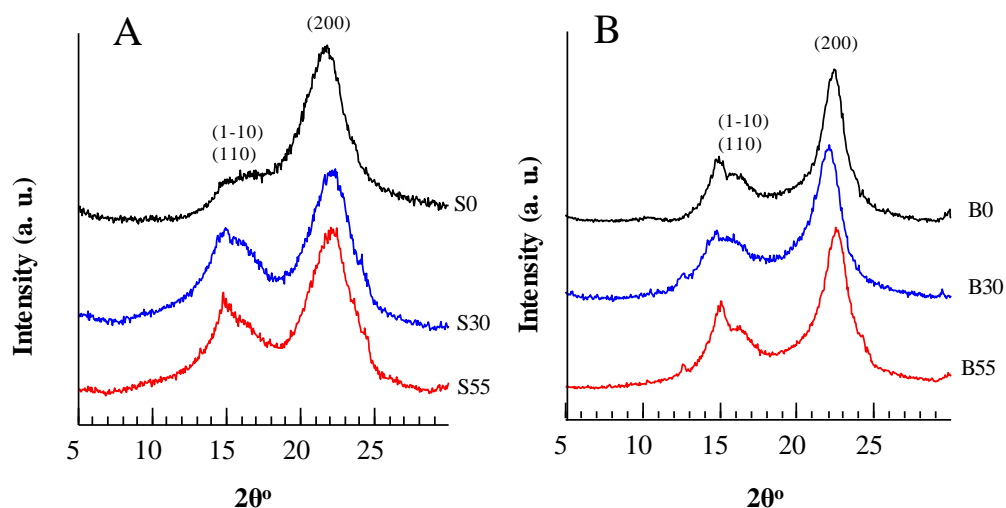


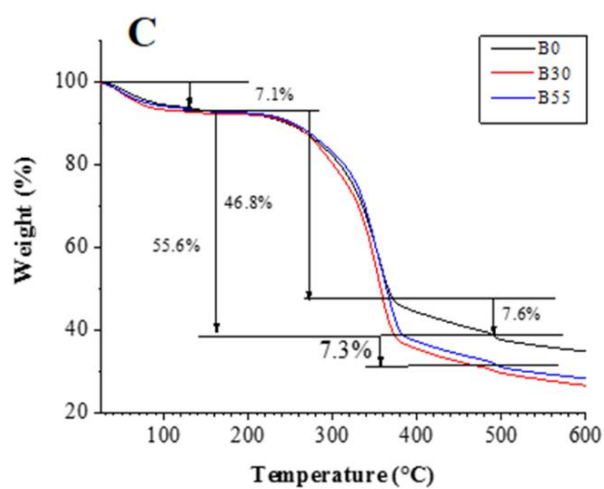
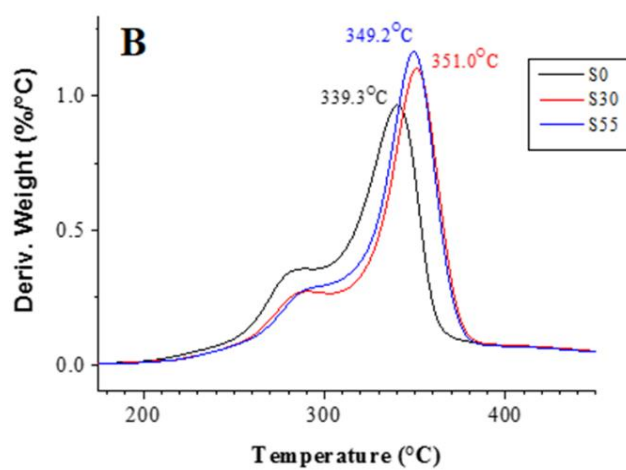
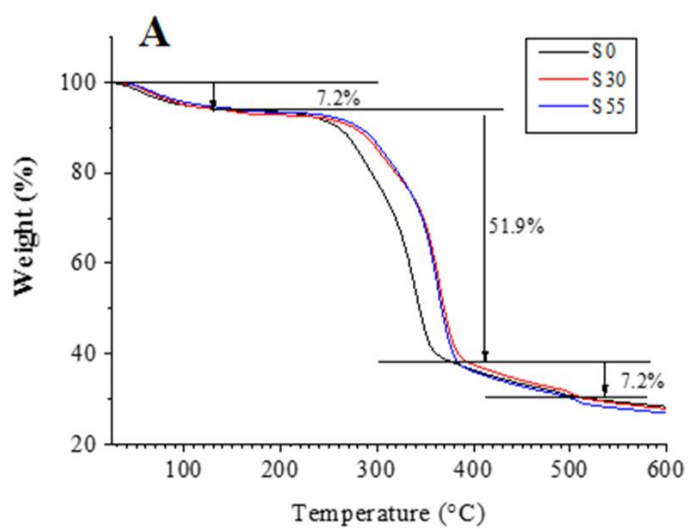
Figure 17: XRD data for the fiber samples. (A) XRD data of *Sterculia villosa* (Roxb.) samples retted for 0 (S0), 30 (S30) and 55 (S55) days. (B) XRD data of *Bauhinia vahlii* samples retted for 0 (B0), 30 (B30) and 55 (B55) days. Data are overlaid vertically for easy comparison. Numbers in parenthesis indicate the reflection planes

2.3.4. Thermal properties

Weight loss around 100°C in both samples (Figure 18 A and C) can be credited to the vaporization of water and/or the emission of low-volatile impurities (Meireles *et al.*, 2010; Poletto *et al.*, 2012; Poletto *et al.*, 2014; Kandel *et al.*, 2022). Hemicellulose is responsible for most of the mass loss between 100 and 300 degrees Celsius because it is less stable than cellulose (Figures 18A and C). Degradation of glycosidic bonding in cellulose results in the formation of organic compounds such as alkenes and other end product of hydrocarbons, which account for most of the weight loss in the 300–400°C temperature range. Lignin (Figure 5A and C) is responsible for the bulk of the mass loss beyond 400°C (Yang, Haiping *et al.*, 2006; Spinace *et al.*, 2009; Elanthikkal *et al.*, 2010).

In water-retted samples, the major DTG peak for *Sterculia villosa* (Roxb.) moves up from 340°C to 350°C. This indicated that thermal stability is improved after water retting (Figure 18 B). As has been noted previously, this may be attributable to a shift in crystalline structure and an increment in cellulose concentration. *Sterculia villosa* (Roxb.) samples (S30 and S55) that were subjected to water retting show a prominent DTG cellulose peak, which is consistent with an increase in cellulose on water retting (figure 18 D). There is a temperature increase of 5°C from the DTG peak at 350°C to 355°C in water-retted samples of *Bauhinia vahlii* (Figure 18 C). This showed that the

thermal stability of water-retted *Bauhinia vahlii* did not vary considerably with water-retting.



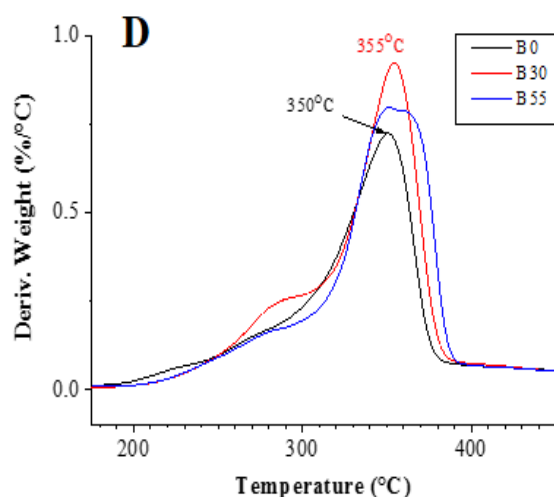


Figure 18: TGA and DTG data for the fiber samples. (A), (B) TGA and DTG for *Sterculia villosa* (Roxb.) water retted for 0 (S0), 30 (S30), and 55 (S55) days. (C), (D) TGA and DTG for *Bauhinia vahlii* water retted for 0 (B0), 30 (B30), and 55 (B55) days

2.3.5. SEM imaging

The surface appearances of the fibers were analyzed by imaging six of the eight samples. Image analysis of *Sterculia villosa* (Roxb.) fibers retted for 0, 30, and 55 days (Figures 19 A, B, and C) demonstrates that sticky constituents were eliminated from the fiber exterior, and fiber bundles are partly separated. The wet loss analysis confirms this finding. The fiber of the *Bauhinia vahlii* plant also undergoes an alike modification (Figures 19 D, E, and F).

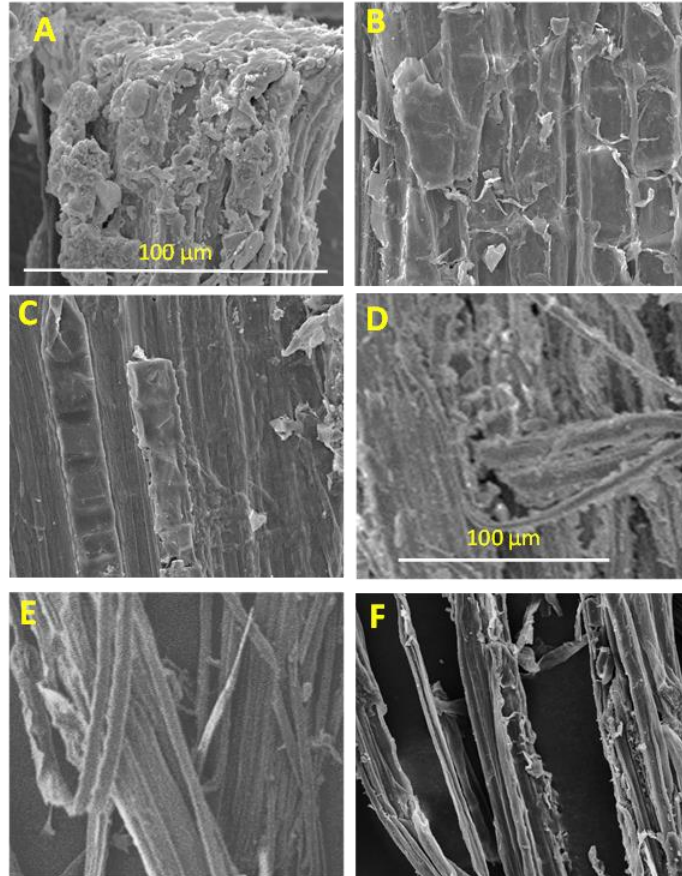


Figure 19: SEM images. A, B, and C are the images of *Sterculia villosa* (Roxb.) fiber retted for 0 (S0), 30 (S30), and 55 (S55) days; respectively. D, E, and F are the corresponding images for *Bauhinia vahlii* fiber. Scale bar of 100 μm are provided in A (also applicable for B and C) and D (also applicable for E and F)

2.4. Conclusions

In conclusion, the lignocellulosic content and water retting efficiency of *Sterculia villosa* and *Bauhinia vahlii* fiber was evaluated after being retted for varying durations of duration. Significant weight loss occurred after retting of *Sterculia villosa* (Roxb.) fiber, which is consistent with the expected decrease in lignin, ash, and extractive contents. *Bauhinia vahlii* fiber showed a smaller percentage increase, indicating less effective retting. *Sterculia villosa* (Roxb.) fiber's mechanical strength significantly improved during the course of the retting period of around 2 months, but *Bauhinia vahlii* fiber's strength remained consistent. After being retted in water, both fibers showed improved thermal stability. XRD and SEM imaging results further confirm these findings. These results suggested that both fibers have exceptional water stability and can be investigated as a key component in the fabrication of cellulose-based composite materials designed for high precipitation or humid conditions.

CHAPTER 3

3. COMPARATIVE STUDY ON MATERIAL PROPERTIES OF WOOD-ASH ALKALI AND COMMERCIAL ALKALI-TREATED *Sterculia villosa* (ROXB.) FIBER

3.1. Introduction

Fiber made from lignocellulose plants is a crucial component of the paper, pulp, and cardboard manufacturing processes. After undergoing chemical and/or mechanical processing, the fiber can be extracted from a variety of plant parts, including bark, leaf, root, and others (Reddy and Yang, 2007; Bajpai, 2018b; Tanpichai *et al.*, 2019a). Hemp, sisal, coir, kenaf, and jute are all examples of lignocellulose fibers that may be processed into materials with low density, high specific strength, and minimal environmental impact. In composites, these fibers are being researched as a possible replacement for traditional materials like glass and plastic. There are various uses for composite materials reinforced with natural fibers due to their many benefits, including those in the automotive and agricultural sectors, as well as in waste water treatment and structural engineering (Manimaran *et al.*, 2020; Vigneshwaran *et al.*, 2020).

Cellulose, hemicellulose, lignin, and extractives are the primary chemical components of raw cellulose fiber. A variety of chemical and mechanical processes must be applied to raw fiber before it can be used in a particular application (Bajpai, 2018b). To prepare fiber biomass for chemical treatment, it is often boiled in either a) a mixture of sodium hydroxide and sodium sulfide (Kraft pulping) or b) an alkali or mixture of alkalis or c) a mixture of sulfurous acid and bisulfite ion (sulfite pulping). Pulping reduces the effective width of fiber bundles and partially or completely separates the bundles by removing non-cellulosic fixing constituents' lignin and hemicellulose and additional residues to varying degrees depending on the fiber-treatment parameters. During the pulping process, changes are made to the fiber's shape, crystallinity, specific strength, and thermal stability (Saha *et al.*, 2010; Liu *et al.*, 2013; Chandrasekar *et al.*, 2017). Approximately 75% of overall pulp output and 91% of chemical pulping worldwide is kraft pulping, which is intended to regenerate energy and cooking chemicals (Bajpai, 2015). Commercial alkali or a combination of alkalis is typically used in the processing of fiber in small-scale or handmade paper companies (Hubbe and Bowden, 2009; Mejouyo *et al.*, 2020; Sannapapamma *et al.*, 2020; Chauhan and Meena, 2021).

The contamination of water, land, and air is intensified by the waste produced by the paper, pulp, and cardboard industries (Chakraborty *et al.*, 2019; Gaur *et al.*, 2020; Sharma and Singh, 2021). For this reason, today's paper and pulp mills are more equipped than ever to retrieve chemicals, renovate waste biomass into additional energy-value products, or adapt the waste biomass for longer to stimulate more beneficial microbes (Chakraborty *et al.*, 2019). The manufacturing cost and worldwide alkali consumption may be lowered with the help of any cheap and environmentally-beneficial option that can be employed in fiber processing and waste reprocessing.

In this investigation, an alkali derived from wood ash was used to treat raw *Sterculia villosa* (Roxb.) fiber. Wood ash alkali-treated fiber was evaluated with both unprocessed and commercially available alkali-treated fiber in terms of its net weight reduction, fiber width, and surface morphology. Mechanical strength, heat resistance, and crystallinity of the cellulose fiber generated from both processes were also evaluated thoroughly. Further consequences of the findings are likewise discussed.

3.2. Materials and methods

3.2.1. Fiber treatment with commercial alkali

Raw *Sterculia villosa* (Roxb.) bark had its scaly outer part. It was peeled off by a knife and then dried in the air. To prepare the biomass, it was first refluxed at 80 degrees Celsius in a combination of hexane and methanol (2:1 v/v) for five hours. Secondly, it was heated at boiling temperature in distilled water for four hours. After being washed and dehydrated, extractive-free fiber was submerged in a 5% NaOH solution, with a mass-to-volume proportion maintained at 1:50. For 4 hours, the temperature of the solution was held at 80 ± 2 degrees Celsius. The contents were then cooled to room temperature, neutralized with a solution of 5% acetic acid, and rinsed many times with distilled water after treatment. For three hours, the biomass was treated with a 2% H₂O₂ solution (1:30 w/v) in a Na₂CO₃ and NaHCO₃ buffer at pH 9. Multiple washes by means of distilled water and drying at $100\pm 5^\circ\text{C}$ were used to bring the fiber's weight stable. The percentage of fiber loss was determined from the starting and ending fiber weights. Hereafter, we will refer to this type of sample preparation as a NaOH-treated sample.

3.2.2. Wood ash alkali extraction and fiber treatment

Wood ash was prepared by flaming dry wood and branches from a *Dalbergia sissoo* (locally known as Sissau) tree in a locally constructed oven at temperatures of about 600 °C. It was determined that the ash yield was around 7%. The ashes were filtered via 500 µm sieves. For this experiment, 40 grams of sieved and dry ash were mixed with 1 L of distilled water, the mixture was agitated for 2 hours and then left to decant for about 30 minutes. As a result of filtering the supernatant through a Whatman 40 filter paper, an ash solution was obtained (hereafter named wood ash alkali; WAA). It was determined that the pH of WAA solution is 11.50 ± 0.1 . Alkalinity was measured to be $3 \times 10^{-3} \text{M}$ (0.02% w/v) using titration and pH meters. It was considered for the calculations that the alkalinity came from $\text{Ca}(\text{OH})_2$, and this is supported by the data presented in the discussion and findings. The results showed that the alkali production was 0.2% w/w (dry ash basis).

The alkali derived from wood ash was then applied to extractive-free *Sterculia villosa* (Roxb.) fiber. The treatment protocol followed the similar steps as described for the NaOH treatment technique in section 3.2.1. Once again, the percentage of weight reduction was determined by comparing the starting and ending weights. For the rest of this article, we will refer to samples processed in this manner as WAA-treated samples. Figure 20 presents a basic schematic diagram of the fiber processing technique.

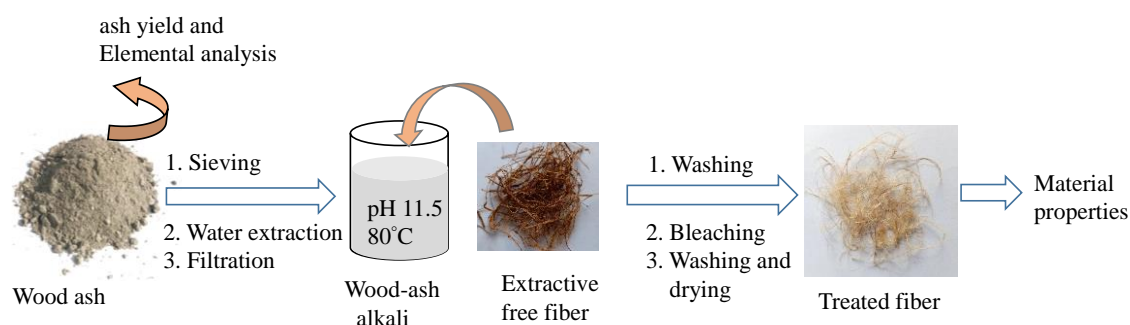


Figure 20: A simple schematic of WAA treatment method. Major steps followed in the treatment method are also indicated

3.2.3. Estimation of cellulose, hemicellulose, and lignin

Utilizing the methods outlined in the literature, the percentages of cellulose, hemicellulose, and lignin in an extractive release fiber and untreated *Sterculia villosa*

(Roxb.) fiber sample were calculated using a gravimetric technique (Boopathi *et al.*, 2012; Das *et al.*, 2014; Adeeyo *et al.*, 2015). The amount of cellulose in 1.00 g of dry fiber was determined by treating the fiber with 5% NaOH (w/v) at a ratio of 1:30 for 5 hours at 80 degrees Celsius. After cooling, the contents were neutralized with 10% sulfuric acid. Vacuum filtration was performed on the leftover biomass using a Buchner funnel and Whatman 40 filter paper. A 2% H₂O₂ solution (fiber biomass to H₂O₂ mass volume ratio 1:30) in a Na₂CO₃ and NaHCO₃ buffer at pH 9 was then used to treat the biomass for 5 hours at room temperature. For 5 hours, while the fiber was thoroughly bleached, the contents were agitated using a magnetic stirrer. Multiple cycles of washing and drying were performed on the biomass until a stable weight was achieved. Cellulose content was calculated as a percentage of the difference between the starting and ending biomass weights.

Hemicellulose was measured by adding 1.000 grams of dry, untreated fiber (without any extractives) to a solution of 2.5% NaOH while maintaining the mass volume ratio constant at 1:50. The contents went through a 4-hour boil. After multiple washes in distilled water, the contents were neutralized, filtered, and dehydrated at 105°C until a consistent weight was achieved. Hemicellulose concentration (in percent) was calculated as differences from the starting and ending dry weights.

Extractive-free, untreated fiber (1.000 g) was mixed with 72% H₂SO₄ at a weight-to-volume ratio of 1:12.5 in order to measure lignin content. After 2 hours of constant stirring and many washes, the supernatant was discarded. The leftovers were dehydrated at 105 degrees Celsius until they reached a steady weight. Lignin concentration was determined by comparing the total amount of fiber to the total amount of dry residue.

Cellulose, hemicellulose along with lignin were estimated in WAA likewise NaOH treated samples for comparison.

3.2.4. Measurement of fiber width

Digital bright field microscopy was used to take pictures of the fiber specimen (AmScope, 5-250X, USA). A high-precision linear calibration grid with a 10 µm lowest grid size was used to calibrate the field of view. In an open-source image analysis program, fiber width was determined from the known size of pixels in micrometers (ImageJ, NIH, USA).

3.2.5. FTIR, XRD, DTA, and SEM measurements

The IR spectra were obtained with a Fourier transform infrared spectrometer in ATR mode with a resolution of 4 cm^{-1} in the $4000\text{-}400\text{ cm}^{-1}$ range (ABB Bomen, MB100, Canada). All fiber samples were pre-conditioned for 12 hours at $23\pm 1^\circ\text{C}$ and 60% RH prior to analysis. All spectra were given as the mean of thirty optical scans to ensure a high signal-to-noise ratio.

The Rigaku MiniFlex600 X-ray diffractometer was used to collect data in the 2θ range of $5\text{-}50^\circ$ at a scan rate of $0.02^\circ/\text{min}$ and a step size of 0.02° . The measurement was performed using a monochromatic X-ray source derived from the $\text{CuK}\alpha$ line ($\lambda=1.540\text{\AA}$).

To perform a thermogravimetric analysis (TGA), 7–10 mg of the sample was heated in an alumina crucible (Perkin Elmer, TGA-7) between 26 and 600°C at a constant rate of $10^\circ\text{C}/\text{minute}$ with nitrogen flow of $80\text{ mL}/\text{min}$. The accuracy of the balance was $0.1\text{ }\mu\text{g}$, while the precision of the thermometer was $\pm 2^\circ\text{C}$.

The samples were investigated by scanning electron microscopy using an X-ray energy-dispersive spectrometer (EDS) attached to a JEOL JXA-8530F field-emission electron probe microanalyzer (EPMA). The accelerating voltage was set to 15 kV. Magnifications of 50-5000X were used to get SEM pictures of each sample. Image analysis was carried out using ImageJ (ImageJ, NIH, USA) in order to get information on the morphology of the fiber surface.

3.2.6. Mechanical strength of fiber

After 24 hours of preconditioning at $23\pm 1^\circ\text{C}$ and 65% RH, both the untreated and alkali-treated fiber samples passed the ASTM test (ASTM, 2004). An equipment from TTS Instruments, India with a maximum load capacity of 7 kg was used to evaluate the fiber's strength. Flat fiber bundles were enclosed in the Pressley Jaw having gauze length 15 mm and the whole component was loaded into the tester for measurement. The fiber was subjected to a steady stress of 1 kg/sec till fracture. Both the load at which the fiber broke and the percentage of elongation were recorded. Pressley Jaw's fragmented fiber was taken out and put on an analytical analyzer (accuracy of 0.0001). The breaking load, grammage, and fiber bundle length (1.5 cm) were used to figure out the fiber bundle strength (breaking tenacity) in g/tex and the tensile strength. To ensure statistical significance, 75 measurements were taken from each sample type.

3.2.7. Statistical analysis

Normal statistical measures, such as mean, standard deviation, and confidence interval, were calculated from the obtained data using a Microsoft Excel spreadsheet. When necessary, paired t-tests were run in OriginPro (OriginLab Corporation, USA) to compare the two datasets.

3.3. Results and discussion

3.3.1. Weight loss, chemical characterization, and fiber width

Unprocessed, dry fiber had $55.6\pm 2.4\%$ cellulose, $28.2\pm 1.7\%$ hemicellulose, and $19.7\pm 2.5\%$ lignin (all percentages are weight-per-weight). The study was performed on extractive-free and dry biomass, therefore the sum of the weights of the three components is equal to 100%. Treatment with 5% NaOH (w/v) at an increased temperature, followed by chlorine-free bleaching, is a typical chemical processing procedure for lignocellulose fiber in both laboratories and factories. NaOH-treated fiber has similar qualities to WAA-treated fiber; therefore, it makes sense to compare the two. It was determined that following NaOH and WAA treatment, the biomass lost a net of $41.33\pm 3.3\%$ and 29.1 ± 2.6 grams, respectively (Table 1). The elimination of hemicellulose and lignin following alkali treatment is the primary contributor to weight reduction in both approaches. To get rid of any residual lignin or pigments in the fiber, an alkaline H_2O_2 bleaching process is performed. Perhaps some little weight reduction might result from this. The brightness of the fibers was significantly improved after bleaching, as predicted (Figure 20).

Other than the amount of alkali used, all of the other treatment parameters were the same across the two approaches. This is because the WAA treatment has a lower alkalinity content, which accounts for less weight loss. Scientific investigations have shown that the amount of weight reduced varies with the type of alkaline solution used and other treatment variables including concentration, duration, and temperature (Saha *et al.*, 2010; Hashim *et al.*, 2017). Consistent with the findings of the weight reduction investigation, cellulose content was raised while hemicellulose and lignin content decreased in both approaches (Table 1).

Table 1: Chemical characterization of fiber samples

Sample type	weight loss	Cellulose	hemicellulose	Lignin
Untreated	0	55.6±2.4	28.2±1.7	19.7±2.5
WAA treated	29.1±2.6	72.0±1.9	18.2±1.2	9.9±1.4
NaOH treated	41.3±3.3%	82.1±1.3	12.5±1.7	8.4±1.1

The effect of the alkalization on the fibers was then investigated by measuring the fiber diameter in each of the samples. Untreated, WAA-treated, and NaOH-treated samples were found to have an average fiber bundle width ($n = 275$) of 446.0 ± 40.2 , 227.0 ± 25.0 , and 227.9 ± 20.0 m, respectively, at 95% CI. We used a fiber bundle for the calculation of fiber strength in spite of a single fiber. Fiber bundle does not ensure their circular nature. Due to this, the diameter could no more be realistic than the fiber width. Fiber width is measured with the help of microscopy and ImageJ. In agreement with the findings shown in Table 1, the loss of lignin, hemicellulose, and other components from the fiber causes a decline in fiber diameter in alkali-treated samples. Thinner fibers are described after the alkali treatment of various plant fibers (Beckermann and Pickering, 2008; Han *et al.*, 2009; Hashim *et al.*, 2017).

3.3.2. SEM, SEM-EDX, and XRD

SEM, SEM-EDX, and XRD data were collected to determine the elemental content of wood ash. Calcium (22.3%), carbon (23%), oxygen (50.5%), aluminum (1%), iron (1.4%), and silicon (1.8%) were identified in the EDX data (Figure 21 and Table 2).

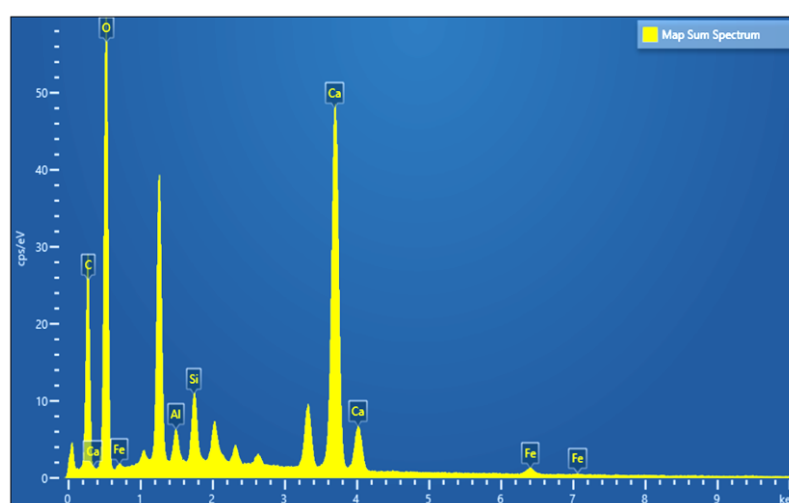
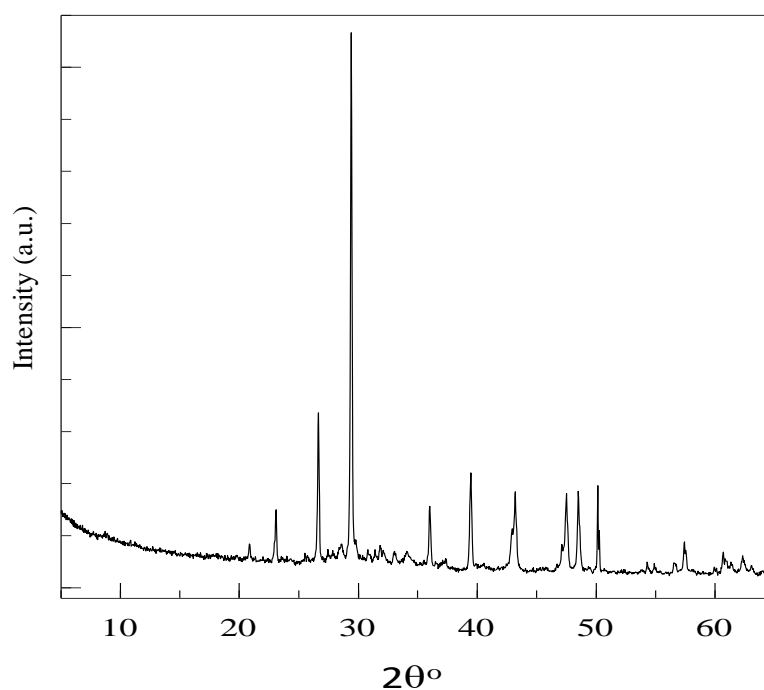


Figure 21: SEM-EDX spectrum of the ash powder

Table 2: Elemental composition of ash

Element	Line Type	Apparent Concentration	k Ratio	Wt%	Wt% Sigma
C	K series	5.80	0.05805	22.96	0.19
O	K series	23.24	0.07821	50.43	0.19
Al	K series	0.92	0.00658	1.07	0.03
Si	K series	1.67	0.01323	1.83	0.03
Ca	K series	20.93	0.18702	22.33	0.11
Fe	K series	1.05	0.01055	1.38	0.07
Total:				100.00	

**Figure 22:** XRD profile of the ash powder

3.3.2.1. FTIR study

The results of the FTIR measurements taken on each sample are presented in figure 23. The bands' spectra were categorized based on information found in the literature. The O-H stretching of hydrogen-bonded systems in cellulose and hemicellulose are responsible for the broad peak between 3000 and 3600 cm^{-1} (Sinha and Rout, 2008; Saha *et al.*, 2010). The hydrogen link between the O-H groups of hemicellulose and the cellulose molecules is broken after alkali treatment, resulting in a decrease in band intensity and width. An acetyl or ester C=O group of (unconjugated) hemicellulose or

lignin is responsible for the 1730 cm^{-1} peak, while the C=O stretching of conjugated lignin is responsible for the 1620 cm^{-1} peak (Haque *et al.*, 2009; Tanpichai *et al.*, 2019a). These peaks weaken after the application of alkali, demonstrating that hemicellulose and lignin have been removed. Alkali treatment also results in a distinctive peak at 1250 cm^{-1} , which matches the C—O stretching of acetyl groups in cellulose and hemicellulose (Sinha, E. and Rout, S., 2008). This also points to the elimination of hemicellulose. These findings are consistent with the results on weight loss given in Table 1.

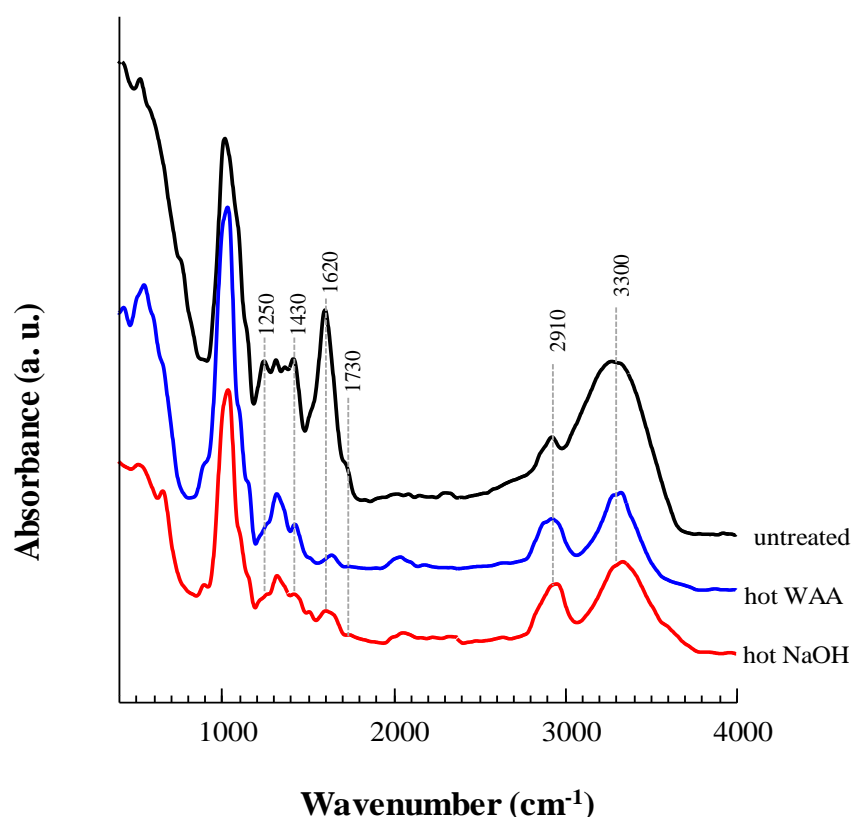


Figure 23: FTIR spectra of untreated and NaOH and WAA-treated fibers. For easy comparison, the spectra as flipped to show absorption bands and overlaid vertically

The CH_2 bending of cellulose is shown by a peak at 1430 cm^{-1} , which weakens significantly in the NaOH-treated sample while being unaffected in the WAA-treated sample. These portions of cellulose that were untouched by the alkali treatment could provide assistance in maintaining the fiber's mechanical strength (Sui *et al.*, 2009; Saha *et al.*, 2010).

3.3.2.2. SEM imaging

SEM imaging shows the cementing components like lignin and hemicellulose, as well as residual wax, pectin, inorganic impurities, and other similar elements, deposited on the surface of untreated fiber (Figure 24 A). After being subjected to alkali, the bulk of the surface materials disappears (Figures 24 B and C). As a result of the elimination of cementing ingredients, fiber bundles are also partially detached. These results agree with past reports of a decrease in weight, narrowing of fibers, and reduction of lignin and hemicellulose characteristic peaks in FTIR data. Since the cementing materials were removed from the inter-fibrillar zone, partial fibrillation was also seen in the alkali-treated samples (Figures 24 B and C). Images of samples treated with alkali also show the formation of micro fractures throughout the fiber's length.

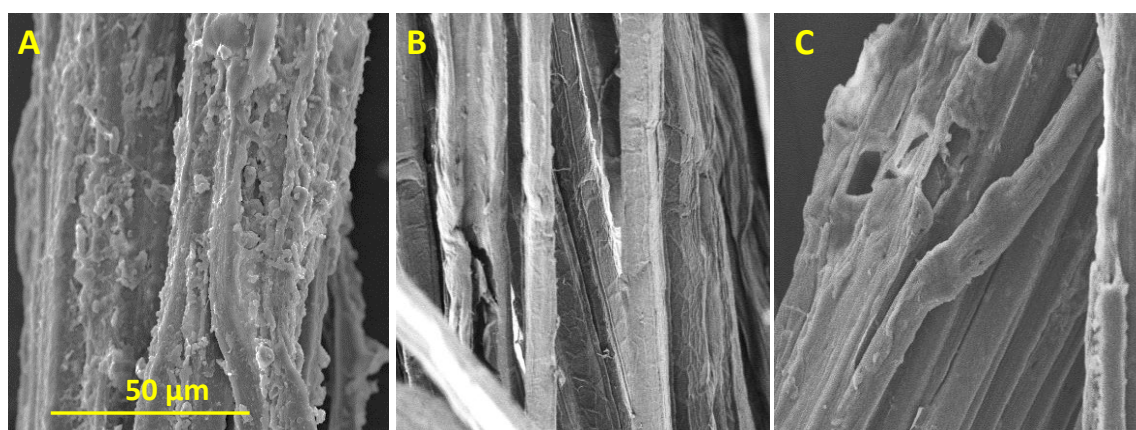


Figure 24: SEM images of A) untreated, B) WAA-treated, and C) NaOH-treated fibers. A scale bar of 50 μm shown in figure A also applies to B and C

3.3.2.3. XRD analysis

The XRD patterns of all the samples are displayed in Figure 25. The planes of crystalline cellulose phase I, (1-10) and (110), (200), and (004); respectively, are where the diffraction peaks at 2θ angles of 15.5° , 21.5° , and 35° originated. Amorphous scattering provides a significant contribution beneath the crystalline peaks (Park *et al.*, 2010b). Information on crystallinity index (CI) was obtained using a six-component peak deconvolution in the 2θ range of $5\text{-}40^\circ$ (inset in Figure 25) (Park *et al.*, 2010b; Yao *et al.*, 2020). Equation 3.1 was utilized to determine CI.

$$CI = \left(\frac{A_t - A_{am}}{A_t} \right) \times 100 \quad \dots\dots\dots\text{Eq. 3.1}$$

Where A_t and A_{am} , respectively, represent the integrated intensities of the crystalline and non-crystalline phases as well as the non-crystalline phases alone. For crystalline and non-crystalline or amorphous contributions, Gaussian and Voigt profiles were utilized (French, 2020; Yao *et al.*, 2020). To remove the instrumental background before to deconvolution, a two-point background correction was performed. This adjustment makes sure that the intensity is zero (2θ at 5° and 40°) away from the crystalline peak position (Yao *et al.*, 2020). The CI was discovered to be 47%, 55%, and 58% in untreated, WAA, and NaOH treated samples, respectively (Table 2). According to various studies, the CI increase is caused by the elimination of amorphous constituents like lignin and hemicellulose, especially from the inter-fibrillar area, resulted by restructuring of cellulose chains (Park *et al.*, 2010b; Saha *et al.*, 2010; Boopathi *et al.*, 2012).

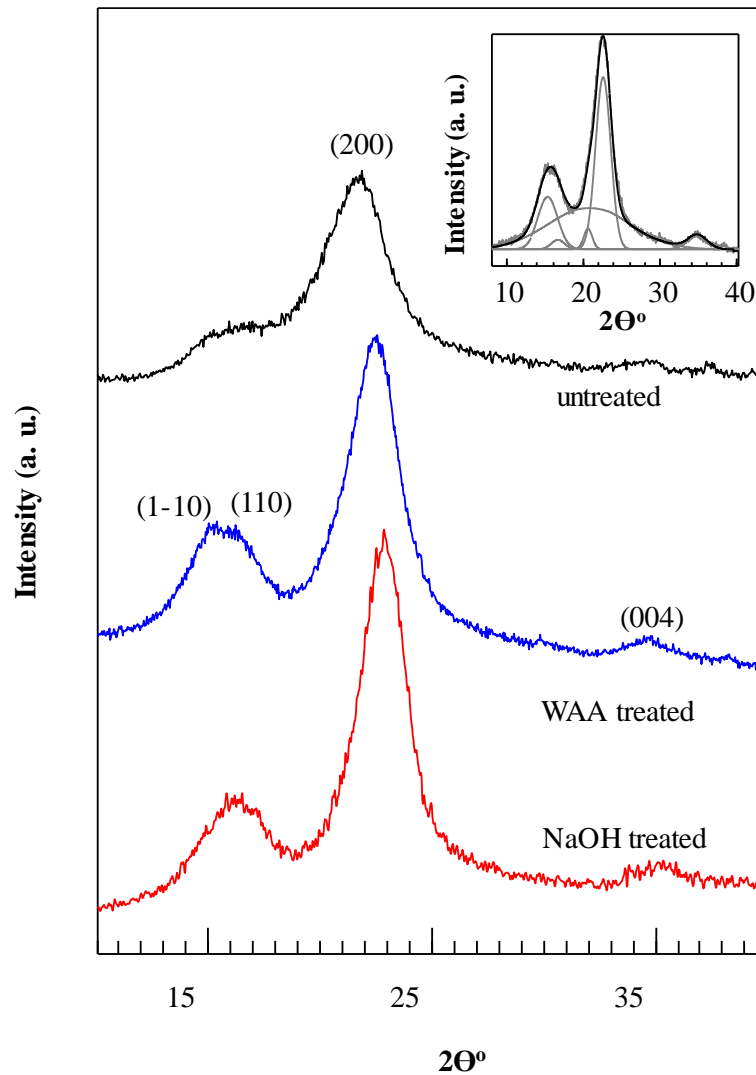


Figure 25: XRD data of untreated, WAA-treated, and NaOH-treated fibers. For easy comparison, data are overlaid vertically. The inset shows six components that fit the XRD data of WAA-treated fiber

The following equation was used in subsequent analysis of the XRD data to determine micro-strain (ϵ) in the crystallites in a direction perpendicular to the diffracting plane (Sinha and Rout, 2008; Ioelovich, 2018):

$$\epsilon = \frac{d_s - d_u}{d_u} \quad \dots\dots\dots\text{Eq. 3.2}$$

Where d_s and d_u represent the inter-planar distance of alkali-treated and untreated samples, respectively. Considering that the treated sample has a negative value of (Table 3), this indicates that there is still some compressive stress on the crystallite surface.

Table 3 also includes the crystallite size (D) determined by the Scherrer equation (Cullity 1978). Alkali treatment results in a 23 percent increase in crystallite size.

Table 3: Crystalline properties of the fiber samples

Sample type	Crystallinity index (%)	Crystallite size (nm)	d₂₀₀, nm	micro-strain
Untreated	47.0	3.0	0.406	0
WAA treated	55.0	3.7	0.394	-0.031
NaOH treated	57.8	3.7	0.388	-0.015

3.3.2.4. Thermal properties

The results obtained from the TGA and DTG are presented in figure 26 and the inset, respectively. TGA data were normalized to 100 in order to accommodate for a minor offset in weight% from 100, which was somewhere in the region of 2–2.5%. The TGA curves for all of the samples are quite comparable to those for commonly-reported lignocellulose fiber samples (Poletto *et al.*, 2014). Table 4 provides a convenient summary of the percentage of weight lost over a range of temperatures. Water molecules and/or volatile substances adsorbing to the fiber are lost at temperatures below 100°C, accounting for the first weight reduction. Changes in crystallinity and equilibrium moisture content may explain why certain substances lose a little more weight than others when heated to $T \leq 100^\circ\text{C}$. Degradation of hemicellulose causes a shoulder in DTG about 300°C (Figure 26 inset) (Poletto *et al.*, 2014). The shoulder is more prominent in the untreated sample, which may indicate a larger concentration of hemicellulose. This finding agrees with the FTIR and chemical analysis results presented previously. Due to its amorphous structure, hemicellulose de-polymerizes at lower temperatures, which reduces its thermal stability (Yang *et al.*, 2006).

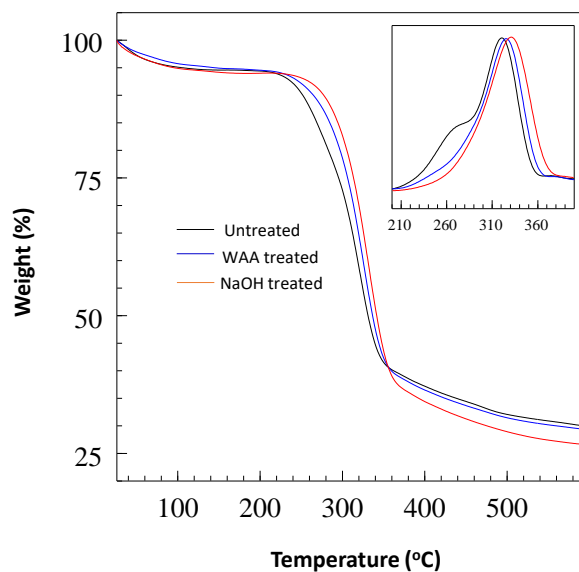


Figure 26: Thermogravimetric analysis. The main frame and inset show the TGA and DTG data of three fiber samples; respectively

It has been recommended that the temperature range of 275°C–350°C is optimal for the breaking of glycosidic linkages. Therefore, the principal DTG peak can be attributable to cellulose degradation (Yang *et al.*, 2006). Cellulose's longer polymeric units are more ordered, making it more resistant to heat than hemicellulose. It was determined that the temperatures at which cellulose degraded were 321, 326, and 332 degrees Celsius for untreated, NaOH-treated, and WAA-treated samples, respectively (Table 4). This indicated that alkali treatment improves thermal stability. An increase in crystallinity and grain size may account for the improved thermal stability of the treated sample. The broad temperature range of 200–600°C is thought to be where lignin breakdown and cleavage occur. As a result of its strong cross-linked structure and large molecular mass, lignin is more resistant to heat. The larger amount of mass that was left in the unprocessed sample could be due to inorganic impurities or to the synthesis of a stable lignin-cellulose complex (Kim, H.-S. *et al.*, 2006).

Table 4: A summary of weight loss data for the fiber samples

Sample type	ΔT , °C	Mass loss, %	Degradation temperature, °C	Residual mass at 600 °C, %
Untreated	26-100	4.9	321	29.8
	100-220	4		
	220-400	57		
	400-600	7.4		
WAA treated	26-100	4.2	326	29.4
	100-220	1.5		
	220-400	57.8		
	400-600	7.1		
NaOH treated	26-100	5.1	332	26.5
	100-220	1.2		
	220-400	59.8		
	400-600	7.9		

3.3.2.5. Mechanical strength

Table 5 lists the mechanical parameters of the fiber samples. Tensile strength values (MPa) are presented for simple comparison in Figure 27. The mean difference between untreated and WAA-treated samples in breaking tenacity and tensile strength is statistically negligible ($p > 0.01$). Untreated and NaOH-treated samples show no statistically significant difference in tensile strength or tenacity ($p > 0.01$). The average change in percentage elongation is statistically significant in all of the samples ($p < 0.01$); this indicated that alkali treatment results in a lower percentage elongation.

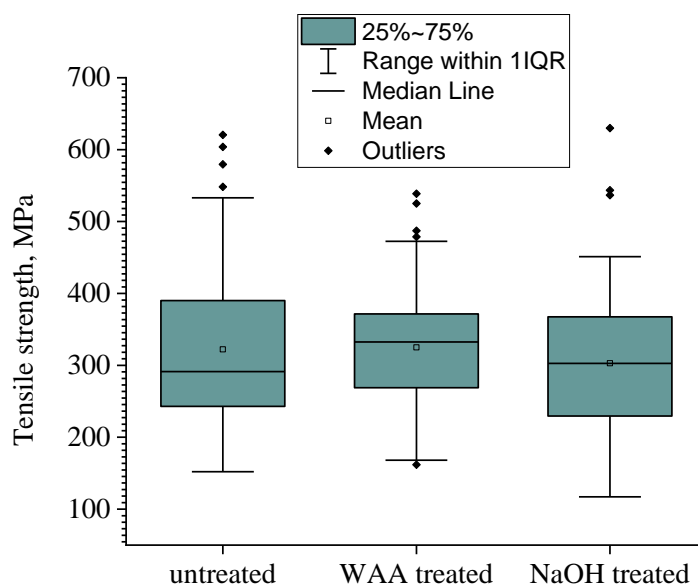


Figure 27: Tensile strength of the fiber samples. For easy comparison, range, mean, and median values along with a few outliers are shown in a box plot

According to reports, the mechanical strength of alkali-treated samples is either maintained, enhanced, or lowered, based on the conditions of the treatment (Saha *et al.*, 2010; Liu *et al.*, 2013; Chandrasekar *et al.*, 2017; Hashim *et al.*, 2017). The

Table 5: Mechanical properties of fiber samples

Sample type	Breaking tenacity (g/tex)	Tensile strength, MPa	Elongation at break, %
Untreated	22.8±7.6	319.2±105.8	4.4±1.8
WAA treated	23.1±5.6	323.5±78.5	2.0±0.8
NaOH treated	21.6±7.0	302.8±97.2	1.24±0.4

elimination of hemicellulose and lignin from the inter-fibrillar area is thought to reduce the internal restriction, allowing for more efficient structuring for microfibrils and cellulose chains. This has the potential to promote crystallinity, leading to enhanced strength. The scanning electron micrographs reveal that the fiber surface is not significantly damaged and that the lignin has been removed from the interfibrillar area (Figures 24 B and C). When fibers are damaged by alkalis and/or bleach, durability suffers. Because of these two competing effects, treated samples may preserve their strength rather than significantly improve it.

3.3.3. Further implications of the research

In this investigation, the material characteristics of *Sterculia villosa* (Roxb.) fiber treated with alkali derived from wood ash and commercial alkali were thoroughly examined. Using the fiber samples, more study may involve the manufacture of paper sheets and composite materials and the assessment of their final qualities. The alkali concentration in this experiment was low, but the solution may be concentrated by evaporating it under lower pressure. Both diluted and concentrated alkali solutions might be used to neutralize acidic left-over and valorize excess materials in the paper and pulp industries. Although we processed *Sterculia villosa* (Roxb.) fiber using a particular type of wood ash, we think that any type of wood ash waste may be processed with alkali to produce lignocellulose fiber. The health risk linked with wood ash handling is lower than that of commercial alkali. In these regards, the technology described here might be an eco-friendly approach for lignocellulose fiber processing.

3.3.4. Conclusions

To sum up, we processed lignocellulose fiber derived from *Sterculia villosa* (Roxb.) using an alkali solution that was extracted from wood ash. Several essential material parameters, given as weight loss, fiber width, fiber shape, mechanical strength, thermal stability, and crystallinity, were evaluated between wood ash alkali-treated fiber and untreated and commercially available alkali-treated fibers. We observed considerable lignin and hemicellulose removal with both WAA and NaOH treatments. Both approaches produced fibers with equivalent tensile strength and breaking tenacity. In comparison to untreated samples, the thermal stability and crystallinity of fibers produced by both techniques were enhanced. These results indicated that wood ash alkali may be utilized to treat lignocellulose fiber on a lab scale. Additionally, the technology might be applied in small-scale paper and pulp factories for the chemical processing of lignocellulose biomass.

CHAPTER 4

4. KINETICS OF WATER SORPTION IN SINGLE *Sterculia villosa* (ROXB.) AND *Bauhinia vahlii* FIBERS AT AMBIENT TEMPERATURE

4.1. Introduction

Plant-based lignocellulose fiber, such as that found in leaves, roots, and bark, is a key ingredient in many composites. In addition, they perform a vital role in the production of paper, pulp, and cardboard (Reddy and Yang, 2007; Bajpai, 2018b; Tanpichai *et al.*, 2019a). In an effort to find more sustainable alternatives to conventional composites made with plastic or glass fiber, lignocellulose fiber-reinforced composites are being researched. In addition to being lightweight (low density), high specific strength, and abrasion-resistant, these materials also have a high thermal stability. These materials have found increasing use in several fields in recent years, including agriculture and the automotive industry, medicine, architecture, and pollution control (Liu *et al.*, 2020; Vigneshwaran *et al.*, 2020; Dasore *et al.*, 2021). One of the major challenges with natural fiber-reinforced composites is their fast degradation in the presence of sunlight, humidity, dampness, and microbes. Because they are hydrophilic, natural fibers absorb more water than synthetic materials, which weakens their structural stability and durability (Joseph *et al.*, 2002; Lin *et al.*, 2002; Brebu, 2020). Composites can be exposed to a wide range of humidity and moisture conditions depending on their intended use. Thus, knowledge of the water-receiving actions of cellulosic fiber might be beneficial in understanding the effects of water absorption in composites and in minimizing water uptake.

Researchers have identified three primary pathways responsible for the water uptake in the polymer. The diffusion of water molecules within micro-gaps generated by polymeric chains is a crucial factor. Minor factors include capillary transfer and transport via microcracks or defects (Naylor, 1989; Espert *et al.*, 2004). Using diffusion as a modeling parameter, it is possible to fit the experimental kinetic data. In the case of I diffusion (pseudo-Fickian and Fickian), polymer segment mobility is substantially greater than the rate of diffusion. To a far greater extent than in the other relaxation stages, penetrant mobility is enhanced in case II. Here, a distinct boundary can be seen separating the swollen from the un-swollen portions, and this barrier shifts in a linear fashion over time. In case III (anomalous or non-Fickian diffusion), the relaxation of

polymer segments and the mobility of the penetrants are similar. Information about the dominant mode may be derived from the outline of the sorption-time curve, which is commonly expressed as: (Eq. 4.1)

$$\frac{M_t}{M_{eq}} = kt^n \quad \dots\dots\dots\text{Eq. 4.1}$$

In this equation, M_t and M_{eq} represent the moisture present at time t and the equilibrium, respectively; k and n are constants. The relationship between $\log(M_t/M_{eq})$ and $\log t$ is a straight line with a slope equal to the n factor. For pseudo Fickian diffusion, $n < 1/2$, for Fickian diffusion, $n = 1/2$, for case II, $n=1$, and for anomalous diffusion (case III), n exhibits an intermediate value ($1/2 < n < 1$) (Naylor, 1989; Espert *et al.*, 2004; Jasso-Gastinel, 2017; Sahu and Gupta, 2022). Several sources (Saikia, 2010; Nosbi *et al.*, 2011; Ronald Aseer *et al.*, 2013) describe the water sorption kinetics of natural fibers and composites made from them.

One of the quickest-growing plant species native to south Asia is *Sterculia villosa* (Roxb.), often known as Murgilo or Mudilo, while the fibers from the *Bauhinia vahlii* plant are known as Bharlo fiber. There has been relatively little research on the material characteristics of fiber derived from plant species. The kinetics of water sorption in unprocessed lignocellulose fiber extracted from plants was the primary focus of this investigation. Sorption data were also compared to those of fibers that had been treated with alkali. The mechanical strength of the alkali-treated fibers was then evaluated in both the absorbed and dehydrated states.

4.2. Materials and methods

Thermo Fisher Scientific India Pvt. Ltd. supplied all of the chemicals for the gravimetric analysis. The chemicals were utilized without any additional processing. The reagents were made in double-distilled water with a $\text{pH}=7.1\pm 0.1$ and a conductivity of $4.5\pm 0.5 \mu\text{S}$.

4.2.1. Chemical characterization

From the Gulmi area of Nepal, raw *Sterculia villosa* (Roxb.) and *Bauhinia vahlii* fiber were collected. The biomass was air-dried and the outermost scaly bark was carefully detached. Soxhlet extraction was used on 1.000 g of oven-dried raw fiber in a 2:1 mixture of hexane and methanol at 80°C for five hours to find out how much extractive

was in the fiber. The biomass was cleaned by means of distilled water and dehydrated at $105\pm 2^{\circ}\text{C}$ in an oven. The proportion of extractive content was calculated using the difference between the starting and ending weights. The sample that has not undergone any extraction processes is referred to as the (alkali) untreated sample.

Following techniques described in the literature (Boopathi *et al.*, 2012; Das *et al.*, 2014; Adeeyo *et al.*, 2015), we used gravimetric analysis to quantify the amounts of hemicellulose, lignin, cellulose, and ash present in unprocessed *Bauhinia vahlii* and *Sterculia villosa* (Roxb.) fiber biomass. 1.000 g of extractive-free samples were immersed for five hours in a 5% NaOH solution (w/v), maintaining a fiber-to-solution ratio of 1:30 (w/v), in order to estimate the amount of cellulose present. Once the contents were cool down to normal temperature, they were neutralized using a 10% H_2SO_4 (w/v) solution. The biomass was bleached in a 2% hydrogen peroxide solution for five hours after being rinsed many times in distilled water. The stuff was then repeatedly cleaned and dried in an oven. Cellulose percentage was calculated from the difference in weight between the starting and ending points. The average and standard deviation of each sample were calculated after three separate estimates were performed.

An untreated sample of 1.000 g was boiled for 4 hours in 0.5 M NaOH to determine the hemicellulose content. Before being dried in an oven at 105°C , the biomass was repeatedly rinsed with distilled water. The hemicellulose concentration was determined by comparing the starting and ending weights. The average and standard deviation of each sample were calculated after three separate estimates were performed.

To determine lignin concentration, one gram of raw biomass was soaked in 72% H_2SO_4 (sample-to-acid ratio 1:12.5 w/v) for two hours while being vigorously shaken. The content was watered down with deionized water, and the topmost layer was removed with care. The leftovers were dried in the oven at 105°C after being filtered with Whatman 40 filter paper. Lignin content was expressed as a percentage based on the difference between the starting and ending weights. The average and standard deviation of each sample were calculated after three separate estimates were performed.

1.000 g of raw fiber bio-mass was burned in a muffle furnace at $550\pm 10^{\circ}\text{C}$ for five hours to determine the approximate ash concentration. The proportion of ash was derived from the difference in weight. Each sample had its mean and standard deviation calculated using data from three replicate measurements.

4.2.2. Alkali treatment

Alkali treatment was performed on 1.000 g of untreated biomass consisting of *Sterculia villosa* (Roxb.) and *Bauhinia vahlii* fiber using a 5% NaOH (w/v) solution while maintaining a 50:1 alkali volume to fiber to mass ratio. The solution was kept at 80°C for 4 hours. Following treatment, a 5% acetic acid solution was used to neutralize the biomass, which was then systematically rinsed with distilled water. The biomass was bleached by soaking it in a carbonate-bicarbonate buffer of pH 9 containing 2% H₂O₂ solution at room temperature. After being bleached, the fiber was cleansed in distilled water and dried at temperatures around 100 degrees Celsius. The percentage of weight reduction was determined using the known starting and ending weights. The cellulose fiber after NaOH treatment is referred to in the text below as the "NaOH treated sample."

The same procedure as with NaOH was utilized with the same ratio of 1:50 of fiber mass to wood ash alkali (WAA) solution (pH11.5). The sample will be referred to as a WAA treated sample moving forward.

4.2.3. Measurement of fiber width

A digital bright field microscope was used to capture optical pictures of the fiber samples (AmScope, 5-250X, USA). A high-accuracy linear calibration grid (grid size 10 μm) was utilized to calibrate the optical field of vision. Fiber width was determined in micrometers using open-source ImageJ image analysis software by transforming picture pixels to micrometers based on the field of view (NIH, USA).

4.2.4. Sorption kinetics study

Sorption research was performed on untreated *Sterculia villosa* (Roxb.) and *Bauhinia vahlii* fiber, as well as fiber that had been treated with NaOH and WAA. The investigation was carried out in accordance with the ASTM D 570-98 standard, with some minor adjustments. A sample of fiber with a known weight was immersed in distilled water kept at 27±2°C. The water was cleansed with a lint-free paper after the fiber was removed from it at various times, and the water was then immediately weighed in an analytical scale (accuracy of 0.001g). The percentage increase in weight was determined by comparing the before and after weights to see how much water was absorbed (Eq. 4.2). This procedure was carried out until a steady rise in weight was achieved.

$$\% \text{ weight gain} = \left(\frac{M_t - M_o}{M_o} \right) \times 100 \quad \dots\dots\dots \text{Eq. 4.2}$$

Where M_o and M_t are the mass of fiber before ($t=0$) and after aging (t).

4.2.5. Fickian diffusion model and data analysis

The experimental kinetic data was processed using the non-linear curve fitting feature of OriginPro (OriginLab Corporation, USA) and the Fickian diffusion model. The modified Fick's equation for a cylinder with thickness t of radius r and concentration c on both sides is (Gouanvé *et al.*, 2007):

$$\frac{M_t}{M_{eq}} = 1 - \sum_{n=1}^{\infty} \frac{4}{\alpha_n^2} \exp(-\alpha_n^2 \tau) \quad \dots\dots\dots \text{Eq. 4.3}$$

where, Where M_t and M_{eq} represent moisture content at time t (sec) and at equilibrium, α_n the root of Bessel's function of the first kind and order zero, and $\tau = \frac{Dt}{r^2}$ is dimensionless time with D being the diffusion coefficient. Using the experimentally determined M_t/M_{eq} and r (taken as half the fiber width, m), equation 4.2 was used to fit the sorption kinetic data and get the value of the average diffusion coefficient D (m^2/sec). The fit was performed using the first 10 roots of Bessel's function, which were as follows: 2.4, 5.52, 8.65, 11.79, 14.93, 18.07, 21.21, 24.35, 27.49, and 30.63.

Different analytical solutions for various sorption regions may be derived by expanding Eq. 4.3 in a convergent series. For the end of the first half of sorption, for instance ($M_t/M_{eq} < 0.5$),

$$\frac{M_t}{M_{\infty}} = \frac{4}{\sqrt{\pi}} \sqrt{\tau} \quad \dots\dots\dots \text{Eq. 4.3}$$

When plotting $(M_t/M_{eq})^2$ vs t in this region, a straight line will result, and the slope k_1 is linked to the diffusion coefficient D_1 as follows:

$$D_1 = \frac{k_1 \pi r^2}{16} \quad \dots\dots\dots \text{Eq. 4.4}$$

For extended time i.e., end of second half sorption ($0.7 < M_t/M_{eq} < 1$),

$$\frac{M_t}{M_\infty} = 1 - 4 \left(\frac{\exp(-\alpha_1^2 \tau)}{\alpha_1^2} \right) \dots\dots\dots \text{Eq. 4.5}$$

The plot of $\ln(1-M_t/M_{eq})$ versus time will produce a straight line in this region, and the slope k_2 being proportional to the diffusion coefficient D_2 as follows:

$$D_2 = -\frac{k_2 r^2}{\alpha_1^2} \dots\dots\dots \text{Eq. 4.6}$$

Finally, the sorption coefficient (S) and permeability (P) were determined as following Sahu and Gupta (2022):

$$S = \frac{M_{eq}}{M_t} \dots\dots\dots \text{Eq. 4.7}$$

$$P = S \times D \dots\dots\dots \text{Eq. 4.8}$$

4.2.6. Measurement of mechanical strength

In accordance with the ASTM test procedure ASTM (2004), the fiber samples were kept under 65% relative humidity and $23 \pm 1^\circ\text{C}$ for 24 hours. Fiber strength was measured with a fiber bundle strength tester (Stelometer, TTS India instruments, India, maximum load 7 kg). Pressley Jaw, with a gauze length of 15 mm, was used to tightly compress a flat bundle of fibers. The assembled fiber was put into the tester and stretched at a steady loading speed of 1 kg/sec until the fiber broke. The breaking load was noted accurately. The fiber was extracted from Pressley Jaw and weighed using a balance with an accuracy of 0.0001. Fiber bundle strength (breaking tenacity) was determined to be in g/tex by using the identified values of breaking load and fiber bundle weight and length. For each fiber type, 40 measurements were taken, and statistical analysis was performed.

Fibers were immersed in distilled water having pH 7.1 ± 1 , conductivity $4.5 \pm 0.5 \mu\text{S}$ for 12 hours to determine their tensile strength when wet. A lint-free blotting paper was used to carefully remove the water from the surface. Then, the mechanical strength was tested using the method described before.

4.2.7. Statistical analysis

The mean, standard deviation, and confidence interval for the mean were calculated from the experimental data using a Microsoft Excel spreadsheet. In order to resolve

whether or not there was a statistically considerable variance between the means of the various data sets, paired t-tests were run as needed (p values).

4.3. Results and discussion

4.3.1. Fiber characterization

The primary objective of this work is to investigate the sorption kinetics of both untreated *Sterculia villosa* (Roxb.) and *Bauhinia vahlii* fibers and those fibers that have been treated with alkali. However, we examined a few of the fiber parameters that are essential to comprehending the sorption results.

It was found that the extractive percentage of unrefined *Bauhinia vahlii* and *Sterculia villosa* (Roxb.) fiber was $13.6\pm 0.5\%$ and $13.0\pm 0.4\%$, respectively. Table 6 provides the lignin, cellulose, hemicellulose, and ash content of the extractive removed samples. *Bauhinia vahlii* fiber was found to have 28% lignin and 31% hemicellulose, which is considerably greater ($p>0.05$) than *Sterculia villosa* (Roxb.) fiber. *Bauhinia vahlii* fiber was discovered to have 54% cellulose, which is substantially lesser ($p<0.05$) than *Sterculia villosa* (Roxb.) fiber. The ash content of these fibers was analogous. Lignocellulose biomass varies in chemical composition based on factors such as plant species, geographic origin, and other factors (Fengel and Wegener, 2011). Therefore, the spotted variations in the composition of fiber biomass derived from these plant species are not unexpected.

Table 6: Chemical composition of lignocellulose biomass

Chemical components	<i>Sterculia villosa</i> (Roxb.)	<i>Bauhinia vahlii</i>
Lignin	21.9 ± 1.7	28.2 ± 1.0
Hemicellulose	28.6 ± 2.3	31.2 ± 1.0
Cellulose	58.7 ± 3.3	54.2 ± 1.3
Ash	6.8 ± 1.3	6.2 ± 0.6

To determine the effect of NaOH and WAA treatment, the net weight loss of both fiber types after treatment was determined. *Sterculia villosa* (Roxb.) and *Bauhinia vahlii* fibers lost $41.9\pm 3.4\%$ and $29.8\pm 2.6\%$, of their weight when treated with NaOH and WAA, and 45.8 ± 1.3 and $30.6\pm 1.3\%$, respectively. Due to the elimination of cementing substances, such as lignin and hemicellulose, alkaline treatment causes a reduction in weight. Type of fiber, treatment duration, temperature, and concentration of alkali

solution are all factors that affect weight loss (Beckermann and Pickering, 2008; Saha *et al.*, 2010; Hashim *et al.*, 2017). Low concentrations of alkali may have contributed to the much-decreased weight loss ($p < 0.05$) observed with WAA (Kandel *et al.*, 2022). According to reports, alkali treatment also reduces the effective fiber bundle diameter (Saha *et al.*, 2010; Hashim *et al.*, 2017). To investigate this, the fiber bundle width of each sample was examined. The 95% confidence interval for the average fiber bundle width ($n = 100$) of untreated, WAA-treated, and NaOH-treated *Sterculia villosa* (Roxb.) samples was 424.4 ± 68.0 , 199.4 ± 28.2 , and 172.1 ± 19.5 μm , in that order. The equivalent *Bauhinia vahlii* measurements were 437.1 ± 75.0 , 252.4 ± 33.5 , and 226.5 ± 36.8 μm . The elimination of lignin, hemicellulose, and other components from the alkali-treated samples ($p < 0.05$) fiber may be the cause of a considerable reduction in fiber width, which is comparable with literature review for other fiber types (Beckermann and Pickering, 2008; Han *et al.*, 2009; Hashim *et al.*, 2017; Kandel *et al.*, 2022).

4.3.2. Sorption kinetics in untreated fiber

The Fickian fit (Equation 4.3) to experimental sorption kinetic data for untreated fiber is shown in Figure 28. The diffusion factor n was estimated by determining the slope of the $\log(M_t/M_{eq})$ versus $\log t$ (Equation 4.1) plot to verify the model's accuracy. During the initial stage of sorption ($M_t/M_{eq} < 0.7$), n values of 0.44 for *Bauhinia vahlii* and 0.34 for *Sterculia villosa* (Roxb.) are consistent with Fickian diffusion.

The fit revealed that the average diffusion coefficient (D) for *Sterculia villosa* (Roxb.) and *Bauhinia vahlii* fibers, respectively, was 10.6×10^{-13} m^2/sec and 6.8×10^{-13} m^2/sec . Further, *Bauhinia vahlii* fibers (~145%) have a far higher equilibrium water absorption compared to *Sterculia villosa* (Roxb.) fiber (~90%). These variations are attributable to the chemical components of the fibers. *Bauhinia vahlii* fiber has a substantially larger content of hydrophilic cementing substances including lignin and hemicellulose. This may result in an increase in equilibrium water sorption.

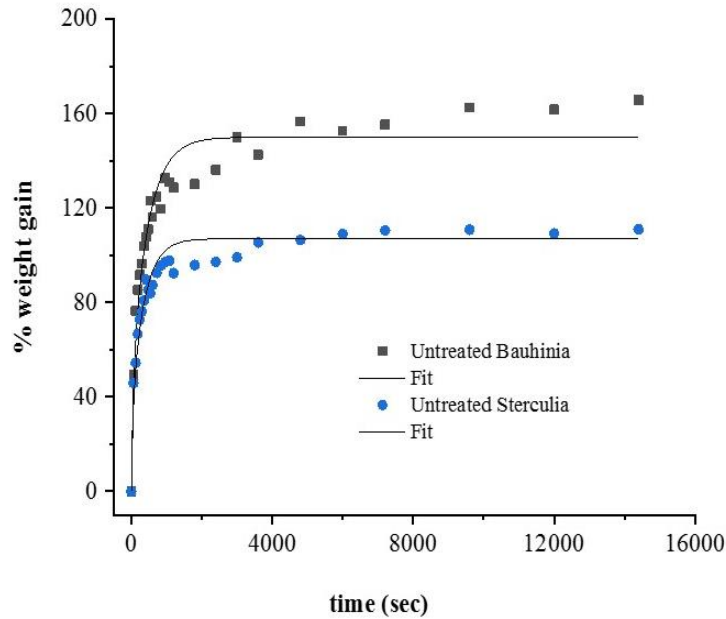


Figure 28: Sorption kinetic data for untreated *Sterculia villosa* (Roxb.) and *Bauhinia vahlii* fibers. Fickian fit to the experimental data points is plotted as solid curves

Further analysis of the kinetic data revealed the diffusion coefficients in the early (D_1) and late (D_2) states of sorption. In accordance with the procedures outlined in methods section, a linear relationship was seen between $(M_t/M_{eq})^2$ and time for both samples at an early stage of sorption ($M_t/M_{eq} < 0.5$) (Figure 29 A). D_1 was determined by utilizing the linear regression slope (Eq. 4.4). Diffusion coefficient D_2 was determined by plotting $\ln(1-M_t/M_{eq})$ with time (Figure 29 B), which resulted in a straight line for extended times ($0.7 < M_t/M_{eq} < 1$) (Eq. 4.5). It was discovered that D_2 was one order of magnitude less than D_1 for both samples (Table 7). Water molecules absorbed at specific places (Langmuir-type sorption) may account for the increased value of the diffusion coefficient in the initial stage. This can occur in a shorter time period, leading to a greater diffusion coefficient. Clusters of water may be less mobile, which may explain why the diffusion coefficient decreases with increasing time (Gouanvé *et al.*, 2007).

Table 7: Diffusion parameters for untreated fiber

Sample	D $\times 10^{-13}$ m ² /sec	D1 $\times 10^{-13}$ m ² /sec	D2 $\times 10^{-14}$ m ² /sec	S	P (barrer)
untreated <i>Sterculia villosa</i> (Roxb.)	10.6	4.72	6.42	0.050	159
untreated <i>Bauhinia vahlii</i>	6.8	4.36	1.28	0.053	108.9

The data was also used to estimate the sorption coefficient (S) and the permeability (P). The solid-to-bulk penetration concentration is measured by the sorption coefficient. The sorption coefficient, in contrast to the diffusion coefficient and the permeability (Table 7), follows the theoretically expected pattern. Once again, the stated variations in fiber composition in Table 6 might account for the varied parameter values.

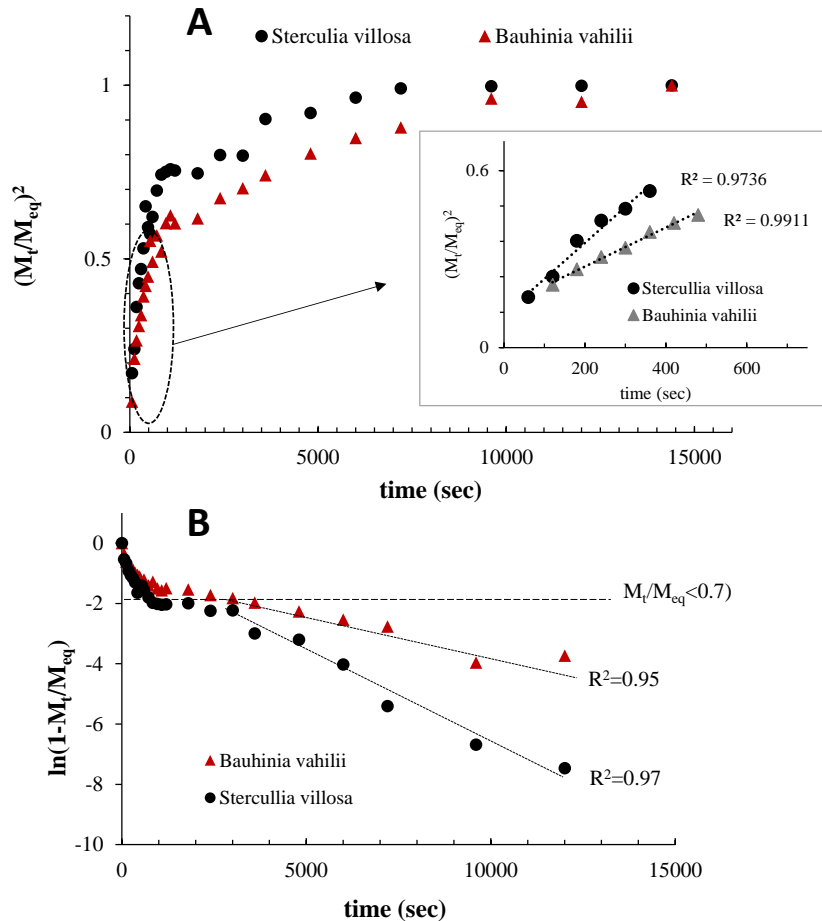


Figure 29: (A) Plot of $(M_t/M_{eq})^2$ versus t and linear regression $(M_t/M_{eq})^2 = f(t)$ derived from the experimental data in the $M_t/M_{eq} < 0.5$ regime (inset). (B) A plot of $\ln(1 - M_t/M_{eq})$ versus t and the linear regression $\ln(1 - M_t/M_{eq}) = f(t)$ derived from the experimental data in the longer time regime ($0.7 < M_t/M_{eq} < 1$)

4.3.3. Sorption kinetics in alkali-treated fiber

The results on the sorption kinetics of the samples that were treated with alkali are presented in Figures 30 A and B. The curve has a substantially different form compared to

Table 8: Diffusion parameters for alkali-treated fiber

Sample	D $\times 10^{-12} \text{ m}^2/\text{sec}$	S	P (barrer)
WAA treated <i>Sterculia villosa</i> (Roxb.)	3.08	0.048	449.5
WAA treated <i>Bauhinia vahlii</i>	3.80	0.049	562.4
NaOH treated <i>Sterculia villosa</i> (Roxb.)	2.35	0.048	348.6
NaOH treated <i>Bauhinia vahlii</i>	3.46	0.049	507.3

that of an untreated fiber; in particular, the percent weight increase approaches near to the equilibrium value within very little time, and the slow and fast sorption regimes are not work out. Table 8 displays the diffusion coefficient calculated from the fitted experimental data.

The average diffusion coefficient of treated samples in comparison with untreated samples is approximately greater than one order of magnitude. This results in decreased sorption coefficient values and dramatically increased permeability (Table 8).

The variation in the form of the sorption curve between untreated and alkali-treated materials may be attributable to variances in chemical composition and fiber width reduction. The narrower fibers might result in greater capillary diffusion.

The equilibrium water content of all the samples was also compared. The equilibrium water absorption is drastically lowered in samples treated with alkali (Figure 31). For instance, the equilibrium water absorption of *Bauhinia vahlii* fiber treated with NaOH and WAA decreases to 80% from 165% in untreated samples.

As indicated previously, alkaline treatment eliminates more hydrophilic cementing substances (lignin and hemicellulose). This might result in a reduction of the equilibrium water sorption. Banana fibers Ronald Aseer *et al.* (2013) and Abaca fibers Punyamurthy *et al.* (2012) have both been observed to have this same phenomenon. It has been hypothesized that the interfibrillar areas of cellulose and hemicellulose are washed out by alkali treatment, leading to a rearrangement of the cellulose chains.

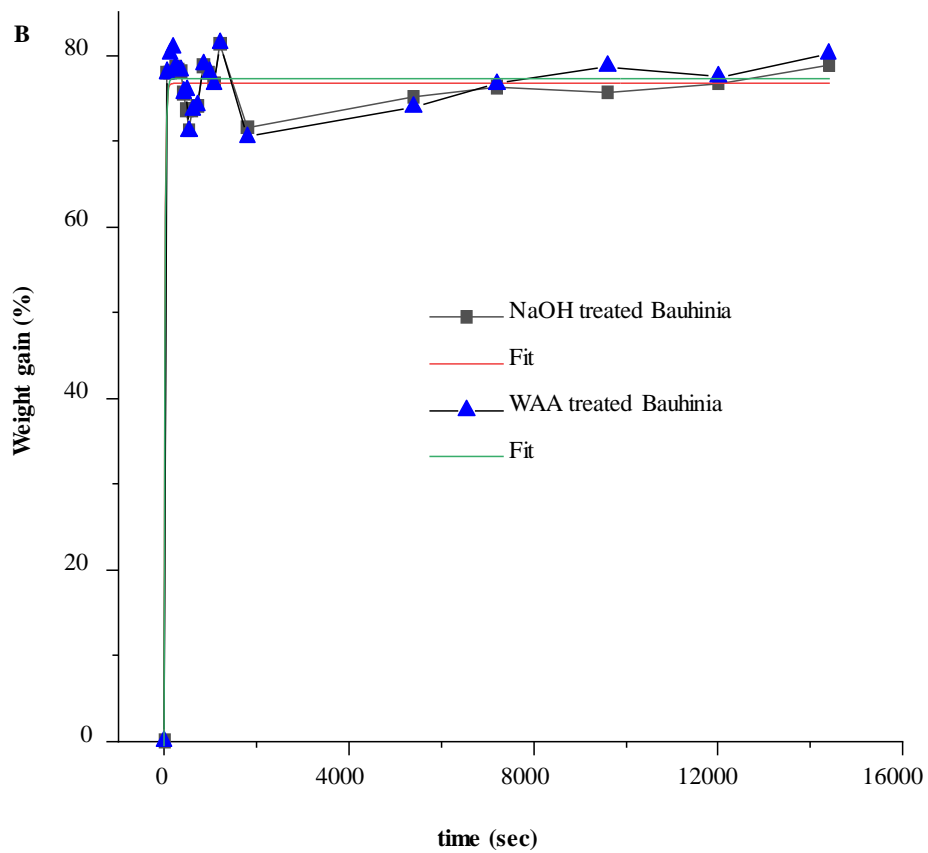
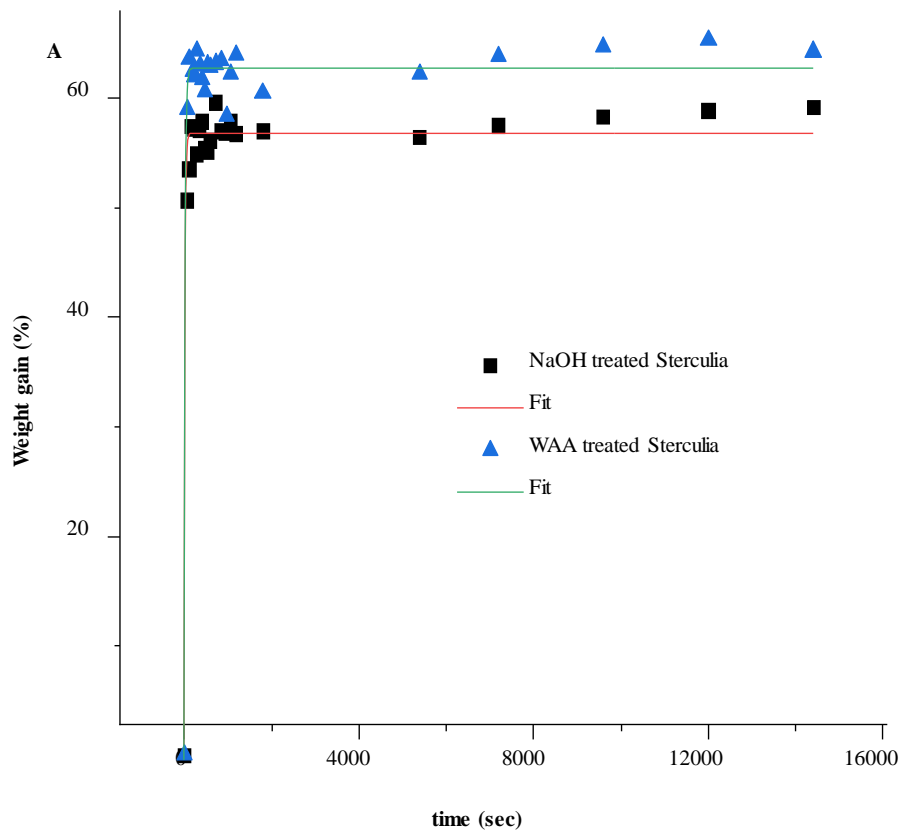


Figure 30: Water sorption kinetic data for alkali-treated *Sterculia villosa* (Roxb.) (A) and *Bauhinia vahlii* fibers (B). The Fickian fit to the experimental data is plotted as solid curves

Consequently, this may cause a rise in crystallinity (Saha *et al.*, 2010). It is possible that enhanced crystallinity following alkali treatment is responsible for the reduced equilibrium water absorption in the treated samples.

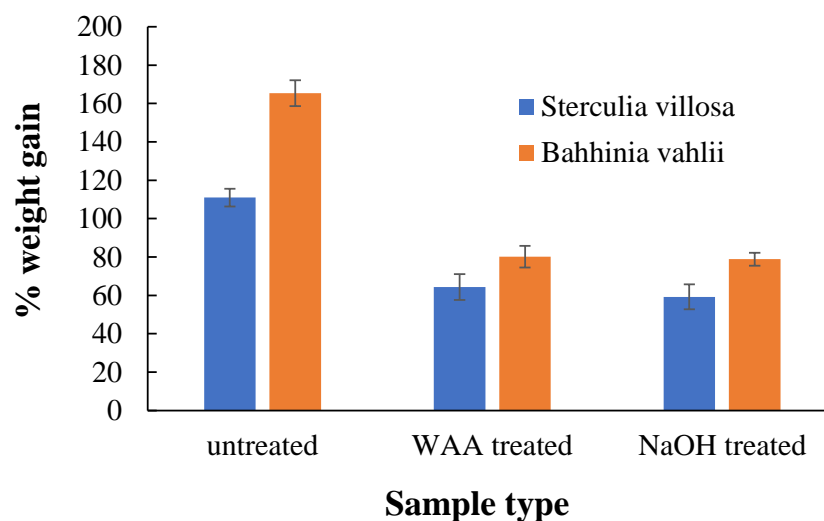


Figure 31: Equilibrium weight gain for untreated and alkali-treated fibers

4.3.4. Mechanical strength of fiber

For clarification, the mechanical strength (breaking tenacity) of the alkali-treated fibers was also tested, both in the dry and wet (absorbent) states (figure 32). Dry WAA-treated *Sterculia villosa* (Roxb.) fiber had a breaking tenacity of 33.6 ± 2.5 g/tex, whereas wet fiber had a breaking tenacity of 24.7 ± 2.7 g/tex. NaOH treatment resulted in values of 32.5 ± 3.5 and 30.0 ± 3.4 for the related variables. The loss in strength in the sorbed state may be the result of weakened hydrogen bonds between cellulose chains or between cellulose and hemicellulose. The mechanical strength of cellulose-polymer composites and other fiber types has also been observed to decrease while wet (Davies and Bruce, 1998; Symington *et al.*, 2009; Céline *et al.*, 2014; Sahu and Gupta, 2022).

An analogous finding was made with *Bauhinia vahlii* fiber (figure 32). In dry and wet conditions, the breaking tenacity of WAA-treated *Bauhinia vahlii* fiber was determined to be 27.8 ± 3.1 and 22.4 ± 3.3 g/tex, respectively. Values of 35.8 ± 3.6 and 28.3 ± 4.3 were discovered for the NaOH-treated sample.

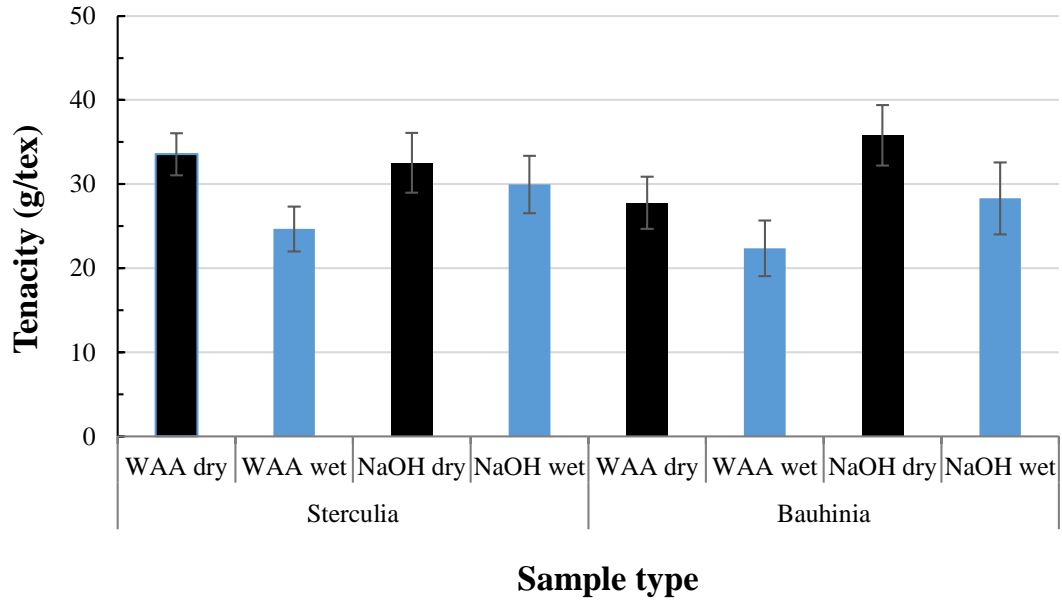


Figure 32: Mechanical strength of different samples. The error bar represents the 95% confidence interval for the mean values

4.4. Conclusions

In conclusion, we applied sorption kinetics to fibers of *Sterculia villosa* (Roxb.) and *Bauhinia vahlii*, both untreated and treated with alkali. In order to learn about the permeability and diffusion coefficients from the experiments, a Fickian model was used to fit the data. The diffusion coefficient was found to be substantially greater in the early state of immersion for untreated fiber compared to the late period. The average diffusion coefficient was discovered to be about one order of magnitude greater in alkali-treated samples compared to untreated samples for both fiber types. As expected, the equilibrium water content of the alkali-treated fiber was significantly lower than that of the untreated fiber. Notably, the mechanical strength of alkali fiber significantly decreased when it was in a sorbed state. Future research might investigate the water sorption kinetics of *Sterculia villosa* (Roxb.) and *Bauhinia vahlii* paper sheets and composite materials.

CHAPTER 5

5. FABRICATION OF Ag-ZnO/CELLULOSE NANOCOMPOSITE MAT FOR DYE DEGRADATION AND ANTIMICROBIAL PACKAGING

5.1. Introduction

A material comprised of nanoparticles that are spread throughout a matrix material, such as a polymer or a metal, is known as a nanocomposite. The dimensions of the nanoparticles is characteristically in the range of 1-100 nanometers, and they can be manufactured from a variety of materials, including metals, ceramics, and polymers. Increased strength, stiffness, and durability are just a few of the distinctive features that nanocomposites possess that are not present in conventional materials. Additionally, they have the potential to be utilized in a diversity of fields, like electronics, aerospace, and biomedical engineering.

Cotton cellulose, sisal fibers, and pineapple leaf fibers were studied as potential reinforcements for polylactic acid and polyester foams. Biodegradable plastics have been researched for use in packaging made from banana trees and Eucalyptus Kraft cellulose. Reinforced concrete containing Cellulose fiber was studied and shown to be useful in a variety of contexts. Coir fiber, jute, and bamboo were studied as potential components of polymeric-reinforced composites. In the processing industries, cellulose fibers are created as a membrane or a pollutant removal adsorbent. In addition, Cellulose fiber sourced from environmental or agricultural wastes is being transformed in novel ways as an asphalt strength-based product used in the transportation sector (Azizan *et al.*, 2023).

Synergistic antibacterial action was also observed in the ZnO-Ag coated nanocomposites cotton material (El-Nahhal *et al.*, 2020). To advance the photocatalytic degradation of methylene blue, silver-zinc oxide nanocomposites were synthesized with varying amounts of Ag-doped to the ZnO (Rafaie *et al.*, 2017). In recent years, photo-catalytic materials have seen significant usage due to the increased focus on water purification and cleaning up the environment (Liu *et al.*, 2019). In another study, Ag-ZnO/cellulose nanocomposite was used to break down methyl orange dye, and it resulted in increased photocatalytic activity, better recovery, more stable catalysts, and multiple reuses (Shi *et al.*, 2021).

To improve the mechanical strength, thermal stability, and gas barrier permeability coefficient for carbon-dioxide, bio-nanocomposite reinforced with ZnO nanoparticles was used in food packaging film (Reis *et al.*, 2021). According to Azizan *et al.* (2023), incorporating nanocomposite into the bacterial cellulose network requires adding the synthesized metal oxide to the nanocomposite via suspension, dispersion, and homogenization at not severe temperatures but with optimal duration. For its potential use in the biomedical treatment of wounds, bacterial cellulose-ZnO has been studied for its effective antibacterial properties. The effectiveness of the nanocomposite in its intended industrial applications was improved by using different processing techniques, such as freeze drying, homogenization, and ultrasonic treatment, to significantly alter the final sizing of the nanocomposite.

Ag-ZnO nanocomposites can be synthesized using a cellulose mat as a substrate. The cellulose mat not only provides mechanical support, but also serves as a porous and biodegradable scaffold for the nanocomposite's development. The cellulose mat can be impregnated using zinc nitrate and silver nitrate solution to create the Ag-ZnO nanocomposite. ZnO nanoparticles and silver nanoparticles can be formed on the cellulose fibers by drying and annealing the mat. Antimicrobial coatings, sensors, and catalysis are just a few of the many possible uses for the Ag-ZnO nanocomposite. Antimicrobial qualities property must come from silver nanoparticles in the nanocomposite, while photocatalytic activity by ZnO nanoparticles. Synthesizing a Ag-ZnO nanocomposite in a cellulose mat matrix offers a greener, biodegradable option to conventional synthetic materials.

The fibers of the *Bauhinia vahlii* plant and *Sterculia villosa* (Roxb.) are locally known as Bharlo and Murgilo or Mudilo respectively. The material properties of fiber generated from these plant species have received comparatively little attention. According to Kandel *et al.* (2022), *Sterculia villosa* (Roxb.) and *Bauhinia vahlii* are found to be high-strength fibers. Their fiber mat can be used as the matrix for synthesizing Ag-ZnO/cellulose nanocomposite material which could be useful in dye degradation and antimicrobial activity. In this study, cellulose mat was prepared using the fiber obtained from two plants species. Phyco-chemical properties of the mats were systematically investigated. The mat was than doped with ZnO and Ag particles and antimicrobial and photocatalytic activities were measured.

5.2. Materials and methods

5.2.1. Materials

Analytical grade sodium hydroxide pellets ethanol, hydrogen peroxide, NaHCO₃, Na₂CO₃, hexamethylene tetramine, zinc nitrate hexahydrate, AgNO₃, CuSO₄, ascorbic acid (Merck Chemicals), was utilized in addition to the extracted fibers of *Sterculia villosa* (Roxb.) and *Bauhinia vahlii*.

5.2.2. Extraction of Fibers

The *Sterculia villosa* (Roxb.) and *Bauhinia vahlii* fiber stems were collected from the Lumbini province of (27°58'22.4"N 83°22'47.6"E) Nepal, specifically from the village of Digam in the Gulmi district. Outer cuticular layer was removed mechanically, then washed multiple times in regular tap water and once in distilled water.

5.2.3. Pulping

Two-stage process was to extract pulp from *Sterculia villosa* (Roxb.) and *Bauhinia vahlii* fibers (Figure 33) (Das *et al.*, 2014; Aryal *et al.*, 2022; Kandel *et al.*, 2022). In the first step, the fibers were delignified using 15% sodium hydroxide at 100°C for four hours under normal atmospheric pressure and fiber-to-liquor ratio of 1:30. After being filtered, the fibers mass was rinsed in distilled water many times to bring pH level to 7. Secondly, fibers were treated with 2% hydrogen peroxide solution prepared in NaHCO₃–Na₂CO₃ buffer system of pH 9 for 5 hours at room temperature. This process isolated the cellulose from the hemicelluloses in the delignified fibers. A mixer grinder was used to grind these fibers into a fine powder. The fine cellulose fiber is called as pulp.

5.2.4. Making paper sheet

The paper sheet of *Sterculia villosa* (Roxb.) and *Bauhinia vahlii* was prepared by following method reported by Obi Reddy *et al.* (2014) with slight modifications. Handmade paper sheets by means of base weight of 65 g/m² were formed from the dried pulp using a 23 x 30 cm² sheet former (homemade equivalent to Hand Sheet Former - UEC-2005). In order to create one liter of the pulp suspension, 4.5 mg of the pulp was added and distributed in water. It was transferred to sheet former. After 10 seconds, water was drained through the wire screen at a 45-degree angle, and the paper sheet was sun dried for 4 hours. The paper sheet was mechanically compressed using 10 kg

steel roller to get final paper. The samples were stored in polyethylene bag in dark for future measurement.

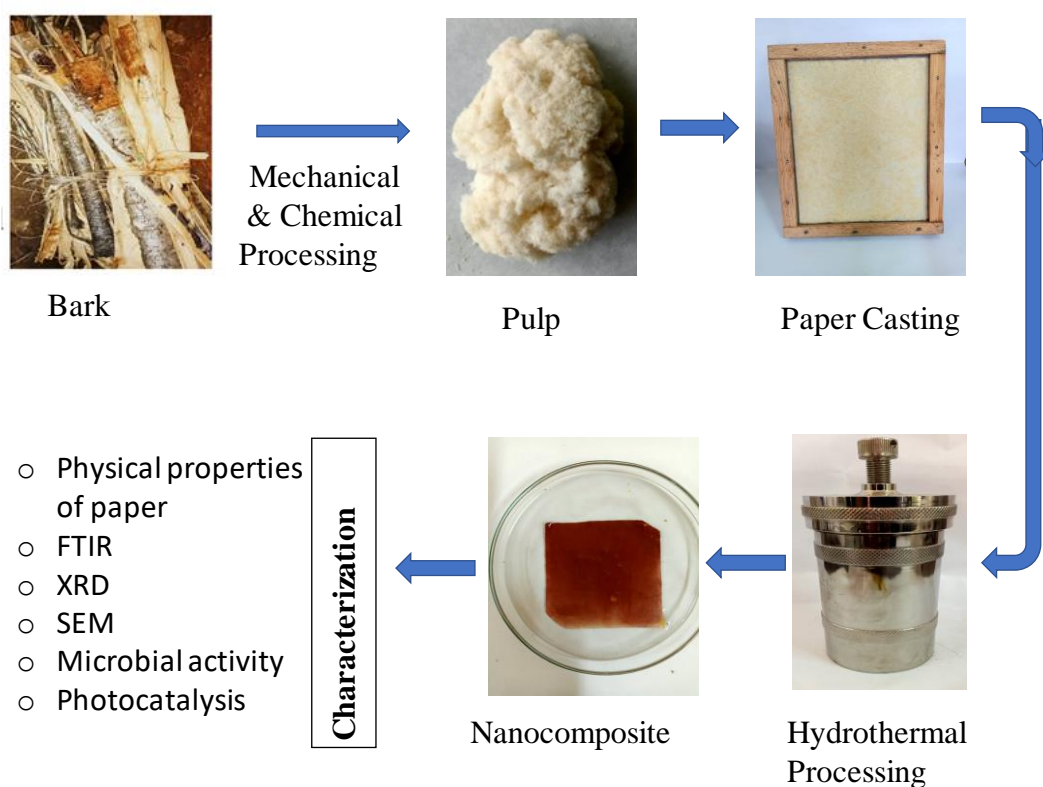


Figure 33: Schematic figure for the conceptual framework used in this work

5.2.5. Characterization

Instruments such as a brightness and opacity tester and a tensile strength tester, the thickness of the paper, Grammage and Cobb 60 were used to evaluate the sheets (Aryal *et al.*, 2022). Weight, thickness, brightness, opacity, tensile strength, and breaking length were determined in accordance with ISO 536, ISO 534, ISO 2470, ISO 2471, ISO 535, ISO 2758, and ISO 1924 standards under standard test environment (23°C and 60% humidity). After doing the above-mentioned tests on five samples from various sheets, the average values (together with the standard deviation) were reported.

5.2.6. Preparation of ZnO-Ag/cellulose sheet

Ag-ZnO/cellulose composite sheet was prepared by following Kim *et al.* (2015) with some modifications. Three different solutions were made: 1.7% hexamethylene tetraamine in distilled water for 30 mL, 2.5% zinc nitrate hexahydrate in distilled water for another 30 mL, and 30 ppm AgNO₃ in 10 mL of distilled water for each bottle. The

solutions of zinc nitrate and hexamethylene tetraamine were combined and agitated actively for 30 minutes. A slurry was made, and then the AgNO₃ solutions were transferred to it. This solution was transferred to a Teflon crucible and 4 x 4 cm² paper mat is added to it. Four hours in an autoclave at 140 degrees Celsius to undergo hydrothermal treatment. The hydrothermal pot was cooled to room temperature, and the composite was filtered, and cleaned several times with of distilled water and ethyl alcohol. After 5 hours of heating at 105°C, the composite was subjected for further testing.

5.2.7. Antimicrobial test preparation

Petri dishes and conical flasks were cleaned, wrapped in paper, and heated at 200°C for 2 hours to sterilize them. Sterilization was performed at 121°C on cotton, loop wire, tips, tips holder, Eppendorf tube, etc. UV light was used to sanitize Laminar for 15 minutes. In terms of composition, Mueller Hinton agar (CM0337B) and Mueller Hinton broth (CM0405B) are almost identical. Both of these products were made from dehydrated beef infusion, hydrolyzed casein, and starch. The powdered agar found in Mueller Hinton agar is what sets it apart as a solid. As a result, the medium will harden at ambient temperature, while liquid Mueller Hinton broth would not. For this experiment, 7.6 grams of Mueller Hinton agar powder (CM0337B) was dissolved in 200 milliliters of distilled water and brought the mixture to a boil while stirring constantly. Once the temperature reached to 47°C, it was stirred thoroughly and 25 ml of the mixture was to clean Petri dishes. They were shielded with a teflon sheet and kept in a refrigerator maintaining 2-8°C for further use. 10 mL MHB solution was prepared by dissolving 0.21 g of Mueller-Hinton broth powder (CM0405B) in sterile water. Autoclave at 121°C for 15 minutes to sterilize, and cooled to room temperature. Bacteria were inoculated by an inoculation loop. The incubation period was 24 hours at 37°C.

5.2.8. Determination of antibacterial efficiency

Ag- ZnO/cellulose paper sheet was investigated for their antimicrobial activities versus different strains by the disk diffusion technique (*Ericsson et al.*, 1960; *Biemer*, 1973; *Sedighi et al.*, 2014). This procedure is often referred to as the ‘Kirby–Bauer method’. The antimicrobial activity of the synthesized paper sheet was assessed by using uncontaminated culture of *Escherichia coli* (*E. coli*) ATCC 8739 (gram - ve), *Bacillus*

subtilis ATCC 6051 (Gram + ve), *Candida Albicans* ATCC 2091. The method consisted of employing 6 mm paper disks with antimicrobial agents on a lawn of bacteria/ fungus scattered on the surface of an agar medium. The Petri dishes were incubated at 5-8°C for 2-3 h to allow appropriate diffusion and then incubated for 24 hours at 37°C. The diameter of the inhibitory zone was calculated after incubation, in millimeters.

5.2.9. Measurement of fiber width

The SEM-image of fiber sample was used to measure its fiber width. Using an open-source image analysis program (ImageJ, NIH, USA) and the known pixel size in micrometers, fiber width measured.

5.2.10. FTIR, XRD, and SEM measurements

The IR spectra were obtained in ATR mode of a Fourier transform infrared spectrometer (Shimadzu IRAffinity-1S) with a resolution of 4 cm⁻¹ in the 4000-400 cm⁻¹ zone. Every fiber sample was conditioned for 12 hours at 23.1 °C and 60% relative humidity before being evaluated. For each spectrum, 100 individual optical scans were averaged to assure a high signal-to-noise proportion. The XRD data was collected using a Rigaku MiniFlex600 X-ray diffractometer in the range of 5-40°, at 30 kV, scan rate of 0.02°/min, and a step size of 0.02°. The X-ray source from Cu K line (= 1.540 Å) was used.

Scanning electron micrographs were undertaken at an accelerating voltage of 15 kV using a JEOL JXA-8530F field-emission electron probe microanalyzer (EPMA) coupled to an X-ray energy-dispersive spectrometer (EDS) for chemical components analysis. Four to six SEM images were acquired for each sample, at magnifications between 50-500. ImageJ (ImageJ, NIH, USA) was used to analyze images and get information on fiber surface morphology.

5.2.11. Measurement of Physical Properties

In compliance with the TAPPI T411 standard, a digital thickness micrometer (Hans Schmidt, D2000C) was used to measure the caliper (thickness) of paper sheet. There were five separate measurements made from different parts of the paper.

The TAPPI-410 method was used to calculate the basis weight of the paper samples at 23°C and 50% relative humidity (RH). Using a circular cutter, a 500 cm² paper sheet

was weighed (0.001 g). The grammage of a sheet of paper was determined by dividing its total mass (g) by its total area (m²). A standard Cobb sizing tool was used to determine the Cobb 60 value in compliance with the TAPPI-T441 guidelines for the non-bibulous paper. The surplus water was pressed out of the wet sample by rolling it back and forth using a 10-kilogram manual roller. The Cobb 60 value was determined by comparing the dry weight of the paper with its wet mass.

The paper's opacity and brightness (ISO brightness) were assessed by means of a standard opacity-brightness instrument (UEC1018, India). The optical characteristics of the paper were determined by cutting five 5 x 5 mm² samples and placing them in the tester. Tensile strength was measured with a 550-kilogram load on a tensile machine (UEC1005B, India) at 23 °C and 50% relative humidity. Paper samples measuring 15 mm to 25 mm were cut from each sheet. The tensile strength of the paper was measured by using the tensile strength tester. The tensile index (Nm/g) was estimated by dividing the tensile strength of the paper (in N/m) by its weight per unit area (in g/m²).

5.3. Results and discussion

5.3.1. Physical Properties of paper mat

The fundamental physical characteristics of all paper samples are listed in Table 9. *Bauhinia vahlii* paper samples had mean thickness values (caliper) between ~269 and ~390 µm (B1 and B3, respectively). Similarly, *Sterculia villosa* (Roxb.) shows variation between ~308 ~ (S5) and 419 µm (S3). The grammage in *Bauhinia vahlii* varied from 51 g/m² (B1) to 71 g/m² (B3). These two variables were found to have a strong positive correlation ($r = 0.83$) in *Bauhinia vahlii* only. *Sterculia villosa* (Roxb.) grammage fluctuated from 47 g/m² (S4) to 102(g/m²) without any obvious trend. The broad range in grammage (Table 9) demonstrates that these sheets can be purposed for distinct uses. Paper sheets with a grammage of 50 or less are typically used for printing, whereas paper with a larger grammage is utilized to create photo albums and packaging for gifts, among other value-added items. A digital micrometer with a 10 µm resolution was used to measure the caliper. For instance, the mean caliper measurement of sample B1 is 268.8±67.5 µm. Since there is such a wide range in caliper measurements, it's safe to assume that handmade paper (HP) samples aren't uniformly thicker. Typically, samples of handmade paper are produced using the chemical-mechanical approach to fiber processing, which produces predominantly long fiber (1 mm).

Table 9: Physical properties of Paper sheet

<i>Bauhinia vahlii</i>	B1	B2	B3	B4	B5	Mean
Thickness	268.80	223.60	389.60	316.60	358.40	311.40±66.85
GSM	50.85	51.12	70.99	54.49	69.38	59.37±10.00
Brightness	58.77	58.70	59.38	58.70	62.07	59.52±1.45
Opacity	94.51	93.87	96.57	94.10	95.87	94.98±1.18
Cobb 60	104.30	99.40	153.90	111.30	145.00	122.78±24.91
Elongation (E) %	0.31	0.49	0.56	0.48	0.64	0.50±0.12
Tensile index (B) Nm/g	3.19	3.67	3.31	3.06	4.83	3.61±0.72
Tensile strength (S) kN/m	0.19	0.22	0.20	0.18	0.29	0.21±0.04
Breaking length (Ls) km	0.35	0.38	0.34	0.31	0.49	0.37±0.07
Absorbed energy (Z) J/m ²	0.65	0.94	0.90	0.77	1.82	1.02±0.46
Apparent density (g/cm ³)	0.19	0.23	0.18	0.17	0.19	0.19±0.02
Apparent porosity (%)	83.64	80.22	84.24	85.11	83.25	83.29±1.85
Thickness/fiber width	24.26	20.18	35.16	28.57	32.35	28.10±6.03
RBA	0.03	0.04	0.03	0.02	0.03	0.03±0.01
<hr/>						
<i>Sterculia villosa</i> (Roxb.)	S1	S2	S3	S4	S5	Mean
Thickness	371.00	323.80	419.20	309.40	308.20	346.32±48.07
GSM	73.74	101.70	61.98	47.22	82.56	73.44±20.62
Brightness	58.42	58.04	54.55	57.38	61.90	58.06±2.63
Opacity	95.46	97.09	90.67	86.32	96.76	93.26±4.65
Cobb 60	174.80	256.70	146.40	77.10	210.00	173.00±67.61
Elongation (E) %	1.85	1.12	1.07	1.04	1.00	1.22±0.36
Tensile index (B) Nm/g	15.07	9.44	9.42	8.65	8.41	10.20±2.76
Tensile strength (S) kN/m	1.11	0.69	0.69	0.64	0.62	0.75±0.20
Breaking length (Ls) km	1.54	0.96	0.96	0.88	0.86	1.04±0.28
Absorbed energy (Z) J/m ²	14.98	8.08	7.03	6.22	5.61	8.38±3.80
Apparent density (g/cm ³)	0.20	0.31	0.15	0.15	0.27	0.22±0.07
Apparent porosity (ε) (%)	83.67	74.19	87.85	87.46	77.99	82.23±5.99
Thickness/fiber width	31.44	27.44	35.53	26.22	26.12	29.35±4.07
RBA	0.03	0.07	0.02	0.02	0.05	0.04±0.02

During the paper-making process, the long fibers have a high tendency to floc formation, leading to inconsistent thickness (Beghella, 1998; Lundell *et al.*, 2011).

The apparent density (g/cm³) was determined by dividing the weight (g/m²) by the sample's thickness (m). *Bauhinia vahlii* had an apparent density between 0.2 ± 0.0

g/cm³ and *Sterculia villosa* (Roxb.) between 0.2 ± 0.1 g/cm³ (Table 10). The volume of air or empty space within a sheet of paper is included in its apparent density. This means that apparent density always falls short of true density. In contrast to papers created from *Bauhinia vahlii* and *Sterculia villosa* (Roxb.), machine-made and commercially available paper sheets have been shown to have a higher apparent density (0.5-0.8 g/cm³) (Bajpai, 2018a; Aryal *et al.*, 2022).

Table 10: Density of *Bauhinia vahlii* and *Sterculia villosa* (Roxb.)

Sample	M1	M2	M3	M4	Mean
<i>Bauhinia</i> cellulose fiber density	1.12	1.19	1.17	1.14	1.16±0.03
<i>Sterculia</i> cellulose fiber density	1.21	1.22	1.23	1.21	1.22±0.01

HPs appear to be lightweight paper based on their low apparent density. The known densities of the paper network and cellulose can be used to evaluate the apparent porosity of paper (Sampson, 2004; Henriksson *et al.*, 2008; Tanpichai *et al.*, 2012; Tanpichai *et al.*, 2019a). In this work, the apparent porosity was determined using eq 5.1.

$$\varepsilon(\%) = \left[1 - \frac{\rho_{adp}}{\rho_{cf}} \right] \times 100 \dots\dots\dots \text{Eq. 5.1}$$

where ρ_{adp} is the apparent density of the paper mat and ρ_{cf} is the density of cellulose fiber. In the calculation, cellulose density of *Sterculia villosa* (Roxb.) and *Bauhinia vahlii* as represented in table 10 was used. The apparent porosity of *Bauhinia vahlii* was determined to be 83%, while that of *Sterculia villosa* (Roxb.) was 82% (Table 9). Specifically, we found that apparent density and porosity are perfectly inversely related to one another ($r = -1$). Some possible causes of the low apparent density (high porosity) of handmade papers include the use of long and inflexible fibers, not enough refining, the lack of fillers and fines, and inadequate calendaring, and their combinations (Bajpai, 2018b). Samples of laboratory-made handmade paper have also been found to have a low apparent density, in the range of 0.2 to 0.5 g/cm³ (Marrakchi *et al.*, 2011; Obi Reddy *et al.*, 2014; Mejouyo *et al.*, 2020).

5.3.2. Cobb 60

Water absorbency is often measured using the Cobb 60 value since it is the most widely applied metric. The weight of water absorbed by one square meter of paper submerged

in one centimeter of water in sixty seconds is known as the Cobb 60. Fiber chemistry, fiber shape and organization, and fiber caliper all affect the Cobb value. In the samples we examined, the Cobb sizing ranged from ~100 (B2) to ~154 (B3) g/m² and from ~77 to ~257 (S4) and (S2), respectively. Differences in chemical composition (given in Table 6) and slight variations in fiber shape and organization may account for the large range in Cobb 60. In the instance of *Bauhinia vahlii*, there is a significant positive association between the Cobb 60 value of handmade paper and the caliper ($r^2 = +0.88$). The grammage of both type of sheets should strong positive correlation ($r > +0.98$) with Cobb 60. It is probable that the experiment's high Cobb 60 value was the result of the residual water being not easy to release with mechanical pressing, using a 10 kg roller.

5.3.3. Optical Properties

The primary optical characteristics of paper are its brightness and opacity. Yellowish paper is less reflective or more absorbent under blue light. Thus, less yellow paper is indicated by a greater brightness. The amount of bleaching and how smooth the surface is will determine how bright the paper sample is. Commercial printing paper that has been bleached and glazed may achieve an ISO brightness of 100% (Bajpai, 2018a). The brightness of paper sheets varied from 59% (B1) to 62% (B5) (Table 9). Handmade paper produced by Lokta Bushes, commonly known as Nepali Kagaj, has a comparable brightness (Aryal *et al.*, 2022). Paper and pulp samples vary in brightness based on factors including lignin and coloring impurity levels and microscopic surface features (Bajpai, 2018a).

5.3.4. Opacity

The capacity of paper to conceal an item on the other side of the sheet is measured by its opacity. A high-opacity paper is needed for double-sided printing so that the front page can be read without being distracted by the letters or graphics on the reverse and the strikethrough is not visible. High opacity is caused by the scattering of blue light by tiny air gaps or pores in thick paper sheets (Bajpai, 2018a). Paper opacity varied from 94% (B2) to 97% (B3), and from 86% (S4) to 97% (S2) in this investigation (Table 8). It is possible that the papers' low apparent density and/or high porosity contribute to their greater opacity.

5.3.5. Mechanical Properties

All the paper samples were tested for tensile strength and the tensile index throughout the length of the wooden frame or paper molds. Tensile strength was between 0.18 (B4) and 0.29 (B5) kN/m (S5) and between 0.62 (S5) and 1.11 (S1). The maximum tension per unit width (N/m or kN/m) required to tear a paper strip is defined as the tensile strength. A sheet of paper may be stressed in a variety of ways in the course of printing and other processes, such as making pasted paper tape. In these situations, the paper's web may break if it lacks sufficient tensile strength (Bajpai, 2018a).

The tensile strength index, also known as tensile strength adjusted for weight, was also determined. Table 9 shows the distribution of tensile indices for the paper samples, which extend from 8.41 for S5 to 15.07 for S1 to 3.06 for B4 to 4.83 for B5.

Several variables affect the tensile strength of paper-based materials, including fiber strength, fiber length, and fiber-to-fiber connection and bonding. The degree of contact connecting two layers may be characterized in terms of relative bonding area (RBA) by observing a paper sheet as multiple layers of fabric composite structure comprising two-dimensional fibrous setups that are not interwinding between layers (Soszynski, 1995; Henriksson *et al.*, 2008). RBA may be roughly estimated from the values of fractional porosity (ϵ) and the number of fiber layers (n), where n is the ratio of thickness to fiber diameter (Sampson, 2004). Table 9 displays the RBA values for all of the available paper samples.

The RBA was calculated using a fiber diameter of 10.8 and 11.8 μm (Figure 34) for *Bauhinia vahlii* and *Sterculia villosa* (Roxb.) fiber in the paper mat, respectively. For fibers with the same length, coarseness, cross-section perimeter, and bonding strength, the tensile strength of a fiber sheet is directly linked to the relative bonding area (Page, 1969; Tao and Liu, 2011).

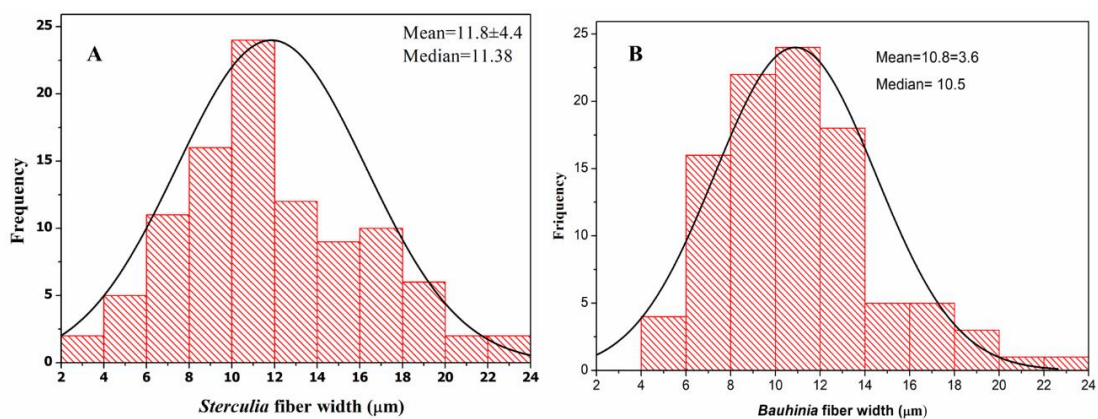


Figure 34: Diameter of fiber distribution A) *Sterculia villosa* (Roxb.) B) *Bauhinia vahlii*

5.3.6. SEM Imaging of the Paper Samples

Figure 35 A-H shows some typical SEM pictures of the paper samples we examined. A network of intertwined fibers shown in the photographs that are randomly organized. Long fibers (more than 1 mm) that intertwine with one another strengthen the paper sheet. Fiber width is a crucial parameter to assess the durability and strength of a paper sheet's fibers. The width of the fibers was determined for each of the samples. From a total of 99 measurements, we find that the average fiber width of *Bauhinia vahlii* and *Sterculia villosa* (Roxb.) is 10.8 and 11.8 μm, respectively, with median values of 10.5 and 11.38 μm. Some fibers may lose their lumen or cell wall stability during processing, resulting in flexible, ribbon-like fibers. There may be a large increase in the apparent diameter of the folded fiber (Hubbe, 1999; Ilyas *et al.*, 2019). High apparent width may also be the consequence of fibers that are not fully separated or that stay linked to create a bundle. The extreme porosity of this cellulose mat is one of its defining features. Isolated cellulose seems to be a dense substance, with the cellulose fibers linked tightly together. The non-woven network of pores in natural cellulose is extremely porous (Maneerung *et al.*, 2008). The hydroxyl of the cellulose is predicted to interact with electro-positive metal ions, and the pores in the material make it easy for zinc ions to adsorb before being washed away in a methanol rinse (Ali *et al.*, 2016).

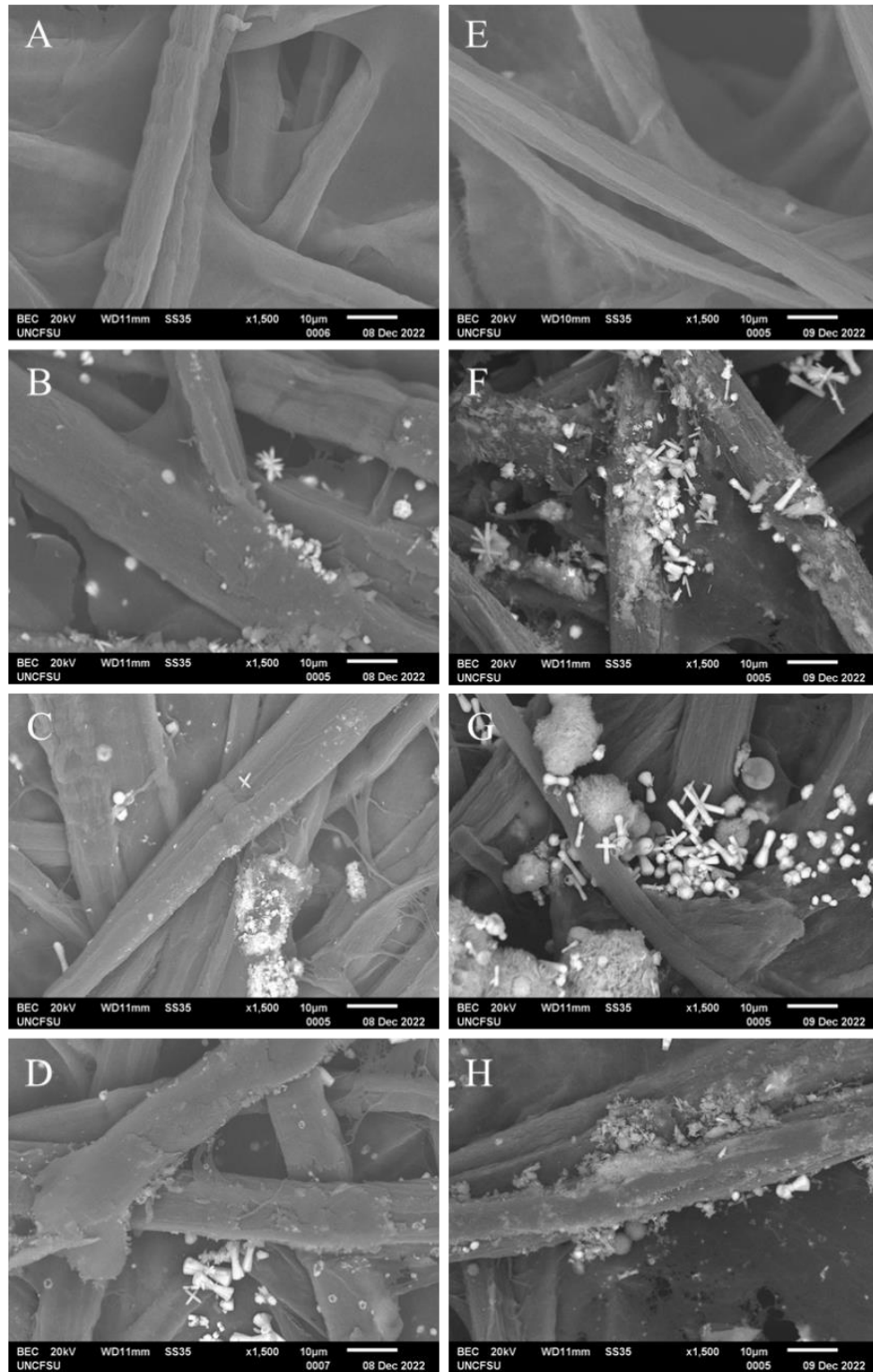


Figure 35: SEM image of *Bauhinia Vahlia*: A) Cellulose paper mat, B) Cellulose-ZnO/Ag, C) 10 min sonicated Cellulose-ZnO/Ag, D) 20 min sonicated cellulose-ZnO/Ag; and E, F, G, H represent the corresponding data for *Sterculia villosa* (Roxb.)

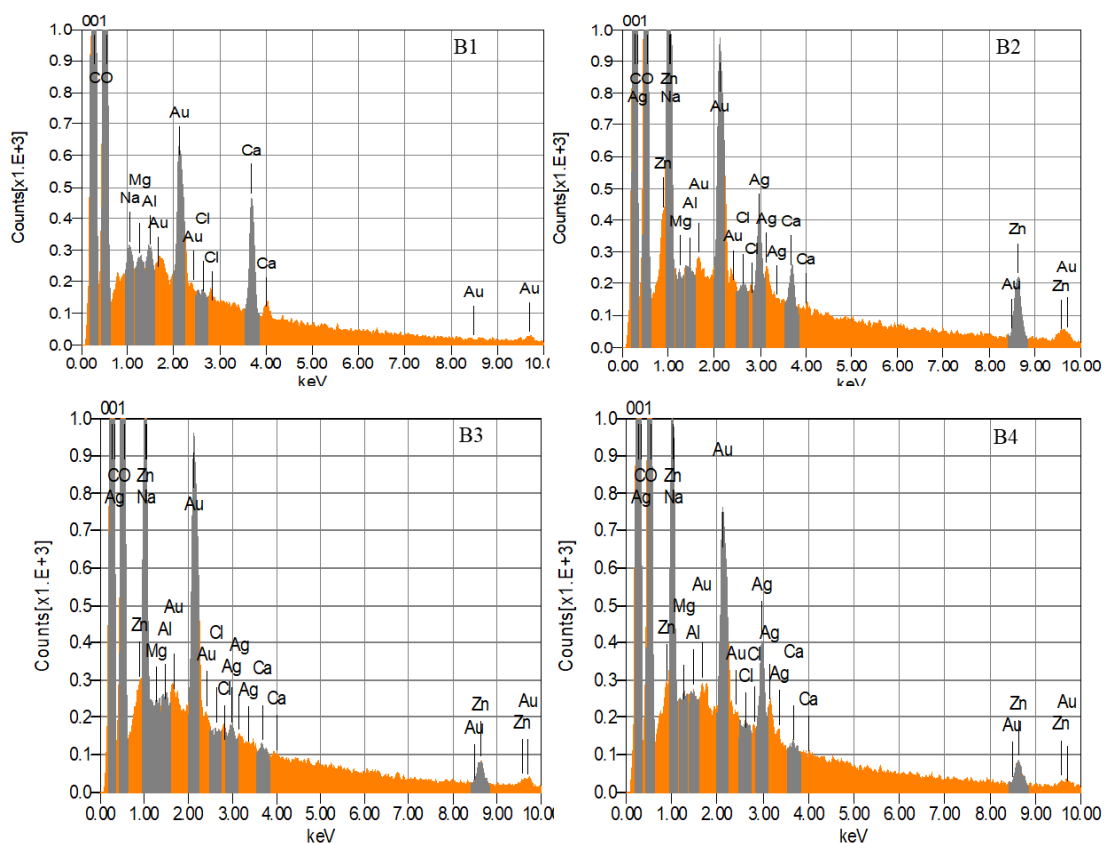


Figure 36: SEMEDX, B1) Cellulose Paper), B2) Cellulose-ZnO/Ag, B3) B2 sonicated for 10 min, B4) B2 sonicated for 20 min

Representative FE-SEM images with EDX spectra of the paper mat and Ag-ZnO/cellulose composites are shown in Figures 35, 36, and 37 respectively. The EDS results demonstrate that the Ag-ZnO/cellulose composite (Figure 37 S2) has the same range of elements as the cellulose mat (Figure 36 B2). Furthermore, the quantity of zinc and silver greatly increased in comparison to cellulose mats, indicating the efficient development of a composite. FE-SEM images (Fig. 35) reveal that a cluster of Nano-sized particles (Ag and ZnO) has been uniformly deposited on the surface of the cellulose mat. Figure 36 B3 and B4 shows SEM EDX showing the concentration of zinc and silver after sonication of Ag-ZnO/cellulose mat. This shows the concentration of these elements does not decrease significantly revealing that, the nanocomposite formed was stable. Based on these findings, it seems that molecules of composite particles interacted with one another actively. Hydrothermal treatment resulted in a uniform distribution of ZnO and Ag NPs over the surface of the cellulose mat.

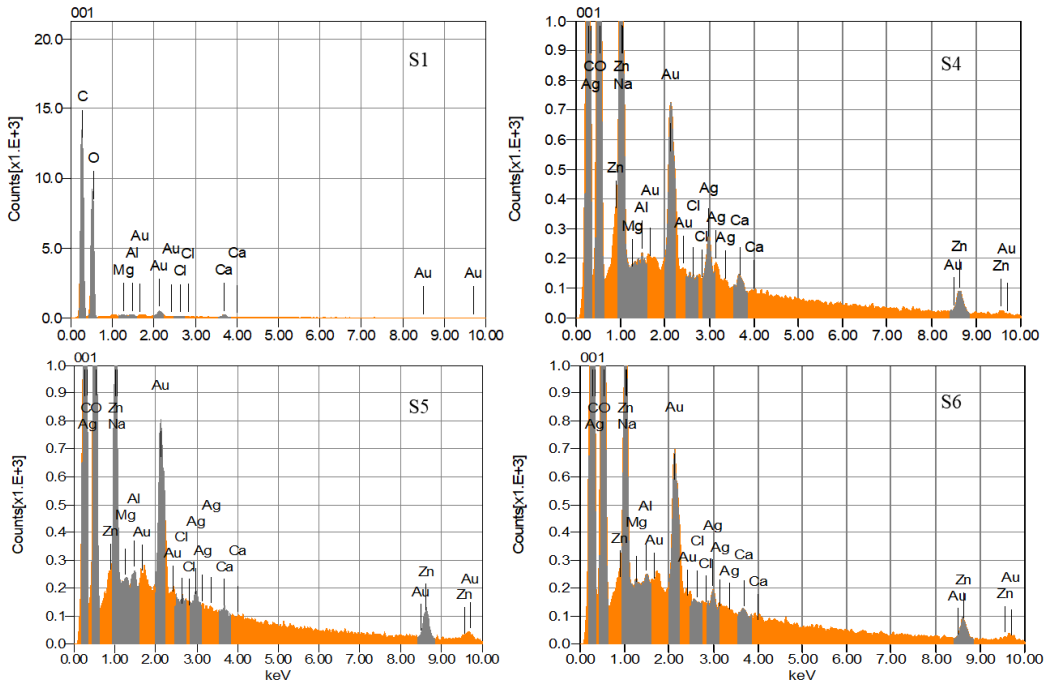


Figure 37: SEM EDX *Sterculia villosa* (Roxb.), S1) Cellulose Paper (CP), S2) CP-ZnO/Ag, S3) CP-Ag-ZnO sonicated for 10 min, S4) CP-Ag-ZnO sonicated for 20 min

5.3.7. XRD Study

XRD data of raw fiber and paper samples were measured (Figure 38). The (200) and (110/110) planes of the cellulose I crystalline phase are responsible for the peak at 2θ values of 21.5° and 15.5° , respectively (Park *et al.*, 2010a; Saha *et al.*, 2010). The amorphous phase accounts for the presence of a uniform backdrop that lies underneath the peaks (Segal *et al.*, 1959; Park *et al.*, 2010a). Following equation 5.2, the XRD crystallinity index (CI) was determined.

$$CI = \left(\frac{A_t - A_{am}}{A_t} \right) \times 100 \dots\dots\dots \text{Eq. 5.2}$$

where A_t is the integrated intensity of both the crystalline and amorphous phases and A_{am} is the intensity of the amorphous phase solely. Gaussian fitting was used in the 2θ range of $5-40^\circ$ to get values for A_t , A_{am} , and CI. The crystallinity Index for B1–B4 were found to be 58.98%, 50.69%, 59.39%, and 50.50%, respectively. Variation in CI of paper mat may be due to the not homogenous nature of fiber mat. The (110), (200), and (004) planes may be identified as sharp peaks at 2θ in the XRD pattern of cellulose, which occurs at 14° , 16° , and 22° , respectively. Peaks at 2θ for ZnO nanoparticles are seen at 31.8° , 34.5° , and 36.3° , which correspond to the (100), (002), and (101), planes

of the hexagonal wurtzite ZnO crystal structure, using JCPDS 36-1451 (Kalpana and Devi Rajeswari, 2018). Peaks at 2θ angles of 38.1° can be seen in the XRD pattern of Ag nanoparticles (Figure 36), which match the (111) planes of face-centered cubic silver (Zhou *et al.*, 2013; Ibănescu *et al.*, 2014). These data conform the incorporation of ZnO and silver on the cellulose mat surface.

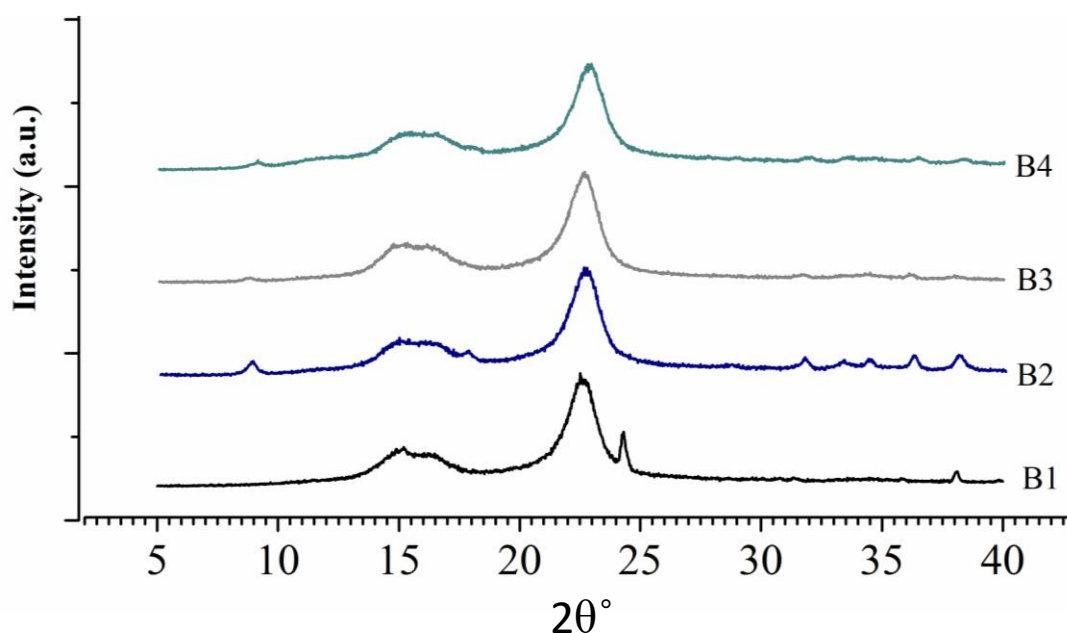


Figure 38: XRD data of cellulose paper (B1), cellulose-ZnO (B2), Ag-ZnO/cellulose (B3 and B4), and Sonicated Ag-ZnO/cellulose mat

Nano crystallite size of Ag and ZnO was calculated by using Scherrer equation.

$$D = K\lambda/\beta\cos\theta \dots\dots\dots \text{Eq. 5.3}$$

Where K is Scherrer’s constant and is equal to 0.89, λ is the wave length of X-ray, θ is the Bragg diffraction angle, and β is the full width at half maximum of the diffraction peak. The Ag particle size was found to be 13.85 and average particle size of ZnO was 23.4 nm in Ag-ZnO/*Sterculia*. Similarly, the size of Ag and ZnO crystallite in *Bauhinia* mat was estimated as 17.7 and 23.6 nm respectively. This result shows the formation of nanocomposite.

5.3.8. FTIR and UV-vis Study

The FTIR data of unprocessed fiber, paper mat, and nanocomposite are shown in Figure 39. The shapes of the spectra are quite similar, with just a little variation in the relative

peak intensities. The spectral labels were determined using data found in published works (Kondo and Sawatari, 1996; Åkerholm *et al.*, 2004; Xu, F. *et al.*, 2013; Poletto *et al.*, 2014; Tanpichai *et al.*, 2019a). The O-H stretching of cellulose is responsible for the large peak between 3000-3600 cm^{-1} (with three weak peaks). The hemicellulose and cellulose aliphatic C-H stretching vibration contributes to the faint peak about $\sim 2900 \text{ cm}^{-1}$ (Poletto *et al.*, 2014). The C—O stretching of conjugated lignin gives rise to the peak at $\sim 1630 \text{ cm}^{-1}$, while acetyl or ester C—O groups in hemicellulose or lignin give rise to the peak at $\sim 1735 \text{ cm}^{-1}$ (Haque *et al.*, 2009; Tanpichai *et al.*, 2019b). Raw fiber has comparatively more prominent versions of these peaks. This finding indicated that pulping only partly removes hemicellulose and lignin. The C—O stretching of acetyl groups in hemicellulose and cellulose accounts for the faint peak at $\sim 1250 \text{ cm}^{-1}$ (Sinha and Rout, 2008). Paper samples show a weaker signal, indicating that hemicellulose was removed during fiber processing. The results of the chemical analysis shown in Table 6 corroborate these findings.

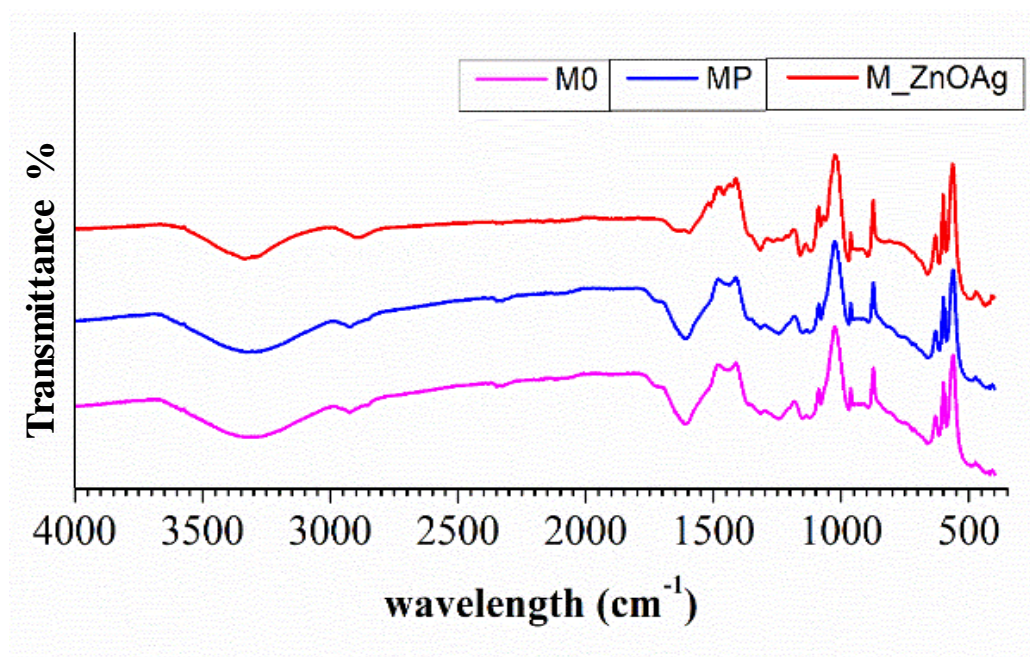


Figure 39: FTIR of paper, and nanocomposite made from *Bauhinia vahlii* fibers

The Ag and ZnO contributed to the appearance of bands with a wavelength of less than 471 cm^{-1} , which are typical of the metal-oxygen band (Elemike *et al.*, 2021).

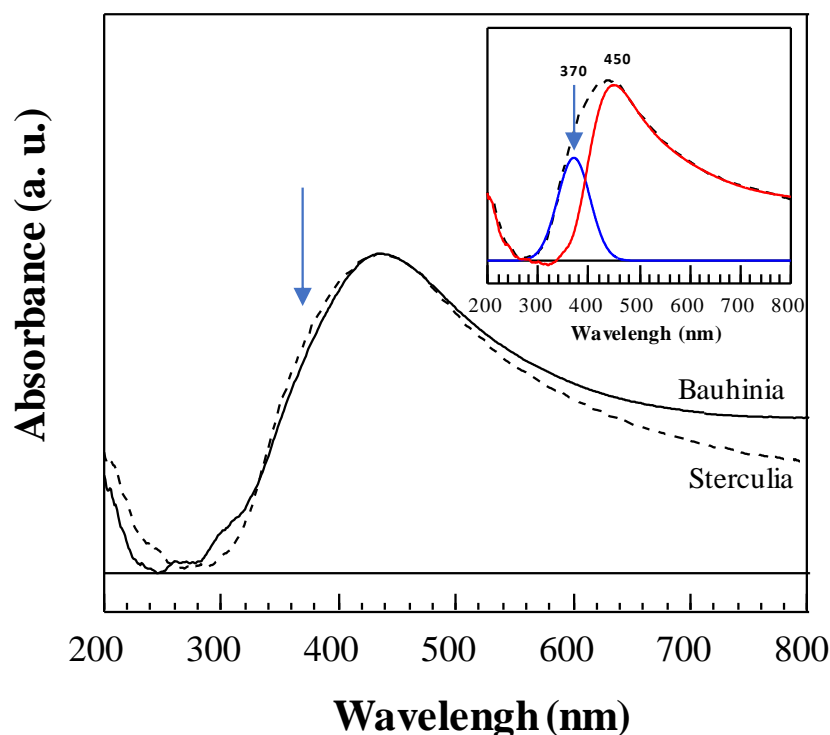


Figure 40: UV-vis spectra of the Ag-ZnO/Cellulose nanocomposites. The spectra are normalized to the peak around 450 nm

The UV-vis spectra of nanocomposites are very similar with a weak shoulder around 370 nm (indicated with an arrow in main frame in figure 40) and peak around 450 nm tailing to longer wavelength. The spectra can be indeed deconvolved to two components (inset in figure 40): a) a peak at 370 nm which can be accounted to ZnO nanoparticles and, b) other contribution peaking at 450 nm corresponds to silver nanoparticles. The broad contribution extending as high as 800 nm can be due to Ag nanoparticle agglomerates. This observation is consistent With SEM images.

5.3.9. Photocatalysis of Methylene blue

Degradation of an aqueous MB (cationic dye) solution under continuous UV irradiation was used to test the photocatalytic activity of the as-synthesized photocatalyst. Figure 41 shows the photocatalytic activity of Ag-ZnO/cellulose nanocomposite. The efficacy of photodegradation may be modified by adjusting the particle size, shape, and method of ZnO attachment to the cellulose mat surface. Hydrothermal development of ZnO NPs on cellulose mat reduced the probability of particle aggregation (Kim, H. J. *et al.*, 2015). Potentially degrading features include a large surface area for ZnO and Ag NPs deposition on cellulose mat. Kansal *et al.* (2007) found that ZnO NPs' surface electron-

hole pairs are responsible for triggering the photodegradation of MB. The Ag NPs on the ZnO NPs' surface operate as an electron sink, facilitating charge transfer across the particle interface. When compared to the ZnO/dye interface, the Schottky junction formed by Ag has a larger potential gradient generated by the Schottky barrier, which might explain why Ag-loaded ZnO is more chemically active (Pant *et al.*, 2013).

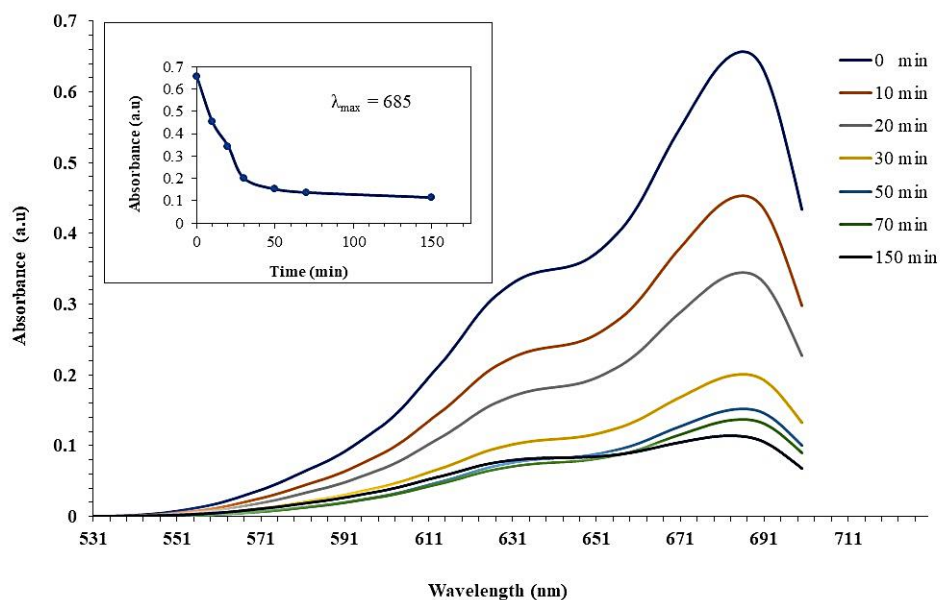


Figure 41: UV-vis absorption spectra of Methyl Blue measured at different time interval of UV-irradiation where 0 to 150 refers time in minutes. Inset shows absorbance versus time plot

Hydrothermal development of ZnO and Ag NPs is facilitated by cellulose particles because of their high surface area, which prevents the NPs from aggregating into larger particles. Ag and ZnO NPs with a high surface area and a small diameter result in a greater number of photocatalytic active sites. When ZnO is activated, electrons rapidly jump to Ag NPs from conduction band, making the Ag-ZnO/cellulose composite catalyst very efficient. This reduces formation of highly reactive species (O_2^- and $\cdot OH$) by photogenerated carriers and speeds up the degradation of the dye. (Kim *et al.*, 2015). The dye degradation test of methyl blue in the presence of UV light shows the decrease of absorption peak indicating degradation of methyl blue.

5.3.10. Determination of antimicrobial efficiency

The antimicrobial activity of the synthesized paper sheet was evaluated by using a pure culture of *Escherichia coli* (*E. coli*) ATCC 8739 (Gram - ve), *Bacillus subtilis* ATCC 6051 (Gram + ve), *Candida Albicans* ATCC 2091. The antimicrobial activity of

synthesized Ag-ZnO/cellulose nanocomposite is shown in Table 12 and Figure 40 A-H. The zone inhibition approach was used to assess their antibacterial performance. *Escherichia coli* (*E. coli*) ATCC 8739 (gram - ve) shows the least response to the nanocomposite prepared. *Bacillus subtilis* ATCC 6051 (gram + ve) and *Candida Albicans* ATCC 2091 show better antimicrobial activity.

Table 11: Zone of inhibition microbial test

Strains	Zone of inhibition			
	<i>Bauhinia Vahlia</i>	<i>Sterculia Villosa</i> (Roxb.)	C-	Standard (c+)
<i>Escherichia coli</i> ATCC 8739 (Gram - ve)	0.0, 0.1, 0.2	0.0, 0.0, 0.1	0	1.1
<i>Bacillus subtilis</i> ATCC 6051 (Gram + ve)	0.4, 0.6, 0.8	0.1, 0.2, 0.2	0	1.0
<i>Candida Albicans</i> ATCC 2091	0.1, 0.2, 0.3	2., 0.3, 0.3	0`	1.3

The result also shows antimicrobial activity increases with the increase in concentrations. According to Yamamoto (2001), ZnO particles inhibited bacterial growth by producing hydrogen peroxide, however, their antibacterial effectiveness appeared poor in comparison to that of Ag NPs. Although the mechanism of antimicrobial activity of nanoparticles is uncertain, there is evidence that Ag NPs may have bactericidal effects by leaking cellular material and disrupting DNA replication straight through the membrane of a bacterial cell (Yamamoto, 2001). These findings provided further evidence that the Ag-ZnO/cellulose composite enhanced antibacterial activity.

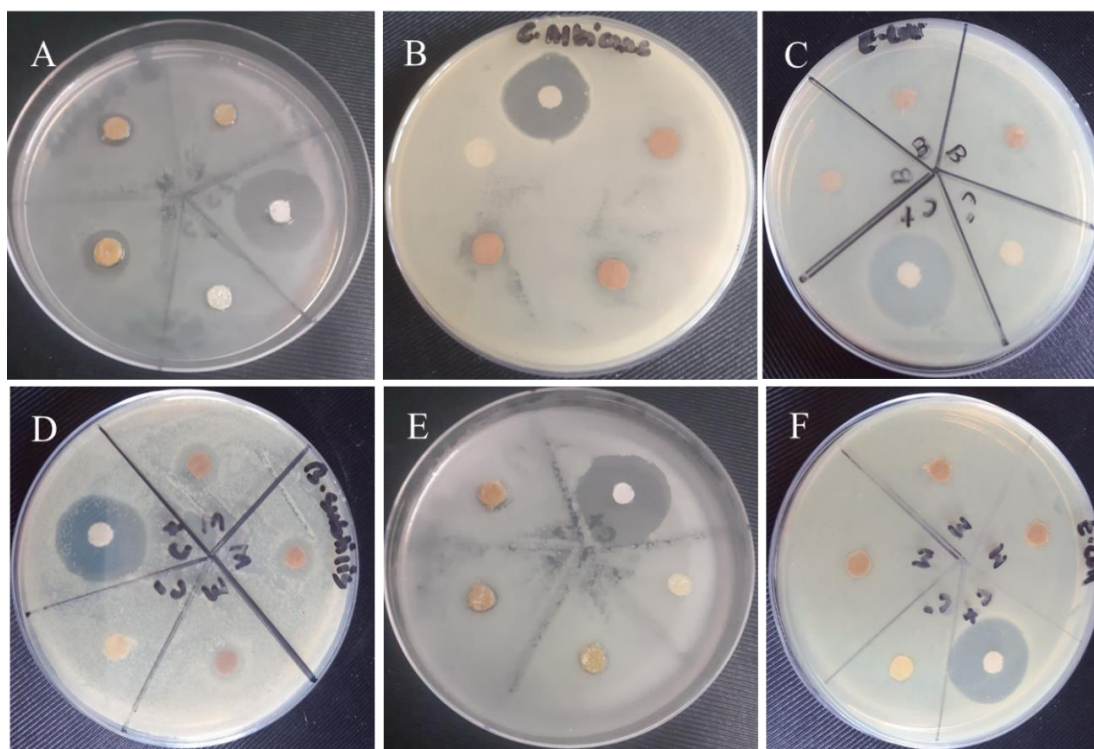


Figure 42: Antimicrobial Activity of Nanocomposite Paper-mat of *Bauhinia* A) *Bacillus subtilis* B) *Candida Albicans* C) *Escherichia coli* and *Sterculia* D) *Bacillus subtilis* E) *Candida Albicans* F) *Escherichia coli*

5.4. Conclusions

In conclusion, hydrothermal treatment was used to produce a stable Ag-doped ZnO/cellulose composite. Photocatalytic activity toward MB dye degradation was observed in the Ag-ZnO/cellulose composite. The hydrothermal treatment brings about the deposition of Ag and ZnO NPs from their precursor solution onto the cellulose's large surface area, with no agglomeration of the NPs. The Ag-ZnO/cellulose nanocomposite showed promising antibacterial characteristics and stability in experimental settings, suggesting it may find use in the removal of pollutants. The antibacterial capabilities of the Ag-ZnO particles placed on the surface of the cellulose mat fibers show that the noble nanocomposite mat may be employed as an affordable and environmentally compatible water filter.

CHAPTER 6

6. SUMMARY AND CONCLUSIONS

6.1. Summary

Sterculia villosa (Roxb.), often known as ‘Murgilo or Mudilo’, and *Bauhinia vahlii* locally known as ‘Bhorlo’ are fast-growing plant species indigenous to south Asia. Comparatively little research has been done on the material characteristics of fiber produced from these plant species. Fiber biomass from these plants is often regarded as water-resistant and high in strength. Therefore, they are used in local levels for fastening purposes in wet or humid settings.

Broadly, this research explored the Physico-mechanical properties of cellulosic fiber obtained from *Sterculia villosa* (Roxb.) and *Bauhinia vahlii* and the nano-composite membrane. The specific objectives were, i) extraction of cellulosic fiber by different chemical methods, ii) chemical composition analysis of cellulose, lignin, and hemicellulose of fiber extracted by different methods, iii) physico-mechanical properties of the fiber obtained from the plants, iv) fabrication of the cellulose membrane, v) incorporation of the ZnO and Ag nanoparticles on the cellulose membrane by hydrothermal method and measure the antimicrobial, photocatalytic dye degradation efficiency of the fabricated nanocomposite membrane.

This dissertation consists of seven chapters, excluding references and appendices. The first chapter of the thesis contains the introduction and discusses the context, rationale, research question, objectives, and thesis organization. Each chapter (2-5) is arranged as an abstract, introduction, materials and methods, result and discussion, and conclusions. Chapter -2 deals with a “systematic study on material properties of water-retted *Sterculia villosa* (Roxb.) and *Bauhinia vahlii* fiber”. It covers the material characteristics of fibers that have been water-retted for long durations. In this study, two kinds of fiber were retted in tank water after 0, 20, 30, and 55 days. The percentage of weight lost by *Sterculia villosa* (Roxb.) fiber after being retted for 20, 30, and 55 days was 10.5, 15.2, and 17.5%, respectively. *Bauhinia vahlii* fiber had similar values of 4.1%, 5.1%, and 8.1%. According to these results, *Sterculia villosa* (Roxb.) fiber is more effective in retting than *Bauhinia vahlii* fiber. The breaking tenacity of *Sterculia*

villosa (Roxb.) fiber went up ($p < 0.05$) during the course of 55 days, from 18.3 ± 1.6 (mean 95% CI) to 26.9 ± 2.7 g/tex ($R^2 = 0.73$). During the same time frame, there was no significant change in the mechanical strength of *Bauhinia vahlii* fiber ($p > 0.05$). It was found that the mechanical strength of *Sterculia villosa* (Roxb.) fiber increased dramatically *Bauhinia vahlii*.

The chapter-3 describes the “Comparative study on material properties of wood-ash alkali and commercial alkali treated *Sterculia villosa* (Roxb.) fiber”. In this study, raw *Sterculia villosa* (Roxb.) fiber was treated with an alkali made from wood ash. Comparisons were made between unprocessed and commercially available alkali-treated fiber, as well as alkali-treated fiber made from wood ash, with regard to net weight reduction, fiber width, and surface morphology. It was determined that following NaOH and WAA treatment, the biomass lost a net of $41.33 \pm 3.3\%$ and $29.1 \pm 2.6\%$, respectively. The weight loss by alkali treatment was also supported by decreased fiber diameter. Untreated, WAA-treated, and NaOH-treated samples were found to have an average fiber bundle diameter ($n = 275$) of 446.0 ± 40.2 , 227.0 ± 25.0 , and 227.9 ± 20.0 μm , respectively, at 95% CI. The cellulose fibers produced by both methods were also thoroughly evaluated for their mechanical strength, heat resistance, and crystallinity. The Crystallinity Index was discovered to be 47%, 55%, and 58% in untreated, WAA, and NaOH treated samples, respectively. The thermal stability and crystallinity of fibers produced using both methods were improved over those of untreated samples. Based on these findings, wood ash alkali might be used to treat lignocellulose fiber in a laboratory setting. Alkali derived from wood ash could be a better option.

Chapter-4 evaluates “Kinetics of water sorption in single *Sterculia villosa* (Roxb.) and *Bauhinia vahlii* fibers at ambient temperature”. The kinetics of water sorption in unprocessed and alkali-treated lignocellulose fiber isolated from plants were the major focus of this study. The sorption results were also compared to those of alkali-treated fibers. The mechanical strength of the alkali-treated fibers was then evaluated in both the absorbed and dehydrated states. Dry and wet WAA-treated *Sterculia villosa* (Roxb.) fiber had a breaking tenacity of 33.6 ± 2.5 and 24.7 ± 2.7 g/tex. NaOH treatment resulted in values of 32.5 ± 3.5 g/tex and 30.0 ± 3.4 g/tex for the related variables. The equilibrium water absorption of *Bauhinia vahlii* fiber treated with NaOH and WAA decreases to 80% from 165% in untreated samples. The equilibrium water content of the alkali-

treated fiber was much lower than that of the untreated fiber. Notably, the mechanical strength of alkali-processed fiber significantly decreased when it was in a sorbed state. The chapter-5 describes “Fabrication of Ag-ZnO/cellulose nanocomposite mat for dye degradation and antimicrobial packaging”. *Sterculia villosa* (Roxb.) and *Bauhinia vahlii* are found to be high-strength fibers. Nanocomposite Ag-ZnO/cellulose is synthesized using their fiber mat as the matrix. In experimental conditions, the Ag-ZnO/cellulose nanocomposite demonstrated encouraging antibacterial properties and stability. Due to the photocatalytic and antibacterial properties of the Ag-ZnO particles coated on the cellulose mat as nanocomposite material has the potential to be used as a cheap and eco-friendly water filter.

Overall findings and suggestions for future research, and the thesis is summed up and highlighted in Chapter 6.

Finally, fibers from *Sterculia villosa* (Roxb.) and *Bauhinia vahlii* fiber are high strength fibers and are highly resistant to water and might be studied further as a crucial component in the production of cellulose-based composite materials optimized for use in wet environments.

6.2. Conclusions

Sterculia villosa (Roxb.) and *Bauhinia vahlii* fibers were retted in water for various periods, and their lignocellulosic content and water retting effectiveness were analyzed. After being subjected to retting, *Sterculia villosa* (Roxb.) fiber loses a significant amount of its lignin, ash, and extractive components, and therefore, its weight. The lower percentage increase in *Bauhinia vahlii* fiber suggests less effective retting. During the roughly 2-month retting period, the mechanical strength of *Sterculia villosa* (Roxb.) fiber rose dramatically whereas *Bauhinia vahlii* fiber maintained its initial strength. The thermal stability of both fibers was improved when they were retted in water.

The lignocellulose fiber obtained from the *Sterculia villosa* (Roxb.) plant was treated with an alkaline solution derived from wood ash. Weight reduction, fiber breadth, fiber shape, mechanical strength, thermal stability, and crystallinity are just a few of the critical material properties that were examined to determine how well wood ash alkali-treated fiber performed in comparison to both untreated and commercially available alkali-treated fibers. WAA and NaOH treatments effectively removed a substantial

amount of lignin and hemicellulose. Both processes produced fibers with comparable tensile and breaking strengths. Both methods provide fibers that are more crystalline and thermally stable than their raw material counterparts. These results indicated that lignocellulose fiber could be treated with alkali derived from wood ash in a controlled environment.

Sorption kinetics were performed on untreated and alkali-treated *Sterculia villosa* (Roxb.) and *Bauhinia vahlii* fibers. The permeability and diffusion coefficients were calculated by fitting the experimental data to a Fickian model. For untreated fiber, it was shown that the diffusion coefficient was much higher during the first stages of immersion compared to the latter stages. Diffusion coefficient measurements showed that alkali-treated samples were nearly an order of magnitude higher than their untreated counterparts for both fiber types. The equilibrium water content of the alkali-treated fiber was much less than that of the untreated fiber. The mechanical strength of alkali-fiber that has been absorbed was shown to drop dramatically.

Using hydrothermal processing, a stable Ag-doped ZnO/cellulose composite was produced. The Ag-ZnO/cellulose composite showed photocatalytic activity in the degradation of MB dye. The hydrothermal treatment of cellulose deposits Ag and ZnO NPs from the precursor solution onto the broad cellulose surface without NP agglomeration. The antibacterial characteristics of the Ag-ZnO/cellulose nanocomposite and its experimental stability suggest that it could have used in pollution control. Since the Ag-ZnO particles placed onto the cellulose mat fibers have antibacterial properties, the nanocomposite mat has the potential to be used as a low-cost, eco-friendly water filter.

6.3. Recommendations for Further work

On the basis of the findings made in this study, following recommendation can be made.

6.3.1. Research recommendations

- The high-water resistance of *Sterculia villosa* (Roxb.) and *Bauhinia vahlii* fibers suggests they might be an important component in the development of cellulose-based composite materials with enhanced performance in damp conditions, and so warrants further research.
- Small-scale paper and pulp mills might use an alkaline solution derived from wood ash for the chemical processing of lignocellulose biomass.

- It may be worthwhile to investigate, in the future, the water sorption kinetics of *Sterculia villosa* (Roxb.) and *Bauhinia vahlii* paper sheets and composite materials.
- The Ag-ZnO/cellulose nanocomposite mat might serve as a low-cost, environmentally friendly water filter. More study is needed to evaluate the effectiveness and economic viability of alternating concentration.

6.3.2. Policy recommendations

- *Sterculia villosa* (Roxb.) and *Bauhinia vahlii* plants available in the hilly region of Nepal and can be promoted as alternative for pulp and paper industries. This will help to rise economic status of local people.
- *Sterculia villosa* (Roxb.) and *Bauhinia vahlii* can be used to prepare high strength material. Further research investment is required to explore this area.

REFERENCES

- Adeeyo, O., Oresgun, O. M., & Oladimeji, T. E. (2015). Compositional analysis of lignocellulosic materials: Evaluation of an economically viable method suitable for woody and non-woody biomass. *American Journal of Engineering Research (AJER)*, **4**(4): 14-19.
- Agger, J. W., Isaksen, T., Várnai, A., Vidal-Melgosa, S., Willats, W. G., Ludwig, R., Horn, S. J., Eijsink, V. G., & Westereng, B. (2014). Discovery of LPMO activity on hemicelluloses shows the importance of oxidative processes in plant cell wall degradation. *Proceedings of the National Academy of Sciences*, **111**(17): 6287-6292. doi:10.1073/pnas.1323629111
- Åkerholm, M., Hinterstoisser, B., & Salmén, L. (2004). Characterization of the crystalline structure of cellulose using static and dynamic FT-IR spectroscopy. *Carbohydrate Research*, **339**(3): 569-578. doi:10.1016/j.carres.2003.11.012
- Akin, D. E., Condon, B., Sohn, M., Foulk, J. A., Dodd, R. B., & Rigsby, L. L. (2007). Optimization for enzyme-retting of flax with pectate lyase. *Industrial Crops and Products*, **25**(2): 136-146. doi:10.1016/j.indcrop.2006.08.003
- Aladpoosh, R., Montazer, M., & Samadi, N. (2014). In situ green synthesis of silver nanoparticles on cotton fabric using *Seidlitzia rosmarinus* ashes. *Cellulose*, **21**(5): 3755-3766. doi:10.1007/s10570-014-0369-1
- Ali, A., Ambreen, S., Maqbool, Q., Naz, S., Shams, M. F., Ahmad, M., Phull, A. R., & Zia, M. (2016). Zinc impregnated cellulose nanocomposites: Synthesis, characterization and applications. *Journal of Physics and Chemistry of Solids*, **98**: 174-182. doi:10.1016/j.jpics.2016.07.007
- Amara, C., El Mahdi, A., Medimagh, R., & Khwaldia, K. (2021). Nanocellulose-based composites for packaging applications. *Current Opinion in Green and Sustainable Chemistry*, **31**: 100512. doi:10.1016/j.cogsc.2021.100512
- Aryal, G. M., Kandel, K. P., Bhattarai, R. K., Giri, B., Adhikari, M., Ware, A., Han, S., George, G., Luo, Z., & Gautam, B. R. (2022). Material Properties of Traditional Handmade Paper Samples Fabricated from Cellulosic Fiber of Lokta Bushes. *ACS Omega*, **7**(36): 32717-32726. doi:10.1021/acsomega.2c04398

- ASTM. (2004). ASTM D1776-04 *Standard Practice for Conditioning and Testing Textiles*, **07.01:5**, American Society for Testing and Materials.
- Azizan, A., Samsudin, A. A., Shamshul Baharin, M. B., Dzulkiflee, M. H., Rosli, N. R., Abu Bakar, N. F., & Adlim, M. (2023). Cellulosic fiber nanocomposite application review with zinc oxide antimicrobial agent nanoparticle: An opt for COVID-19 purpose. *Environmental Science and Pollution Research*, **30(7)**: 16779-16796. doi:10.1007/s11356-022-18515-5
- Bajpai, P. (2015). Green Chemistry and Sustainability in Pulp and Paper Industry. *Basic Overview of Pulp and Paper Manufacturing Process*. Manhattan: Cham, Springer International Publishing.
- Bajpai, P. (2018). Paper and Board Making, *Biermann's Handbook of Pulp and Paper*, **2**: Elsevier.
- Bajpai, P. (2018). Brief Description of the Pulp and Papermaking Process. *Biotechnology for Pulp and Paper Processing*. Singapore: Springer Singapore.
- Banik, S., Basak, M., Paul, D., Nayak, P., Sardar, D., Sil, S., Sanpui, B., & Ghosh, A. (2003). Ribbon retting of jute-a prospective and eco-friendly method for improvement of fibre quality. *Industrial Crops Products*, **17(3)**: 183-190. doi:10.1016/S0926-6690(02)00097-3
- Beadle, C., Turnbull, C., & Dean, G. (1996). Environmental effects on growth and kraft pulp yield of Eucalyptus globulus and E. nitens. *Appita Journal*, **49(4)**: 239-242.
- Beckermann, G., & Pickering, K. L. (2008). Engineering and evaluation of hemp fibre reinforced polypropylene composites: fibre treatment and matrix modification. *Composites Part A: Applied Science and Manufacturing*, **39(6)**: 979-988. doi:10.1016/j.compositesa.2008.03.010
- Beghelo, L. (1998). The influence of carboxymethylation on the fiber flocculation process. *Nordic Pulp & Paper Research Journal*, **13(4)**: 269-273. doi:10.3183/npprj-1998-13-04-p269-273
- Biemer, J. J. (1973). Antimicrobial susceptibility testing by the Kirby-Bauer disc diffusion method. *Annals of Clinical & Laboratory Science*, **3(2)**: 135-140.

- Boopathi, L., Sampath, P., & Mylsamy, K. (2012). Investigation of physical, chemical and mechanical properties of raw and alkali treated Borassus fruit fiber. *Compos. B. Eng.*, **43**(8): 3044-3052. doi:10.1016/j.compositesb.2012.05.002
- Booth, I., Goodman, A. M., Grishanov, S. A., & Harwood, R. J. (2004). A mechanical investigation of the retting process in dew-retted hemp (*Cannabis sativa*). *Annals of Applied Biology*, **145**(1): 51-58. doi:10.1111/j.1744-7348.2004.tb00358.x
- Brebu, M. (2020). Environmental degradation of plastic composites with natural fillers- a review. *Polymers*, **12**(1): 166. doi:10.3390/polym12010166
- Brindha, R., Narayana, C., Vijayalakshmi, V., & Nachane, R. (2019). Effect of different retting processes on yield and quality of banana pseudostem fiber. *Journal of Natural Fibers*, **16**(1): 58-67. doi:10.1080/15440478.2017.1401505
- Camargo, P. H. C., Satyanarayana, K. G., & Wypych, F. (2009). Nanocomposites: synthesis, structure, properties and new application opportunities. *Materials Research*, **12**: 1-39. doi:10.1590/S1516-14392009000100002
- Céline, A., Fréour, S., Jacquemin, F., & Casari, P. (2014). The hygroscopic behavior of plant fibers: a review. *Frontiers in Chemistry*, **1**: 43. doi:10.3389/fchem.2013.00043
- Chabbert, B., Padovani, J., Djemiel, C., Ossemond, J., Lemaître, A., Yoshinaga, A., Hawkins, S., Grec, S., Beaugrand, J., & Kurek, B. (2020). Multimodal assessment of flax dew retting and its functional impact on fibers and natural fiber composites. *Industrial Crops and Products*, **148**: 112255. doi:10.1016/j.indcrop.2020.112255
- Chakraborty, D., Dahiya, S., Amulya, K., Srivastav, V., & Mohan, S. V. (2019). Valorization of paper and pulp waste: Opportunities and prospects of biorefinery. *Industrial and Municipal Sludge*. Oxford: Butterworth-Heinemann.
- Chandrasekar, M., Ishak, M., Sapuan, S., Leman, Z., & Jawaid, M. (2017). A review on the characterisation of natural fibres and their composites after alkali treatment and water absorption. *Plastics, Rubber and Composites*, **46**(3): 119-136. doi:10.1080/14658011.2017.1298550

- Subash, M. c., & Muthiah, P. (2021). Eco-friendly degumming of natural fibers for textile applications: A comprehensive review. *Cleaner Engineering and Technology*, **5**: 100304. doi:10.1016/j.clet.2021.100304
- Chauhan, S., & Meena, B. L. (2021). Introduction to pulp and paper industry: Global scenario. *Physical Sciences Reviews*, **6**(5), 81–109. doi:10.1515/psr-2020-0014
- Chauhan, S., Sharma, A. K., Jain, R. K., & Jain, R. K. (2013). Enzymatic Retting: A Revolution in the Handmade Papermaking from *Calotropis procera*. In R. C. Kuhad & A. Singh (Eds.), *Biotechnology for Environmental Management and Resource Recovery*. India: Springer India.
- Das, A. M., Ali, A. A., & Hazarika, M. P. (2014). Synthesis and characterization of cellulose acetate from rice husk: eco-friendly condition. *Carbohydrate Polymers*, **112**: 342-349. doi:10.1016/j.carbpol.2014.06.006
- Dasore, A., Rajak, U., Balijepalli, R., Verma, T. N., & Ramakrishna, K. (2022). An overview of refinements, processing methods and properties of natural fiber composites. *Proceedings of the Materials Today, 2021*, **49**: 296-300. doi:10.1016/j.matpr.2021.02.103
- Davies, G. C., & Bruce, D. M. (1998). Effect of environmental relative humidity and damage on the tensile properties of flax and nettle fibers. *Textile Research Journal*, **68**(9): 623-629. doi:10.1177/0040517598068009
- Djemiel, C., Grec, S., & Hawkins, S. (2017). Characterization of bacterial and fungal community dynamics by high-throughput sequencing (HTS) metabarcoding during flax dew-retting. *Frontiers in Microbiology*, **8**: 2052. doi:10.3389/fmicb.2017.02052
- Du, H., Liu, W., Zhang, M., Si, C., Zhang, X., & Li, B. (2019). Cellulose nanocrystals and cellulose nanofibrils based hydrogels for biomedical applications. *Carbohydrate Polymers*, **209**: 130-144. doi:10.1016/j.carbpol.2019.01.020
- Ebringerová, A., Hromádková, Z., & Heinze, T. (2005). Hemicellulose. In T. Heinze (Ed.), *Polysaccharides I: Structure, Characterization and Use*. Berlin, Heidelberg: Springer Berlin Heidelberg.
- El-Nahhal, I. M., Salem, J., Anbar, R., Kodeh, F. S., & Elmanama, A. (2020). Preparation and antimicrobial activity of ZnO-NPs coated cotton/starch and

- their functionalized ZnO-Ag/cotton and Zn (II) curcumin/cotton materials. *Scientific Reports*, **10**(1): 5410. doi:10.1038/s41598-020-61306-6
- Elanthikkal, S., Gopalakrishnapanicker, U., Varghese, S., & Guthrie, J. T. (2010). Cellulose microfibrils produced from banana plant wastes: Isolation and characterization. *Carbohydrate Polymers*, **80**(3): 852-859. doi:10.1016/j.carbpol.2009.12.043
- Elemike, E. E., Onwudiwe, D. C., Ogeleka, D. F., & Obasi, E. C. (2021). Biomediated cellulose-Ag-ZnO nanocomposites and their ecotoxicological assessment using onion bulb plant. *Journal of Cluster Science*, **32**: 651-656. doi:10.1007/s10876-020-01826-3
- Ericsson, B. H., Tunevall, G., & Wickman, K. (1960). The paper disc method for determination of bacterial sensitivity to antibiotics: Relationship between the diameter of the zone of inhibition and the minimum inhibitory concentration. *Scandinavian Journal of Clinical and Laboratory Investigation*, **12**(4): 414-422. doi:10.3109/00365516009065406
- Espert, A., Vilaplana, F., & Karlsson, S. (2004). Comparison of water absorption in natural cellulosic fibres from wood and one-year crops in polypropylene composites and its influence on their mechanical properties. *Composites Part A: Applied Science and Manufacturing*, **35**(11): 1267-1276. doi:10.1016/j.compositesa.2004.04.004
- Fengel, D., & Wegener, G. (2011). *Wood: chemistry, ultrastructure, reactions*. Berlin : Walter de Gruyter.
- Fornari, A., Rossi, M., Rocco, D., & Mattiello, L. (2022). A Review of Applications of Nanocellulose to Preserve and Protect Cultural Heritage Wood, Paintings, and Historical Papers. *Applied Sciences*, **12**(24). 12846. doi:10.3390/app122412846
- French, A. D. (2020). Increment in evolution of cellulose crystallinity analysis. *Cellulose*, **27**(10): 5445-5448. doi:10.1007/s10570-020-03172-z
- Ganan, P., Zuluaga, R., Velez, J. M., & Mondragon, I. (2004). Biological natural retting for determining the hierarchical structuration of banana fibers. *Macromolecular Bioscience*, **4**(10): 978-983. doi:10.1002/mabi.200400041

- Gandini, A., & Belgacem, M. N. (2012). The state of the art of polymers from renewable resources *Handbook of Biopolymers and Biodegradable Plastics: Properties, procession and applications*, Boston: William Andrew Publishing.
- Gaur, V. K., Sharma, P., Sirohi, R., Awasthi, M. K., Dussap, C.-G., & Pandey, A. (2020). Assessing the impact of industrial waste on environment and mitigation strategies: A comprehensive review. *Journal of Hazardous Materials*, **398**: 123019. doi:10.1016/j.jhazmat.2020.123019
- Ghosh, S. R., & Baruah, P. P. (1997). Sterculia villosa Roxb — A potential source of wood-fibre for pulp and paper making. *Bioresource Technology*, **62**(1): 43-46. doi:10.1016/S0960-8524(97)00047-3
- Gierer, J. (1980). Chemical aspects of kraft pulping. *Wood Science and Technology*, **14**(4): 241-266. doi:10.1007/BF00383453
- Gong, W., Liu, C., Mu, X., Du, H., Lv, D., Li, B., & Han, S. (2015). Hydrogen peroxide-assisted sodium carbonate pretreatment for the enhancement of enzymatic saccharification of corn stover. *ACS Sustainable Chemistry & Engineering*, **3**(12): 3477-3485. doi:10.1021/acssuschemeng.5b01278
- Gouanvé, F., Marais, S., Bessadok, A., Langevin, D., & Métayer, M. (2007). Kinetics of water sorption in flax and PET fibers. *European Polymer Journal*, **43**(2): 586-598. doi:10.1016/j.eurpolymj.2006.10.023
- Han, G., Cheng, W., Deng, J., Dai, C., Zhang, S., & Wu, Q. (2009). Effect of pressurized steam treatment on selected properties of wheat straws. *Industrial Crops and Products*, **30**(1): 48-53. doi:10.1016/j.indcrop.2009.01.004
- Haque, M. M., Hasan, M., Islam, M. S., & Ali, M. E. (2009). Physico-mechanical properties of chemically treated palm and coir fiber reinforced polypropylene composites. *Bioresource Technology*, **100**(20): 4903-4906. doi:10.1016/j.biortech.2009.04.072
- Hashim, M. Y., Amin, A. M., Marwah, O. M. F., Othman, M. H., Yunus, M. R. M., & Chuan Huat, N. (2017). The effect of alkali treatment under various conditions on physical properties of kenaf fiber. *Journal of Physics: Conference Series*, **914**(1): 012030. doi:10.1088/1742-6596/914/1/012030

- Haslinger, S., Ye, Y., Rissanen, M., Hummel, M., & Sixta, H. (2019). Cellulose fibers for high-performance textiles functionalized with incorporated gold and silver nanoparticles. *ACS Sustainable Chemistry & Engineering*, **8**(1): 649-658. doi:10.1021/acssuschemeng.9b06385
- Heinze, T. (2016). Cellulose: Structure and Properties. *Cellulose Chemistry and Properties: Fibers, Nanocelluloses and Advanced Materials*. Manhattan, Cham: Springer International Publishing.
- Heinze, T., El Seoud, O. A., & Koschella, A. (2018). Production and Characteristics of Cellulose from Different Sources. *Cellulose Derivatives: Synthesis, Structure, and Properties*. Manhattan, Cham: Springer International Publishing.
- Henriksson, G., Akin, D. E., Rigsby, L. L., Patel, N., & Eriksson, K.-E. L. (1997). Influence of chelating agents and mechanical pretreatment on enzymatic retting of flax. *Textile Research Journal*, **67**(11): 829-836. doi:10.1177/004051759706701107
- Henriksson, M., Berglund, L. A., Isaksson, P., Lindström, T., & Nishino, T. (2008). Cellulose nanopaper structures of high toughness. *Biomacromolecules*, **9**(6): 1579-1585. doi:10.1021/bm800038n
- Hu, L., Du, H., Liu, C., Zhang, Y., Yu, G., Zhang, X., Si, C., Li, B., & Peng, H. (2019). Comparative Evaluation of the Efficient Conversion of Corn Husk Filament and Corn Husk Powder to Valuable Materials via a Sustainable and Clean Biorefinery Process. *ACS Sustainable Chemistry & Engineering*, **7**(1): 1327-1336. doi:10.1021/acssuschemeng.8b05017
- Hubbe, M. A. (2000). Difficult furnishes. Proceedings of the *Proceedings TAPPI*, 1999. Atlanta, GA: TAPPI.
Retrieved from <http://www.lib.ncsu.edu/resolver/1840.2/48>
- Hubbe, M. A., & Bowden, C. (2009). Handmade paper: A review of its history, craft, and science. *BioResources*, **4**(4): 1736-1792.
- Hurren, C. J., Wang, X., Dennis, H. G., & Clarke, A. F. K. (2002). *Evaluation of bast fibre retting systems on hemp*. Proceedings of the 82nd Textile Institute World Conference, Cairo, Egypt.

- Ibănescu, M., Muşat, V., Textor, T., Badilita, V., & Mahltig, B. (2014). Photocatalytic and antimicrobial Ag/ZnO nanocomposites for functionalization of textile fabrics. *Journal of Alloys and Compounds*, **610**: 244-249.
doi:10.1016/j.jallcom.2014.04.138
- Ilyas, R., Sapuan, S., Ishak, M., & Zainudin, E. (2019). Sugar palm nanofibrillated cellulose (*Arenga pinnata* (Wurmb.) Merr): Effect of cycles on their yield, physic-chemical, morphological and thermal behavior. *International Journal of Biological Macromolecules*, **123**: 379-388. doi:10.1016/j.ijbiomac.2018.11.124
- Ioelovich, M. (2018). Determination of distortions and sizes of cellulose nanocrystallites. *Research Journal of Nanoscience and Engineering*, **2**(1): 1-5.
- Jankauskiene, Z., Lugauskas, A., & Repeckiene, J. (2007). New methods for the improvement of flax dew retting. *Journal of Natural Fibers*, **3**(4): 59-68.
doi:10.1300/J395v03n04_05
- Jaspal, D., & Malviya, A. (2020). Composites for wastewater purification: A review. *Chemosphere*, **246**: 125788. doi:10.1016/j.chemosphere.2019.125788
- Jasso-Gastinel, C. F. (2017). 8 - Gradients in Homopolymers, Blends, and Copolymers, *Modification of Polymer Properties*. New York : William Andrew Publishing.
- Jensen, C. U., Rodriguez Guerrero, J. K., Karatzos, S., Olofsson, G., & Iversen, S. B. (2017). Fundamentals of Hydrofaction™: Renewable crude oil from woody biomass. *Biomass Conversion and Biorefinery*, **7**(4): 495-509.
doi:10.1007/s13399-017-0248-8
- Joseph, P., Rabello, M. S., Mattoso, L., Joseph, K., & Thomas, S. (2002). Environmental effects on the degradation behaviour of sisal fibre reinforced polypropylene composites. *Composites Science and Technology*, **62**(10-11): 1357-1372. doi:10.1016/S0266-3538(02)00080-5
- Kalpana, V., & Devi Rajeswari, V. (2018). A review on green synthesis, biomedical applications, and toxicity studies of ZnO NPs. *Bioinorganic Chemistry and Applications*, **2018**. doi:10.1155/2018/3569758
- Kandel, K. P., Adhikari, M., Kharel, M., Aryal, G. M., Pandeya, S., Joshi, M. K., Dahal, B., Gautam, B., & Neupane, B. B. (2022). Comparative study on material

properties of wood-ash alkali and commercial alkali treated Sterculia fiber. *Cellulose*. doi:10.1007/s10570-022-04610-w

- Kandel, K. P., Aryal, G. M., & Neupane, B. B. (2023). Kinetics of water sorption in single Sterculia and Bauhinia fibers at ambient temperature. *Results in Chemistry*, **5**: 100872. doi:10.1016/j.rechem.2023.100872
- Kansal, S., Singh, M., & Sud, D. (2007). Studies on photodegradation of two commercial dyes in aqueous phase using different photocatalysts. *Journal of Hazardous Materials*, **141**(3): 581-590. doi:10.1016/j.jhazmat.2006.07.035
- Kapoor, V. P., Chanzy, H., & Taravel, F. R. (1995). X-ray diffraction studies on some seed galactomannans from India. *Carbohydrate Polymers*, **27**(3): 229-233. doi:10.1016/0144-8617(95)00045-9
- Keller, A., Leupin, M., Mediavilla, V., & Wintermantel, E. (2001). Influence of the growth stage of industrial hemp on chemical and physical properties of the fibres. *Industrial Crops and Products*, **13**(1): 35-48. doi:10.1016/S0926-6690(00)00051-0
- Kim, H.-S., Kim, S., Kim, H.-J., & Yang, H.-S. (2006). Thermal properties of bio-flour-filled polyolefin composites with different compatibilizing agent type and content. *Thermochimica Acta*, **451**(1-2): 181-188. doi:10.1016/j.tca.2006.09.013
- Kim, H. J., Joshi, M. K., Pant, H. R., Kim, J. H., Lee, E., & Kim, C. S. (2015). One-pot hydrothermal synthesis of multifunctional Ag/ZnO/fly ash nanocomposite. *Colloids and Surfaces A: Physicochemical and Engineering Aspects*, **469**: 256-262. doi:10.1016/j.colsurfa.2015.01.032
- Klemm, D., Heublein, B., Fink, H.-P., & Bohn, A. (2005). Cellulose: Fascinating Biopolymer and Sustainable Raw Material. *Angewandte Chemie International Edition*, **44**(22): 3358-3393. doi:10.1002/anie.200460587
- Kondo, T. (1997). The relationship between intramolecular hydrogen bonds and certain physical properties of regioselectively substituted cellulose derivatives. *Journal of Polymer Science Part B: Polymer Physics*, **35**(4): 717-723. doi:10.1002/(SICI)1099-0488(199703)35:4<717::AID-POLB18>3.0.CO;2-J

- Kondo, T., & Sawatari, C. (1996). A Fourier transform infra-red spectroscopic analysis of the character of hydrogen bonds in amorphous cellulose. *Polymer*, **37**(3): 393-399. doi:10.1016/0032-3861(96)82908-9
- Kozłowski, R., Batog, J., Konczewicz, W., Mackiewicz-Talarczyk, M., Muzyczek, M., Sedelnik, N., & Tanska, B. (2006). Enzymes in bast fibrous plant processing. *Biotechnology Letters*, **28**(10): 761-765. doi:10.1007/s10529-006-9044-4
- Kozłowski, R. M., & Różańska, W. (2020). Enzymatic treatment of natural fibres *Handbook of Natural Fibres*, 227-244: Elsevier.
- Krässig, H. A. (1993). *Cellulose: structure, accessibility and reactivity*. Philadelphia: Gordon and Breach Science Publishers.
- Larocque, G., & Maass, O. (1941). The mechanism of the alkaline delignification of wood. *Canadian Journal of Research*, **19**(1): 1-16. doi:10.1139/cjr41b-001
- Lee, C., Khalina, A., Lee, S. H., & Liu, M. (2020). A Comprehensive Review on Bast Fibre Retting Process for Optimal Performance in Fibre-Reinforced Polymer Composites. *Advances in Materials Science and Engineering*, **2020**: 6074063. doi:10.1155/2020/6074063
- Lee, C. M., Kafle, K., Park, Y. B., & Kim, S. H. (2014). Probing crystal structure and mesoscale assembly of cellulose microfibrils in plant cell walls, tunicate tests, and bacterial films using vibrational Sum Frequency Generation (SFG) spectroscopy. *Physical Chemistry Chemical Physics*, **16**(22): 10844-10853. doi:10.1039/C4CP00515E
- Lin, Q., Zhou, X., & Dai, G. (2002). Effect of hydrothermal environment on moisture absorption and mechanical properties of wood flour-filled polypropylene composites. *Journal of Applied Polymer Science*, **85**(14): 2824-2832. doi:10.1002/app.10844
- Liu, H., You, L., Jin, H., & Yu, W. (2013). Influence of alkali treatment on the structure and properties of hemp fibers. *Fibers and Polymers*, **14**(3): 389-395. doi:10.1007/s12221-013-0389-8
- Liu, H., Zhong, L., Govindaraju, S., & Yun, K. (2019). ZnO rod decorated with Ag nanoparticles for enhanced photocatalytic degradation of methylene blue. *Journal of Physics and Chemistry of Solids*, **129**: 46-53.

doi:10.1016/j.jpccs.2018.12.040

Liu, K., Du, H., Zheng, T., Liu, H., Zhang, M., Zhang, R., Li, H., Xie, H., Zhang, X., Ma, M., & Si, C. (2021). Recent advances in cellulose and its derivatives for oilfield applications. *Carbohydrate Polymers*, **259**: 117740.

doi:10.1016/j.carbpol.2021.117740

Liu, W., Du, H., Zhang, M., Liu, K., Liu, H., Xie, H., Zhang, X., & Si, C. (2020). Bacterial cellulose-based composite scaffolds for biomedical applications: a review. *ACS Sustainable Chemistry & Engineering*, **8**(20): 7536-7562.

doi:10.1021/acssuschemeng.0c00125

López, F., Ariza, J., Pérez, I., & Jiménez, L. (2000). Comparative study of paper sheets from olive tree wood pulp obtained by soda, sulphite or kraft pulping. *Bioresource Technology*, **71**(1): 83-86. doi:10.1016/S0960-8524(99)00044-9

Lundell, F., Söderberg, L. D., & Alfredsson, P. H. (2011). Fluid mechanics of papermaking. *Annual Review of Fluid Mechanics*, **43**: 195-217.

Luo, Y., Li, Z., Li, X., Liu, X., Fan, J., Clark, J. H., & Hu, C. (2019). The production of furfural directly from hemicellulose in lignocellulosic biomass: A review. *Catalysis Today*, **319**: 14-24. doi:10.1016/j.cattod.2018.06.042

Manimaran, P., Pillai, G. P., Vignesh, V., & Prithiviraj, M. (2020). Characterization of natural cellulosic fibers from Nendran Banana Peduncle plants. *International Journal of Biological Macromolecules*, **162**: 1807-1815.

doi:10.1016/j.ijbiomac.2020.08.111

Marrakchi, Z., Khiari, R., Oueslati, H., Mauret, E., & Mhenni, F. (2011). Pulping and papermaking properties of Tunisian Alfa stems (*Stipa tenacissima*)—effects of refining process. *Industrial Crops and Products*, **34**(3): 1572-1582.

doi:10.1016/j.indcrop.2011.05.022

Mazian, B., Bergeret, A., Benezet, J.-C., & Malhautier, L. (2018). Influence of field retting duration on the biochemical, microstructural, thermal and mechanical properties of hemp fibres harvested at the beginning of flowering. *Industrial Crops and Products*, **116**: 170-181. doi:10.1016/j.indcrop.2018.02.062

- Mboowa, D. (2021). A review of the traditional pulping methods and the recent improvements in the pulping processes. *Biomass Conversion and Biorefinery*, doi:10.1007/s13399-020-01243-6
- Mckean, W., & Jacobs, R. (1997). Wheat straw as a paper fiber source. *Washington, USA: Clean Washington Center*.
- Meireles, C. d. S., Filho, G. R., Fernandes Ferreira Jr, M., Cerqueira, D. A., Assunção, R. M. N., Ribeiro, E. A. M., Poletto, P., & Zeni, M. (2010). Characterization of asymmetric membranes of cellulose acetate from biomass: Newspaper and mango seed. *Carbohydrate Polymers*, **80**(3): 954-961. doi:10.1016/j.carbpol.2010.01.012
- Mejouyo, P., Nkemaja, E. D., Beching, O., Tagne, N., Kana'a, T., & Njeugna, E. (2020). Physical and Tensile Properties of Handmade *Sida rhombifolia* Paper. *International Journal of Biomaterials*, **2020**. doi:10.1155/2020/3967641
- Moon, R. J., Martini, A., Nairn, J., Simonsen, J., & Youngblood, J. (2011). Cellulose nanomaterials review: structure, properties and nanocomposites. *Chemical Society Reviews*, **40**(7): 3941-3994. doi:10.1039/C0CS00108B
- Naylor, T. d. (1989). 20 - Permeation Properties. *Comprehensive Polymer Science and Supplements*. 643-668. Amsterdam: Pergamon.
- Negahdar, L., Delidovich, I., & Palkovits, R. (2016). Aqueous-phase hydrolysis of cellulose and hemicelluloses over molecular acidic catalysts: Insights into the kinetics and reaction mechanism. *Applied Catalysis B: Environmental*, **184**: 285-298. doi:10.1016/j.apcatb.2015.11.039
- Nosbi, N., Akil, H. M., Ishak, Z. A. M., & Bakar, A. A. (2011). Behavior of kenaf fibers after immersion in several water conditions. *BioResources*, **6**(2): 950-960.
- Nykter, M., Kymäläinen, H.-R., Thomsen, A. B., Lilholt, H., Koponen, H., Sjöberg, A.-M., & Thygesen, A. (2008). Effects of thermal and enzymatic treatments and harvesting time on the microbial quality and chemical composition of fibre hemp (*Cannabis sativa* L.). *Biomass and Bioenergy*, **32**(5): 392-399. doi:10.1016/j.biombioe.2007.10.015

- Obi Reddy, K., Uma Maheswari, C., Shukla, M., & Muzenda, E. (2014). Preparation, chemical composition, characterization, and properties of Napier grass paper sheets. *Separation Science and Technology*, **49**(10): 1527-1534.
doi:10.1080/01496395.2014.893358
- Page, D. H. (1969). A theory for the tensile strength of paper. *Tappi*, **52**: 674-681.
Retrieved from <https://cir.nii.ac.jp/crid/1573387449845857408>
- Paridah, M. T., Basher, A. B., SaifulAzry, S., & Ahmed, Z. (2011). Retting process of some bast plant fibres and its effect on fibre quality: A review. *BioResources*, **6**(4): 5260-5281.
- Park, S., Baker, J. O., Himmel, M. E., Parilla, P. A., & Johnson, D. K. (2010). Cellulose crystallinity index: measurement techniques and their impact on interpreting cellulase performance. *Biotechnology for Biofuels*, **3**(1): 1-10.
doi:10.1186/1754-6834-3-10
- Pauly, M., Albersheim, P., Darvill, A., & York, W. S. (1999). Molecular domains of the cellulose/xyloglucan network in the cell walls of higher plants. *The Plant Journal*, **20**(6): 629-639. doi:10.1046/j.1365-313X.1999.00630.x
- Peng, P., & She, D. (2014). Isolation, structural characterization, and potential applications of hemicelluloses from bamboo: A review. *Carbohydrate Polymers*, **112**: 701-720. doi:10.1016/j.carbpol.2014.06.068
- Pérez, S. and Mazeau, K. (2005) Conformations, Structures, and Morphologies of Celluloses. *Polysaccharides: Structural Diversity and Functional Versatility*, 41-68. New York: Marcel Dekker, Inc.
- Peterson, A. A., Vogel, F., Lachance, R. P., Fröling, M., Antal, J. M. J., & Tester, J. W. (2008). Thermochemical biofuel production in hydrothermal media: A review of sub- and supercritical water technologies. *Energy & Environmental Science*, **1**(1): 32-65. doi:10.1039/B810100K
- Poletto, M., Ornaghi Junior, H. L., & Zattera, A. J. (2014). Native cellulose: structure, characterization and thermal properties. *Materials*, **7**(9): 6105-6119.
doi:10.3390/ma7096105

- Poletto, M., Pistor, V., Santana, R. M. C., & Zattera, A. J. (2012). Materials produced from plant biomass: part II: evaluation of crystallinity and degradation kinetics of cellulose. *Materials Research*, **15**: 421-427.
doi:10.1590/S1516-14392012005000048
- Punyamurthy, R., Sampathkumar, D., Srinivasa, C. V., & Bennehalli, B. (2012). Effect of alkali treatment on water absorption of single cellulosic abaca fiber. *BioResources*, **7**(3): 3515-3524.
- Rafaie, H., Nor, R., Azmina, M., Ramli, N., & Mohamed, R. (2017). Decoration of ZnO microstructures with Ag nanoparticles enhanced the catalytic photodegradation of methylene blue dye. *Journal of Environmental Chemical Engineering*, **5**(4): 3963-3972. doi:10.1016/j.jpcs.2018.12.040
- Rao, V. S. R., Sundararajan, P. R., Ramakrishnan, C., & Ramachandran, G. N. (1967). Conformational Studies of Amylose††Contribution No. 204 from the Centre of Advanced Study in Biophysics, University of Madras, Madras 25, India. In G. N. Ramachandran (Ed.), *Conformation of Biopolymers*. Massachusetts: Academic Press.
- Ray, R., Das, S. N., Mohapatra, A., & Das, H. C. (2020). Comprehensive characterization of a novel natural Bauhinia Vahlia stem fiber. *Polymer Composites*, **41**(9): 3807-3816. doi:10.1002/pc.25678
- Reddy, N., & Yang, Y. (2007). Natural cellulose fibers from switchgrass with tensile properties similar to cotton and linen. *Biotechnology & Bioengineering*, **97**(5): 1021-1027. doi:10.1002/bit.21330
- Reis, R. S., Souza, D. d. H. S., Marques, M. d. F. V., da Luz, F. S., & Monteiro, S. N. (2021). Novel bionanocomposite of polycaprolactone reinforced with steam-exploded microfibrillated cellulose modified with ZnO. *Journal of Materials Research and Technology*, **13**: 1324-1335. doi:10.1016/j.jmrt.2021.05.043
- Ribeiro, A., Pochart, P., Day, A., Mennuni, S., Bono, P., Baret, J.-L., Spadoni, J.-L., & Mangin, I. (2015). Microbial diversity observed during hemp retting. *Applied Microbiology and Biotechnology*, **99**: 4471-4484. doi:10.1007/s00253-014-6356-5

- Ronald Aseer, J., Sankaranarayanan, K., Jayabalan, P., Natarajan, R., & Priya Dasan, K. (2013). Morphological, physical, and thermal properties of chemically treated banana fiber. *Journal of Natural Fibers*, **10**(4): 365-380. doi:10.1080/15440478.2013.824848
- Roubroeks, J. P., Andersson, R., & Åman, P. (2000). Structural features of (1→3),(1→4)-β-d-glucan and arabinoxylan fractions isolated from rye bran. *Carbohydrate Polymers*, **42**(1): 3-11. doi:10.1016/S0144-8617(99)00129-0
- Ruan, P., Raghavan, V., Garipey, Y., & Du, J. (2015). Characterization of flax water retting of different durations in laboratory condition and evaluation of its fiber properties. *BioResources*, **10**(2): 3553-3563. doi:10.15376/biores.10.2.3553-3563
- Saha, P., Manna, S., Chowdhury, S. R., Sen, R., Roy, D., & Adhikari, B. (2010). Enhancement of tensile strength of lignocellulosic jute fibers by alkali-steam treatment. *Bioresource Technology*, **101**(9): 3182-3187. doi:10.1016/j.biortech.2009.12.010
- Sahu, P., & Gupta, M. (2022). Water absorption behavior of cellulosic fibres polymer composites: a review on its effects and remedies. *Journal of Industrial Textiles*, **51**(5_suppl): 7480S-7512S. doi:10.1177/1528083720974424
- Saikia, D. (2010). Studies of Water Absorption Behavior of Plant Fibers at Different Temperatures. *International Journal of Thermophysics*, **31**(4-5): 1020-1026. doi:10.1007/s10765-010-0774-0
- Sampson, W. (2004). A model for fibre contact in planar random fibre networks. *Journal of Materials Science*, **39**(8): 2775-2781. doi:10.1023/B:JMSC.0000021453.00080.5a
- Sannapapamma, K., Mariyappanavar, S., Sangannavar, V. V., Jamadar, D., Vastrad, J. V., & Byadagi, S. A. (2020). Development and quality assessment of handmade papers using underutilized agro based natural fibres. *Journal of Pharmacognosy and Phytochemistry*, **9**(2): 1410-1417.
- Scheller, H. V., & Ulvskov, P. (2010). Hemicelluloses. *Annual Review of Plant Biology*, **61**: 263-289. doi:10.1186/s40694-018-0052-7

- Sedighi, A., Montazer, M., & Hemmatinejad, N. (2014). Copper nanoparticles on bleached cotton fabric: in situ synthesis and characterization. *Cellulose*, **21**(3): 2119-2132. doi:10.1007/s10570-014-0215-5
- Segal, L., Creely, J. J., Martin Jr, A., & Conrad, C. (1959). An empirical method for estimating the degree of crystallinity of native cellulose using the X-ray diffractometer. *Textile Research Journal*, **29**(10): 786-794. doi:10.1177/004051755902901003
- Sharma, A., Thakur, M., Bhattacharya, M., Mandal, T., & Goswami, S. (2019). Commercial application of cellulose nano-composites—A review. *Biotechnology Reports*, **21**: e00316. doi:10.1016/j.btre.2019.e00316
- Sharma, P., & Singh, S. P. (2021). Pollutants Characterization and Toxicity Assessment of Pulp and Paper Industry Sludge for Safe Environmental Disposal. *Emerging Treatment Technologies for Waste Management*. Singapore: Springer Singapore.
- Shi, C., Zhang, L., Bian, H., Shi, Z., Ma, J., & Wang, Z. (2021). Construction of Ag–ZnO/cellulose nanocomposites via tunable cellulose size for improving photocatalytic performance. *Journal of Cleaner Production*, **288**: 125089. doi:10.1016/j.jclepro.2020.125089
- Sinha, E., & Rout, S. K. (2009). Influence of fibre-surface treatment on structural, thermal and mechanical properties of jute fibre and its composite. *Bulletin of Materials Science*, **32**(1): 65-76. doi:10.1007/s12034-009-0010-3
- Soszynski, R. (1995). Relative bonded area—a different approach. *Nordic Pulp and Paper Research Journal*. doi:10.3183/npprj-1995-10-02-p150-151
- Spinace, M. A., Lambert, C. S., Fermoselli, K. K., & De Paoli, M.-A. (2009). Characterization of lignocellulosic curaua fibres. *Carbohydrate Polymers*, **77**(1): 47-53. doi:10.1016/j.carbpol.2008.12.005
- Sui, G., Fuqua, M., Ulven, C., & Zhong, W. (2009). A plant fiber reinforced polymer composite prepared by a twin-screw extruder. *Bioresource Technology*, **100**(3): 1246-1251. doi:10.1016/j.biortech.2008.03.065


- Sun, S., Sun, S., Cao, X., & Sun, R. (2016). The role of pretreatment in improving the enzymatic hydrolysis of lignocellulosic materials. *Bioresource Technology*, **199**: 49-58. doi:10.1016/j.biortech.2015.08.061
- Symington, M. C., Banks, W. M., West, O. D., & Pethrick, R. (2009). Tensile testing of cellulose based natural fibers for structural composite applications. *Journal of Composite Materials*, **43**(9): 1083-1108. doi:10.1177/0021998308097740
- Tanpichai, S., Sampson, W. W., & Eichhorn, S. J. (2012). Stress-transfer in microfibrillated cellulose reinforced poly(lactic acid) composites using Raman spectroscopy. *Composites Part A: Applied Science and Manufacturing*, **43**(7): 1145-1152. doi:10.1016/j.compositesa.2012.02.006
- Tanpichai, S., Witayakran, S., Srimarut, Y., Woraprayote, W., & Malila, Y. (2019). Porosity, density and mechanical properties of the paper of steam exploded bamboo microfibers controlled by nanofibrillated cellulose. *Journal of Materials Research and Technology*, **8**(4): 3612-3622. doi:10.1016/j.jmrt.2019.05.024
- Tao, J., & Liu, H. (2011). A method to determine sheet relative bonded area using the fiber flexibility index. *Instrumentation Science and Technology*, **39**(2): 161-172. doi:10.1080/10739149.2010.545849
- Thakur, K. K., Bhat, P., Kumar, A., Ravikanth, G., & Saikia, P. (2022). Distribution mapping of *Bauhinia vahlii* Wight & Arn. in India using ecological niche modelling. *Tropical Ecology*, **63**(2): 286-299. doi:10.1007/s42965-021-00197-8
- Veerasingh, A., Shanmugam, V., Rajendran, S., Johnson, D. J., Subbiah, A., Koilpichai, J., & Marimuthu, U. (2022). Thermal Properties of Natural Fiber Sisal Based Hybrid Composites – A Brief Review. *Journal of Natural Fibers*, **19**(12): 4696-4706. doi:10.1080/15440478.2020.1870619
- Vigneshwaran, S., Sundarakannan, R., John, K., Johnson, R. D. J., Prasath, K. A., Ajith, S., Arumugaprabu, V., & Uthayakumar, M. (2020). Recent advancement in the natural fiber polymer composites: A comprehensive review. *Journal of Cleaner Production*, **277**: 124109. doi:10.1016/j.jclepro.2020.124109

- von Schenck, A., Berglin, N., & Uusitalo, J. (2013). Ethanol from Nordic wood raw material by simplified alkaline soda cooking pre-treatment. *Applied Energy*, **102**: 229-240. doi:10.1016/j.apenergy.2012.10.003
- Wang, H., Xie, H., Du, H., Wang, X., Liu, W., Duan, Y., Zhang, X., Sun, L., Zhang, X., & Si, C. (2020). Highly Efficient Preparation of Functional and Thermostable Cellulose Nanocrystals via H₂SO₄ Intensified Acetic Acid Hydrolysis. *Carbohydrate Polymers*, **239**: 116233. doi:10.1016/j.carbpol.2020.116233
- Wyman, C., Decker, S., Himmel, M., Brady, J., Skopec, C., & Viikari, L. (2004). Hydrolysis of cellulose and hemicellulose. *Polysaccharides*. doi:10.1201/9781420030822.ch43
- Xu, F., Yu, J., Tesso, T., Dowell, F., & Wang, D. (2013). Qualitative and quantitative analysis of lignocellulosic biomass using infrared techniques: a mini-review. *Applied Energy*, **104**: 801-809. doi:10.1016/j.apenergy.2012.12.019
- Xu, H., Li, B., & Mu, X. (2016). Review of alkali-based pretreatment to enhance enzymatic saccharification for lignocellulosic biomass conversion. *Industrial & Engineering Chemistry Research*, **55**(32): 8691-8705. doi:10.1021/acs.iecr.6b01907
- Yamamoto, O. (2001). Influence of particle size on the antibacterial activity of zinc oxide. *International Journal of Inorganic Materials*, **3**(7): 643-646. doi:10.1016/S1466-6049(01)00197-0
- Yang, H., Xie, Y., Zheng, X., Pu, Y., Huang, F., Meng, X., Wu, W., Ragauskas, A., & Yao, L. (2016). Comparative study of lignin characteristics from wheat straw obtained by soda-AQ and kraft pretreatment and effect on the following enzymatic hydrolysis process. *Bioresource Technology*, **207**: 361-369. doi:10.1016/j.biortech.2016.01.123
- Yang, H., Yan, R., Chen, H., Zheng, C., Lee, D. H., & Liang, D. T. (2006). In-depth investigation of biomass pyrolysis based on three major components: hemicellulose, cellulose and lignin. *Energy & Fuels*, **20**(1): 388-393. doi:10.1021/ef0580117
- Yang, X., Xie, H., Du, H., Zhang, X., Zou, Z., Zou, Y., Liu, W., Lan, H., Zhang, X., & Si, C. (2019). Facile extraction of thermally stable and dispersible cellulose

- nanocrystals with high yield via a green and recyclable FeCl₃-catalyzed deep eutectic solvent system. *ACS Sustainable Chemistry & Engineering*, **7**(7): 7200-7208. doi:10.1021/acssuschemeng.9b00209
- Yao, W., Weng, Y., & Catchmark, J. M. (2020). Improved cellulose X-ray diffraction analysis using Fourier series modeling. *Cellulose*, **27**(10): 5563-5579. doi:10.1007/s10570-020-03177-8
- Yu, H., & Yu, C. (2010). Influence of various retting methods on properties of kenaf fiber. *The Journal of The Textile Institute*, **101**(5): 452-456. doi:10.1080/00405000802472564
- Zafeiropoulos, N. E. (2008). 3 - Engineering the fibre – matrix interface in natural-fibre composites. In K. L. Pickering (Ed.), *Properties and Performance of Natural-Fibre Composites*. Cambridge: Woodhead Publishing.
- Zhang, D., Chen, L., Zang, C., Chen, Y., & Lin, H. (2013). Antibacterial cotton fabric grafted with silver nanoparticles and its excellent laundering durability. *Carbohydrate Polymers*, **92**(2): 2088-2094. doi:10.1016/j.carbpol.2012.11.100
- Zhou, Y., Cheng, X., Yang, J., Zhao, N., Ma, S., Li, D., & Zhong, T. (2013). Fast and green synthesis of flexible free-standing silver nanoparticles–graphene substrates and their surface-enhanced Raman scattering activity. *RSC Advances*, **3**(45): 23236-23241. doi:10.1039/C3RA43400A

APPENDIX

Appendix I: Permission letter from Department of Plant Resources, MoFE, Government of Nepal, for collection of plant samples




नेपाल सरकार
वन तथा वातावरण मन्त्रालय

वनस्पति विभाग

(.....जैविक विविधता तथा सार्वटिस शाखा) फ्याक्स नं.: ४२५११६१

नेपाल सरकार
वन तथा वातावरण मन्त्रालय
वनस्पति विभाग

४२६१५६६
४२६१५६७
४२५११६०
४२५११६१



नेपालको लागि पर्यावरण
PLANTS FOR LIFE

पत्र संख्या:- ०६६/०६६
चलानी नम्बर:- ३२६९

इमेल:- info@dpr.gov.np
वनस्पतिमार्ग, थापाथली
काठमाडौं

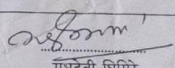
मिति: २०७६/०७/१९

विषय: अनुसन्धान अनुमति सम्बन्धमा ।

श्री कृष्ण प्रसाद कडेल ।




प्रस्तुत विषयमा यस विभागको मिति २०७६/०७/०६ को निर्णयानुसार तपाईंलाई देहाय बमोजिमका शर्तहरूमा रही वनस्पति स्रोतको अनुसन्धान कार्यविधि, २०७० (पहिलो संशोधन, २०७३) बमोजिम अनुसन्धान गर्न निम्नानुसार अनुमति प्रदान गरिएको छ ।

अनुसन्धानकर्ताको नाम	पहिलो		बीचको		शर
	कृष्ण		प्रसाद		कडेल
अनुसन्धानकर्ताको ठेगाना	स्थायी : भरतपुर-४, चितवन । अस्थायी : कीर्तिपुर, काठमाडौं ।		ईमेल : kandelkrishnaji@gmail.com		फोन नं. : ९८५०६०४२८
सम्बद्ध संस्था	संस्थाको नाम :		ठेगाना :		
पद	श्री रासानशास्त्र केन्द्रीय विभाग, त्रि.वि., कीर्तिपुर । कीर्तिपुर, काठमाडौं ।				
अनुसन्धान तह	उप-प्राध्यापक (श्री वीरेन्द्र बहुमुखी क्याम्पस, भरतपुर, चितवन) ।		संस्थागत : राष्ट्रिय / अन्तर्राष्ट्रिय		
अनुसन्धानको शीर्षक	व्यक्तिगत : स्नातक तह / स्नातकोत्तर तह / पि.एच.डी. अन्य :				
अनुसन्धानको क्षेत्र	"Characterization of Bast Fiber Obtained From <i>Sterculia villosa</i> (Roxb.), <i>Bauhinia vahlii</i> and explore its application as Reinforced Composite Material"				
अनुसन्धानको विधि	गुरुमी जिल्लाको विभिन्न स्थान ।				
अनुसन्धानको समयावधि	Instrumental/ wet Lab		नमूना संकलन		नमूनाको परीक्षण
			गर्ने		नेपालमा
अनुसन्धानको शर्तहरू	वि.सं. २०७६ कात्तिक देखि २०७९ चैत्र सम्म ।				
	<ol style="list-style-type: none"> अनुसन्धानकर्ताले विभाग र सम्बन्धित कार्यालयसँग समन्वय गरी गर्नु पर्नेछ । अनुसन्धानकर्ताले आफ्नो अनुसन्धानको प्रस्ताव सम्बन्धित कार्यालयमा समेत बुझाउनु पर्नेछ । अनुसन्धानकर्ताले अनुसन्धान समाप्त भएपछि एक प्रति कामजी प्रतिवेदन र एक प्रति विद्युतिय प्रतिवेदन विभागमा बुझाउनु पर्नेछ । अनुसन्धानकर्ताले नतिजाहरू प्रकाशित गर्दा अनुसन्धानमा संलग्न कर्मचारीको योगदानको आधारमा सह-लेखकको रूपमा समावेश गराउनु पर्नेछ । संकलित नमूना नेपाल सरकारको पूर्व स्वीकृती नलिई विदेश लैजान पाईने छैन । संकलित प्रत्येक प्रजातिका मृत नमूनाहरू एक / एक थान श्री राष्ट्रिय हर्बेरियम तथा वनस्पति प्रयोगशाला (KATH) गोदावरी, ललितपुरमा बुझाउने । 				



मधुदेवी घिमिरे
वैज्ञानिक अधिकृत
(१६३७७९)

Appendix II: Identification of Plants from National Herbarium and Plant Laboratories (KATH), Department of Plant Resources, Government of Nepal.



नेपाल सरकार
वन तथा वातावरण मन्त्रालय
वनस्पति विभाग
राष्ट्रिय हर्बेरियम तथा वनस्पति प्रयोगशाला
गोदावरी, ललितपुर

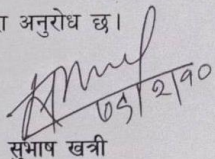
पत्र संख्या: ०६८७६३
च.नं. २६३

गोदावरी, ललितपुर
मिति २०७९/०२/१०

विषय: नमूनाहरू पहिचान सम्बन्धमा।

श्री कृष्ण प्रसाद कँडेल
वीरेन्द्र बहुमुखी क्याम्पस
भरतपुर, चितवन।

प्रस्तुत विषयमा तर्पौंको मिति २०७९/०२/१० को निवेदन साथ हर्बेरियमका नमूनाहरू प्राप्त भई व्यहोरा अवगत भयो। निवेदन माफत ल्याइएका नमूनाहरूको पहिचान गरी प्राविधिक विशेषज्ञको प्रतिवेदन (पाना १) यसै पत्रसाथ संलग्न गरी पठाइएको व्यहोरा अनुरोध छ।


सुभाष खत्री
वरिष्ठ अनुसन्धान अधिकृत
(१६३६८१)
कार्यालय प्रमुख

फोन नं.: ५१७४२७७, ५१७४०४७, फ्याक्स: ९७७-०१-५१७४३४९, पोष्ट बक्स नं.: ३७०८
Website: www.kath.gov.np

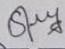


प्राविधिक विशेषज्ञको प्रतिवेदन



१. नमूना परिक्षण गर्न पठाउने व्यक्ति/निकाय:- श्री वीरेन्द्र बहुमुखी क्याम्पस, भरतपुर, चितवन।
- १(क) विद्यार्थीको नाम:- श्री कृष्ण प्रसाद कँडेल
२. प्राप्त नमूनाको विवरण:- हर्वेरियमको नमूना थान २
३. यस कार्यालयमा प्राप्त मिति:- २०७९/०२/१०
४. परिक्षणका आधारहरू:- (क) हर्वेरियममा भएको नमूनाहरू संगको तुलनात्मक अध्ययन ।
(ख) सन्दर्भ सामग्रीहरूको अध्ययन ।
५. पहिचान प्रतिवेदन:- प्राप्त नमूनाहरूको Morphological अध्ययन र यस राष्ट्रिय हर्वेरियम तथा वनस्पति प्रयोगशालाको हर्वेरियम संग्रहालयमा राखिएका नमूनाहरू संगको तुलनात्मक अध्ययन गर्दा उक्त नमूनाहरू निम्नानुसार पहिचान हुन गएको ।
६. हर्वेरियम नमूनाको विवरण:-

S.No.	Scientific Name	Family	Collection No.	Remarks
1	<i>Bauhinia vahlii</i> Wight & Arn.	Fabaceae	01	
2	<i>Sterculia villosa</i> Roxb. ex Sm.	Sterculiaceae	02	

७. परिक्षण गर्ने अधिकारी:-


सजिता ढकाल
अनुसन्धान अधिकृत
(२२५७०४)

Appendix III: Deposition of Plant to the National Herbarium and Plant Laboratories (KATH), Department of Plant Resources, Government of Nepal. "Voucher specimen: Gulmi district, C Nepal, Chhatrakot-4, BB Neupane & KP Kandel 03, 26.04.2023, KATH"



नेपालि सरकार
वन तथा वातावरण विभाग
राष्ट्रिय हर्बेरियम तथा वनस्पति प्रयोगशाला

गोदावरी, ललितपुर

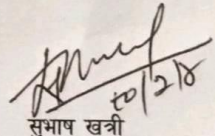
पत्र संख्या: ०६३१०८०
च.नं. ३३२

मिति २०८०/०२/०४

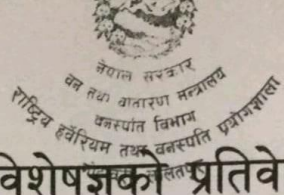
विषय: नमूना पहिचान सम्बन्धमा।

श्री रसायन शास्त्र केन्द्रीय विभाग,
त्रिभुवन विश्वविद्यालय,
विज्ञान तथा प्रविधि अध्ययन संस्थान,
कीर्तिपुर काठमाडौं, नेपाल।

प्रस्तुत विषयमा तपाईंको मिति २०८०/०२/०३ को पत्र साथ वनस्पतिका नमूना प्राप्त भई व्यहोरा अवगत भयो। पत्र माफत ल्याइएको नमूनाको पहिचान गरी प्राविधिक विशेषज्ञको प्रतिवेदन (पाना १) यसै पत्र साथ संलग्न गरी पठाइएको व्यहोरा अनुरोध छ।


सुभाष खत्री
वरिष्ठ अनुसन्धान अधिकृत
(१६३६८१)
कार्यालय प्रमुख

फोन नं: ५१७४२७७, ५१७४०४७, फ्याक्स: ९७७-०१-५१७४३४९, पोस्ट बक्स नं: ३७०८
Website: www.kath.gov.np



प्राविधिक विशेषज्ञको प्रतिवेदन

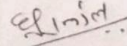
१. नमूना परिक्षण गर्न पठाउने व्यक्ति/निकाय:- श्री रसायन शास्त्र केन्द्रीय विभाग, कीर्तिपुर, काठमाडौं।
- १(क) विद्यार्थीहरूको नाम:- श्री कृष्ण प्रसाद कँडेल
२. प्राप्त नमूनाको विवरण:- वनस्पतिको नमूना १ थान।
३. यस कार्यालयमा प्राप्त मिति:- २०८०/०२/०३
४. परिक्षणका आधारहरू:- (क) हर्बेरियममा भएको नमूनाहरू संगको तुलनात्मक अध्ययन ।
(ख) सन्दर्भ सामग्रीहरूको अध्ययन ।
५. पहिचान प्रतिवेदन:- प्राप्त नमूनाको Morphological अध्ययन र यस राष्ट्रिय हर्बेरियम तथा वनस्पति प्रयोगशालाको हर्बेरियममा राखिएका नमूनाहरू संगको तुलनात्मक अध्ययन गर्दा उक्त नमूना निम्नानुसार भएको पहिचान हुन गएको।

S.N	Scientific Name	Family	Voucher Code	Remarks
1	<i>Bauhinia vahlii</i> Wight & Arn.	Fabaceae	03	

६. हर्बेरियम नमूनाको विवरण:-

Bauhinia vahlii Wight & Arn.
Central Nepal: Chhatrakot-4, Gulmi District,
26.04.2023, B.B.Neupane & K.P.Kandel, 03. (KATH).

७. परिक्षण गर्ने अधिकारी:-


धन राज कँडेल
अनुसन्धान अधिकृत
(१९८१९८)

Appendix IV: Publications

First authorship

- Kandel, K. P., Adhikari, M., Kharel, M., Aryal, G. M., Pandeya, S., Joshi, M. K., Dahal, B., Gautam, B., & Neupane, B. B. (2022). Comparative study on material properties of wood-ash alkali and commercial alkali treated Sterculia fiber. *Cellulose*, doi:10.1007/s10570-022-04610-w
- Kandel, K. P., Aryal, G. M., KC, S. A., Joshi, M. K., Dahal, B., & Neupane, B. B. (2023). A systematic study on material properties of water retted Sterculia and Bauhinia fiber. *BIBECHANA*, **20**(1): 27-35. doi:10.3126/bibechana.v20i1.51793
- Kandel, K. P., Aryal, G. M., & Neupane, B. B. (2023). Kinetics of water sorption in single Sterculia and Bauhinia fibers at ambient temperature. *Results in Chemistry*, **5**: 100872. doi:10.1016/j.rechem.2023.100872

Contributing authorship

- Aryal, G. M., Aryal, B., Kandel, K. P., & Neupane, B. B. (2021). Cellulose-based microfibrillar materials imaged with a home-built smartphone microscope. *Microscopy Research and Technique*, **84**(8): 1794-1801. doi:10.1002/jemt.23736
- Aryal, G. M., Kandel, K. P., Bhattarai, R. K., Giri, B., Adhikari, M., Ware, A., Han, S., George, G., Luo, Z., Gautam, B. R., & Neupane, B. B. (2022). Material Properties of Traditional Handmade Paper Samples Fabricated from Cellulosic Fiber of Lokta Bushes. *ACS Omega*, **7**(36): 32717-32726. doi:10.1021/acsomega.2c04398
- Aryal, G. M., Ware, W., Han, S., George, G., Luo, Z., Kandel, K. P., Gautam, B., & Neupane, B. (2021). Microscopic Characterization of Eco-friendly Lokta Paper. *Microscopy and Microanalysis*, **27**(S1): 720-721. doi:10.1017/S1431927621002932
- Giri, B., Pandey, S., Shakya, S., Neupane, B. B., Kandel, K. P., Yadav, C. K., Yadav, R. P., Neupane, B. P., GC, R. B., Saud, P. S., & Yonjan, M. (2022). Excessive iodine in iodized household salt in Nepal. *Annals of the New York Academy of Sciences*, **1514**(1): 166-173. doi:10.1111/nyas.14793

A systematic study on material properties of water retted *Sterculia* and *Bauhinia* fiber

Krishna Prasad Kandel, Girja Mani Aryal, Sishir Achyarya KC
Mahesh Kumar Joshi, Bipeen Dahal, Bhanu Bhakta Neupane*

¹Central Department of Chemistry, Tribhuvan University, Kathmandu 44613, Nepal

*Corresponding author. Email: newbhanu@gmail.com

Abstract

Lignocellulose biomass forms an important component of traditional and next generation composite materials. To obtain desired properties, the biomass needs to be chemo-mechanically processed at different levels. The raw lignocellulose fiber obtained from *sterculia villosa* (Roxb.) and *Bauhinia vahlii* is traditionally believed to have high water stability; and therefore used in rural areas of South Asian regions to secure objects submerged under water. In this research, we systematically studied several material properties of raw *Sterculia* and *Bauhinia* fiber samples retted for 0, 20, 30 and 55 days ($n=8$). Water retting resulted in significant decrease in lignin and extractives content ($p<0.05$) and increase in cellulose content. Fiber bundle strength of *Sterculia* fiber increased with retting time ($R^2=0.7$) but *Bauhinia* fiber did not show significant change ($p>0.05$). Interestingly, water retting resulted in increased thermal stability in both fiber types. These findings suggested that the fiber studied have excellent water stability. The observed trend in mechanical and thermal properties could have resulted from crystallinity change and/or nominal fiber damage as supported by XRD and SEM imaging data; respectively. These findings suggested that *Sterculia* and *Bauhinia* fiber biomass could be an important component of biodegradable composite materials which are intended for high wetting and/or humid conditions.

Keywords

Lignocellulose, Water retting, Fiber processing, Cellulose fiber, Mechanical strength.

Article information

Manuscript received: January 26, 2023; Accepted: March 28, 2023

DOI <https://doi.org/10.3126/bibechana.v20i1.51793>

This work is licensed under the Creative Commons CC BY-NC License. <https://creativecommons.org/licenses/by-nc/4.0/>

1 Introduction

Lignocellulose biomass is one of cheap, environmentally friendly, and most abundant terrestrial biomass. The biomass can be obtained from leaf, seed, fruit, and bast portion of different plant species or other plant derived wastages following

different processing methods [1–5]. Bast fibers are the soft woody fiber obtained from phloem tissues of plant stem. The fibers are usually long and strong and form an important components of next generation materials and finding applications in waste water treatment, biomedical applications, agro and automotive industries [6–10]. Cellulose



Comparative study on material properties of wood-ash alkali and commercial alkali treated Sterculia fiber

Krishna Prasad Kandel · Menuka Adhikari · Madhav Kharel ·
Girja Mani Aryal · Shiva Pandeya · Mahesh Kumar Joshi · Bipeen Dahal ·
Bhoj Gautam · Bhanu Bhakta Neupane

Received: 4 January 2022 / Accepted: 22 April 2022 / Published online: 23 May 2022
© The Author(s), under exclusive licence to Springer Nature B.V. 2022

Abstract Pulp, paper, and related industries consume large amount of commercial alkali to process raw fiber and/or recycle waste. A low-cost alternative to commercial alkali would be useful to reduce production and recycling costs and global alkali use. In this research, we extracted alkali from wood ash and, as a proof of concept, used the alkali to process lignocellulose fiber obtained from *Sterculia villosa* (locally known as Murgilo or Mudilo), a traditionally important fibrous plant. Material properties of wood-ash alkali (WAA) treated fiber were compared with 5% sodium hydroxide treated fiber. The net weight loss on WAA and sodium hydroxide treatment was found

to be 29.1 ± 2.6 and $41 \pm 3.3\%$, respectively. In both methods, the weight loss resulted from the removal of hemicellulose and lignin consistent with reduction of fiber width and weakening of lignin and hemicellulose characteristic bands in FTIR spectra. Interestingly, both methods resulted in fiber having very similar mechanical strength. Cellulose crystallinity, fiber-surface morphology, and thermal stability of cellulose fiber obtained from two methods were systematically compared. These findings suggested that WAA treatment method could be a low-cost method for processing lignocellulose biomass.

Supplementary information The online version contains supplementary material available at <https://doi.org/10.1007/s10570-022-04610-w>.

K. P. Kandel · M. Kharel · G. M. Aryal · S. Pandeya ·
M. K. Joshi · B. Dahal · B. B. Neupane (✉)
Central Department of Chemistry, Tribhuvan University,
Kathmandu, Nepal
e-mail: bbneupane@cdctu.edu.np; newbhanu@gmail.com

M. Adhikari · B. Gautam
Department of Chemistry, Physics and Materials Science,
Fayetteville State University, Fayetteville 28301, NC, USA



Kinetics of water sorption in single *Sterculia* and *Bauhinia* fibers at ambient temperature

Krishna Prasad Kandel, Girja Mani Aryal, Bhanu Bhakta Neupane*

Central Department of Chemistry, Tribhuvan University, Kirtipur, Kathmandu, Nepal

ARTICLE INFO

Keywords:

Material properties
Lignocellulose biomass
Fickian diffusion
Diffusion coefficient
Mechanical strength

ABSTRACT

Fundamental study on material properties of lignocellulose fiber is important to understand the performance of composite materials. In this study, we explored several material properties of untreated, commercial and wood ash alkali retted fiber obtained from relatively less studied and traditionally important wild plant species *Sterculia villosa* (local name Murgilo or Mudilo) and *Bauhinia vahlii* fibers (local name Bharlo). Water sorption kinetics in all fiber types was measured at ambient temperature. Fickian model then was used to fit experimental sorption kinetic data and information on diffusion coefficients at early and late stages of sorption, average diffusion coefficient, sorption coefficient, and water permeability were obtained. The average diffusion coefficient (D) for untreated, wood ash alkali and commercial alkali treated *Sterculia* was found to be $10.6 \times 10^{-13} \text{ m}^2/\text{sec}$, $3.08 \times 10^{-12} \text{ m}^2/\text{sec}$, and $2.35 \times 10^{-12} \text{ m}^2/\text{sec}$; respectively. The corresponding values for *Bauhinia* fiber were found to be $6.8 \times 10^{-13} \text{ m}^2/\text{sec}$, $3.80 \times 10^{-12} \text{ m}^2/\text{sec}$, and $3.46 \times 10^{-12} \text{ m}^2/\text{sec}$; respectively. The equilibrium water sorption in the alkali treated fiber was significantly reduced due to removal of cementing materials and also increase of crystallinity. Significant decrease in mechanical strength of fiber in sorbed state was found. These findings will be useful to understand stability of fiber and potential end products such as paper sheets and reinforced composite materials exposed under different moisture conditions.

Introduction

Lignocellulose fiber can be obtained from leaf, root, and bark regions of different plant species. The biomass forms an important components of composite materials. It is also a major starting material for pulp, paper, and cardboard industries [1–3]. Lignocellulose fiber reinforced composite materials such as bio-composites are reported to have low density, good thermal stability and specific strength, lower abrasiveness and are being explored as ecofriendly alternative to the traditional plastic or glass fiber incorporated composite materials. Such materials also contribute significantly to achieve major goals of circular economy i.e. recycle the materials, eliminate or reduce waste, and regenerate nature [4]. In recent years, such materials are finding wide range of applications in agro and automobile based industries, biomedical applications, structural engineering, waste water treatment, and many more [5–7].

One of the important issues of natural fiber reinforced materials is fast environmental degradation at different conditions such as sunlight, humidity, moisture, and microorganisms. The hydrophilic nature of

natural fibers lead to increased water absorption leading to decreased stability and mechanical strength [8–10]. Depending on mode of applications, composite materials can be subjected to varying levels of moisture and humidity. Thus, information on water uptake behavior of cellulosic fiber can be important to understand the consequences of water absorption in composite and be useful to minimize the water uptake.

Transport of small permeants in polymer is reported to occur mainly by three mechanisms. The major contributor is diffusion of the water molecules inside micro-gaps formed by the polymeric chains. The minor contributors are capillary transport and transport by micro-cracks or defects [11,12]. The experimental kinetic data can be modeled considering diffusion behavior. In case I diffusion (pseudo Fickian and Fickian), polymer segment mobility is much higher than the rate of diffusion. In case II (or super case II), mobility of penetrant is significantly higher than the other relaxation processes. Here a sharp boundaries exist between the swollen and un-swollen regions and the boundary moves linearly with time. In case III (non-Fickian or anomalous diffusion), polymer segment relaxation and penetrant mobility are comparable.

* Corresponding author.

E-mail address: bbneupane@cdctu.edu.np (B.B. Neupane).

<https://doi.org/10.1016/j.rechem.2023.100872>

Received 8 August 2022; Accepted 24 February 2023

Available online 8 March 2023

2211-7156/© 2023 The Author(s). Published by Elsevier B.V. This is an open access article under the CC BY license (<http://creativecommons.org/licenses/by/4.0/>).

Cellulose-based micro-fibrous materials imaged with a home-built smartphone microscope

Girja Mani Aryal^{1,2} | Bishwa Aryal¹ | Krishna Prasad Kandel¹ |
Bhanu Bhakta Neupane¹ 

¹Central Department of Chemistry, Tribhuvan University, Kathmandu, Nepal

²Research Centre for Applied Science and Technology, Tribhuvan University, Kathmandu, Nepal

Correspondence

Bhanu Bhakta Neupane, Central Department of Chemistry, Tribhuvan University, Kathmandu, Nepal.
Email: bbneupane@cdctu.edu.np

Funding information

University Grants Commission, Nepal, Grant# MRS-74/75/S&T-19

Review Editor: Paolo Bianchini

Abstract

Micro-fibrous materials are one of the highly explored materials and form a major component of composite materials. In resource-limited settings, an affordable and easy to implement method that can characterize such material would be important. In this study, we report on a smartphone microscopic system capable of imaging a sample in transmission mode. As a proof of concept, we implemented the method to image handmade paper samples—cellulosic micro-fibrous material of different thickness. With 1 mm diameter ball lens, individual cellulose fibers, fiber web, and micro-porous regions were resolved in the samples. Imaging performance of the microscopic system was also compared with a commercial bright field microscope. For thin samples, we found the image quality comparable to commercial system. Also, the diameter of cellulose fiber measured from both methods was found to be similar. We also used the system to image surfaces of a three ply surgical facemask. Finally, we explored the application of the system in the study of chemical induced fiber damage. This study suggested that the smartphone microscope system can be an affordable alternative in imaging thin micro-fibrous material in resource limited setting.

KEYWORDS

bright field microscope, contrast, handmade paper, micro-fibrous material, resolution

1 | INTRODUCTION

An imaging system helps to visualize small specimen or the details within the larger specimens which are not visible to naked eyes. Different versions of imaging techniques are available, such as far and near field optical, electron, and scanning probe. The choice of an imaging technique depends on the nature of sample, availability of resources, and the level of spatial details required. Optical microscopic systems are normally the method of choice for the study of soft and biological specimens at their native environments (Hell, 2007; Sawyer, Grubb, & Meyers, 2008; Stender et al., 2013; Xiong et al., 2013). Although super-resolution far field optical microscopic techniques provide significantly improved resolution (Hell, 2007; Iketaki, Watanabe, Bokor, & Fujii, 2006; Kuang, Zhao, & Wang, 2010; Li, Wu, & Chou, 2009; B. Neupane et al., 2015; Puthukodan, Murtezi,

Jacak, & Klar, 2020), resolution of traditional optical microscopic systems is lower than that of electron microscopic methods. Nonetheless, different versions of conventional optical microscopic systems are being used in the characterization different fibrous materials (Choong, Yi, & Rutledge, 2015; Hayes & Gammon, 2010; Singh, Lim, & Manickavasagan, 2020). Electron and scanning probe microscopic techniques, depending on the nature of sample, can provide resolution from few nanometer to atomic scale, therefore these techniques are highly used in characterization of diverse materials including micro-fibrous materials (De Jonge & Ross, 2011; Hörber & Miles, 2003; Lee, Kim, Choi, Takeuchi, & Park, 2017; Venkateshaiah et al., 2020).

In recent years, smartphone microscopic systems are being explored as an affordable alternative to image and/or quantify specimens of few micrometer to few tenths of micrometer. Different

Material Properties of Traditional Handmade Paper Samples Fabricated from Cellulosic Fiber of Lokta Bushes

Girja Mani Aryal, Krishna Prasad Kandel, Ram Kumar Bhattarai, Basant Giri, Menuka Adhikari, Alisha Ware, Shubo Han, Gibin George, Zhiping Luo, Bhoj Raj Gautam,* and Bhanu Bhakta Neupane*

Cite This: <https://doi.org/10.1021/acsomega.2c04398>

Read Online

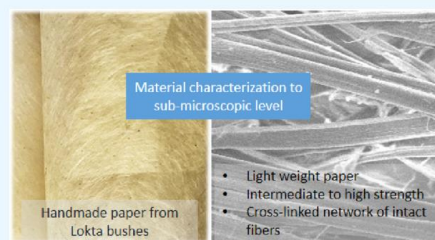
ACCESS |

Metrics & More

Article Recommendations

Supporting Information

ABSTRACT: Handmade papers (HPs) are fabricated from fibrous biomass of Lokta bushes and other plant species following traditional eco-friendly method in Nepal. Although HP fabricated from Lokta bushes is believed to be durable and resistant to bugs and molds, material properties of this paper are not reported in literature. In this study, we measured several material properties of 10 handmade Lokta paper samples collected from local enterprises and paper industries. The mean caliper, grammage, apparent density, equilibrium moisture content, Cobb 60, brightness, opacity, tensile strength, and tensile index values in the paper samples ranged from ~90 to 700 μm , 50 to 150 g/m^2 , 0.2 to 0.4 g/cm^3 , 4 to 7%, 50 to 400 g/m^2 , 56 to 67%, 83 to 98%, 30 to 2900 N/m , and 1 to 27 Nm/g , respectively. These properties suggested that the HPs are lightweight papers with intermediate to high strength. The tensile strength was found to be significantly higher along the length direction ($p < 0.05$). Characteristic features of cellulose, hemicellulose, and lignin were observed in FTIR spectra. The crystalline and amorphous phases were also identified in X-ray diffraction (XRD) data. Electron microscopy images revealed a nicely cross-linked network of intact fibers having almost parallel arrangement of microfibrils. These features could provide strength and durability to the paper samples. Understanding the material properties of HPs down to the sub-microscopic level may help improve the paper quality and find novel applications in the future.



1. INTRODUCTION

Handmade paper (HP) making has been practiced across the globe since 105 AD.¹ It is believed that handmade paper making started, at least, in the 12th century AD in the western district of Baglung in Nepal.² In Nepal, HP is known as Nepali Kagaj. It is a traditional paper made from fibrous biomass of Lokta (*Daphne bholua* and *Daphne papyracea*) and Argeli (*Edgeworthia gardneri*) or their combinations. These plants are found at an elevation of 1600–4000 m in Nepal.^{2–5} HP is believed to be a durable and bug- and mold-resistant paper and therefore is mostly used in official record keeping and religious texts.³ Furthermore, a number of value-added products such as notebooks, photo albums, gift boxes and bags, and paper jewelries are fabricated from HP. The HP made from Lokta bushes is traditionally named Loka paper. However, any HP made from other plants is loosely termed as Lokta paper these days. There are ~200 small- and medium-sized paper-making enterprises in Nepal, which support the livelihood of ~55,000 families with an annual sell value of ~\$2.5 and ~5.5 million in Nepal and abroad, respectively.³

HP making starts from harvesting stalks and manual removal of outer scaly bark. The long fiber mass is cut into small pieces and soaked in cold water for 6–12 h, and debris is removed manually. The biomass is boiled in water or ash solution for

around 5–10 h. Next, the softened fiber biomass is beaten to make pulp and dispersed in water to make slurry. The slurry is poured in a wooden mesh frame or paper molds over a water tank, drained, and air-dried to obtain the paper sheet. In recent years, the hot water or ash solution digestion step of paper making is replaced by 4–5% hot alkali solution treatment for 3–10 h. Depending on the customers' need, additional steps such as chemical bleaching, calendaring, and machine glazing are performed.^{3,4} The paper can be colored using traditional plant-based or commercial dyes if needed. Traditional HP making is considered an eco-friendly process since it requires low energy consumption, and little or no chemicals are used compared to the commercial paper-making process.

In recent years, several research groups are exploring the handmade paper making in laboratory settings. The paper sheets are fabricated from woody or non-woody parts of different plant species following mechanical and chemical methods of fiber

Received: July 12, 2022

Accepted: August 23, 2022

Microscopic Characterization of Eco-friendly Lokta Paper

Girja Mani Aryal¹, Washat Ware², Shubo Han³, Gibin George², Zhiping Luo³, Krishna Prasad Kandel¹, Bhoj Gautam² and Bhanu Neupane¹

¹Tribhuvan University, Kathmandu, Nepal, ²Fayetteville State University, Fayetteville, North Carolina, United States, ³Fayetteville State University, FAYETTEVILLE, North Carolina, United States

Lokta paper is a handmade paper indigenous to Nepal. The paper is made from inner fibrous bark of Lokta bushes; evergreen shrubs that grow in Himalayan forests ranging from 1600 to 4000 m. Because of its durability and resistance to bugs and moulds, the paper in its original or modified form is being used in official documents, calligraphy, holy books, packaging materials, and even to make paper bills [1]. The paper is fabricated in local levels following the traditional eco-friendly method of fiber processing. Firstly, outer scaly bark from raw fiber is manually removed and cut to small pieces and soaked in cold water for 5–6 hours. The biomass is boiled in water for around 5–10 hours and then washed with ash or alkali solution. The softened fiber biomass is beaten to make pulp and then dispersed to make slurry. The slurry is poured in a wooden mesh frame or paper moulds over a water tank. The frame is then drained and air dried to get paper sheet. Depending on the demand, the paper can be colored using natural dyes obtained from different plants and or patterned for artistic purposes. A systematic characterization of lokta paper sheet from material perspective, which helps to explain its novel properties, is missing in literature. In this work, we studied fiber organization, morphology and elemental distribution in lokta paper sheet with the help of scanning electron microscope (SEM) coupled to an electron probe micro analyzer (EPMA). For SEM imaging the paper sample was sputter coated with carbon and imaged in a JEOL field-emission JXA-8530F EPMA equipped with an SDD X-ray energy-dispersive spectrometer (EDS). Finally, we also did atomic force microscopy (AFM) imaging in tapping mode to explore surface roughness and structural details in the sample at nanoscopic level. AFM was performed at ambient condition in tapping mode. Finally, the X-ray diffraction (XRD) data were collected at Bragg's angle 2θ ranging from 5 to 40° by a X-ray diffractometer. The Cu K α line ($\lambda=1.540\text{\AA}$) was used as X-ray source. The SEM micrographs of lokta paper imaged at different magnification is shown in figure 1A–D. The micrographs show that in the paper the cellulosic fibers are randomly oriented so as to form densely packed interwoven networks (Figure 1 and B). It is known that strength of paper sheet is largely determined by strength of individual fiber and degree of cross linking within the individual fibers. The presence of long interconnecting fibers having no or low curl could provide durability and strength to the paper sheet. With further zooming individual fiber surface can be imaged (Figure 1C and D). We found fiber diameter in the range of 10–14 micrometer. In most of the fibers, individual micro-fibrils that run straight along the length of fiber are clearly visible (yellow dotted regions in Figure C and D). In some fibers gummy material is found attached on the surface (white dotted region in Figure 1C). The micro-fibrils are visible due to removal of gummy materials such as lignin and hemicellulose from the fiber surface during processing. We found micro-fibril diameter and spacing in the range of 100–350 nm and 100–500 nm, respectively. The almost parallel arrangement of micro-fibril could provide excellent strength to individual fiber and to the paper sheet. The observation of micro-fibrils is also reported in fiber processed from other plant types and biomass [2, 3]. In a cellulose fiber amorphous and crystalline phases are known to exist in different proportions but these phases are not visible in SEM images. However, we observed the contribution from two cellulose forms in the XRD data (Figure 1E). The peak at 2θ values of ~16° and 22° originate from the crystalline planes (101) and (002), respectively. A broad background underlying the crystalline peaks originates from the amorphous regions [4].

Excessive iodine in iodized household salt in Nepal

Basant Giri¹ | Shishir Pandey¹ | Sadiksha Shakya¹ | Bhanu Bhakta Neupane^{1,2} |
Krishna Prasad Kandel³ | Chandradip Kumar Yadav⁴ | Ram Prabodh Yadav⁵ |
Bishnu Prasad Neupane⁶ | Rajendra Bahadur GC⁷ | Prem Singh Saud⁸ |
Meghraj Yonjan⁹

¹Center for Analytical Sciences, Kathmandu Institute of Applied Sciences, Kathmandu, Nepal

²Central Department of Chemistry, Tribhuvan University, Kathmandu, Nepal

³Birendra Multiple Campus, Tribhuvan University, Chitwan, Nepal

⁴Dhankuta Multiple Campus, Tribhuvan University, Dhankuta, Nepal

⁵J.S. Murarka Multiple Campus, Lahan, Nepal

⁶Faculty of Health Sciences, School of Health and Allied Sciences, Pokhara University, Kaski, Nepal

⁷Butwal Multiple Campus, Tribhuvan University, Butwal, Nepal

⁸Kailali Multiple Campus, Far-western University, Kailali, Nepal

⁹Amrit Science Campus, Tribhuvan University, Kathmandu, Nepal

Correspondence

Basant Giri, Center for Analytical Sciences, Kathmandu Institute of Applied Sciences, P. O. Box 23002, Kathmandu 44600, Nepal.
Email: bgiri@kias.org.np

Bhanu Bhakta Neupane, Central Department of Chemistry, Tribhuvan University, Kathmandu 44600, Nepal.
Email: bbneupane@cdctu.edu.np

Abstract

Iodine is an essential trace element required for the regulation of physiological processes involving the thyroid gland. However, inadequate and excessive intake of iodine are responsible for health problems, such as iodine deficiency disorders, hypothyroidism, hyperthyroidism, thyroiditis, thyroid papillary cancer, and thyrotoxicosis. The Universal Salt Iodization (USI) program has become successful in providing supplemental iodine at the population level globally. Packaging quality, fortification level, and transportation and storage conditions of iodized salt determine the availability of iodine. Previous studies have reported severe health issues caused by excessive iodine intake after the implementation of the USI program. To understand the levels of iodine, we collected 2117 household salt samples from seven districts of Nepal and tested them for iodine content; among them, 98.1% were iodized. Overall median concentration of iodine was 53.9 ppm (range: 43.5–61.4 ppm). The majority (67.2%) of samples had iodine in the range of 45–75 ppm. Approximately 0.9% of samples had inadequate, 13.3% contained adequate, and 83.9% had excessive iodine than the World Health Organization-recommended value. Iodine content varied among the sampling districts and seasons, to some extent. Our study confirmed that iodized salt is widely used in Nepal and is excessively iodized. Excessive intake of iodine through iodized salt requires further attention by policy makers. The iodine level may need adjustment to address the health impact.

KEYWORDS

fortified salt, iodine deficiency disorders, iodometric titration, paper analytical device, supplemental iodine, Universal Salt Iodization

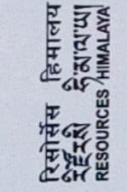
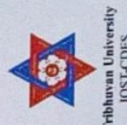
INTRODUCTION

Iodine is an essential trace element required for the regulation of several physiological processes involving the thyroid gland in the human body.¹ However, inadequate and excessive intake of iodine are responsible for several health problems. Inadequate iodine is responsible for iodine deficiency disorders (IDDs) and hypothyroidism resulting in functional and developmental abnormalities, such as endemic goiter,

abortions, still births, cretinism, retarded physical development, brain damage, and irreversible mental retardation.² Furthermore, excessive iodine intake can also have adverse chronic health effects, such as iodine-induced hyperthyroidism (IIH), thyroiditis, thyroid papillary cancer, and thyrotoxicosis. Several studies have reported that chronic exposure to higher amounts of iodine disrupts thyroid function.^{3–8} Chronic iodine intake (urinary iodine > 500 µg/L) was found to be associated with increasing thyroid volume in children.⁹

Appendix V: Conference

- 1) Poster Presentation on the topic “**Material properties of water retted Sterculia and Bauhinia fibers**” at Eighth Graduate Conference 2022, Himalayan knowledge conclave organized by Mid-West University.
- 2) Oral presentation on the topic of “**Material properties of lignocellulosic fiber obtained from traditional Himalayan plants**” at 4th International conference on bioscience & biotechnology”, Sauraha, Nepal.
- 3) Poster presentation on the topic of “**Wood-ash Alkali for Economical Processing of Natural Fiber**” International scientific conference, “Kathmandu Humboldt-Kolleg 2022”
- 4) Poster presentation on the topic of “**Cellulose-Ag-ZnO Nanocomposite Mat for Dye Degradation and Antimicrobial Use**” at 6th international Symposium on Advance in Sustainable Polymers, Lalitpur, Nepal., organized by Nepal Polymer Institute.
- 5) Oral presentation on the topic of “**A comprehensive investigation on the structural characteristics of water-retted *Sterculia* and *Bauhinia* fibers**” at National Conference on Multidisciplinary Innovations, Organized by Research management Cell, Birendra Multiple Campus, Chitwan, Nepal.
- 6) Poster presentation on the topic of “**Fabrication of cellulose–Ag-ZnO nanocomposite mat for dye degradation and antimicrobial packaging**” on National Conference on Advances in Polymer Material, G.B Pant University of Agriculture & Technology, Pantnagar, India.



Eight Graduate Conference 2022

HIMALAYAN KNOWLEDGE CONCLAVE

Connecting Dots: Resources and Prosperity



CERTIFICATE OF APPRECIATION

This certificate is awarded to

Krishna Pd. Kandel.

in recognition as a PRESENTER in the Eighth Graduate Conference held in Mid-West University, Birendranagar, Surkhet, Nepal on April 4-5, 2022.

(Signature)

Prof. Nanda Bahadur Singh, PhD
Patron
Vice-Chancellor
Mid-West University

(Signature)

Sudeep Thakuri, PhD
Convener
Dean, Faculty of Science and Technology
Mid-West University

CERTIFICATE

OF PARTICIPATION

THIS IS TO CERTIFY THAT

Mr. Krishna Prasad Kandel

HAS PARTICIPATED AS **GRADUATE STUDENT TALK IN**
4th INTERNATIONAL CONFERENCE ON BIOSCIENCE & BIOTECHNOLOGY
(ICBB – 2022)

Sauraha, Nepal | March 3-6, 2022



Prajwal Rajbhandari

Chair, ICBB - 2022
Research Institute for Bioscience
and Biotechnology (RIBB), Nepal



Suvechhya Bastola

Secretary, ICBB - 2022
Research Institute for Bioscience
and Biotechnology (RIBB), Nepal



काठमाडौं हुम्बोल्ड सम्मेलन

KATHMANDU HUMBOLDT-KOLLEG 2022

Interdisciplinary Collaboration for Strengthening Science and Culture

October 16-19, 2022, Kathmandu, Nepal

Unterstützt von / Supported by



Alexander von Humboldt
Stiftung/Foundation

Certificate of Appreciation

is hereby awarded to Dr. / Mr. / Ms.

KRISHNA PRASAD JKANDEL

for Poster Presentation in the international scientific conference
"Kathmandu Humboldt-Kolleg 2022" organized by Humboldt Club Nepal
generously supported by Alexander von Humboldt Foundation, Germany.

PROF. DR. RAMESHWAR ADHIKARI

Coordinator

Kathmandu Humboldt-Kolleg 2022

Humboldt Club Nepal

DR. JUDITH SCHILDIT

*Sponsorship and Network Department,
Alexander von Humboldt Foundation,
Germany*

ASP-23

**6th International Symposium on
Advances in Sustainable Polymers**

Certificate of Participation

This is to certify that

Mr. Krishna Prasad Kandel

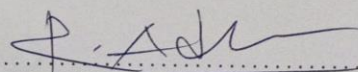
has participated as an Poster presenter on

*“Cellulose-Ag/ZnO Nanocomposite Mat for Dye Degradation
and Antimicrobial Use”*

ASP-23 (6th International Symposium
on Advances in Sustainable Polymers),

April 11 (Tue) to 13 (Thu), 2023
Lalitpur, NEPAL

Organized by **Nepal Polymer Institute (NPI)**



Prof. Rameshwar Adhikari
(Chair, Local Organizing Committee)



Tribhuvan University

Birendra Multiple Campus

Research Management Cell

Bharatpur, Chitwan, Nepal

Certificate of Presentation

Krishna Prasad Kandel

Birendra Multiple Campus,

Tribhuvan University, Chitwan, Nepal

presented a paper in the

National Conference on Multidisciplinary Innovations

April 7-8, 2023

organized by Research Management Cell,

Birendra Multiple Campus, Chitwan, Nepal

Prof. Dr. Sita Ram Bahadur Thapa
RMC Coordinator

Prof. Daya Ram Paudyal
Campus Chief

Prof. Dr. Dharma Kanta Baskota
Vice-Chancellor
Tribhuvan University

Supported by:



University Grants Commission



Bharatpur Metropolitan City



NAST



Ratnanagar Municipality

G. B. Pant University of Agriculture and Technology, Pantnagar, Uttarakhand, India



*National Conference on
Advances in Polymer Materials*

APM-2023

April 25 - 26, 2023

Department of Chemistry, College of Basic Sciences and Humanities

Supported by

Defence Research & Development Organization, India

Certificate

This is to certify that.....K.RISHNA.....P.RASAD.....K.ANDEL.....
From.....&D.C.....T.R.B.HUMAN.....UNIVERSITY.....K.R.I.P.U.R.....NEPAL.....
Presented/delivered/participated.....
in the two days National Conference, APM-2023 held from at GBPU&T Pantnagar.

Sameena
Dr. Sameena Mehtab
Convener

[Signature]
Dr. Sandeep Arora
Coordinator & Dean, CBS&H



Appendix VI: Laboratory equipment used during research



High precision Hydrothermal Oven (20-300 °C, $\pm 2^{\circ}\text{C}$) Equipment



Bright field, Digital and Stereo microscopes



Soxhlet Setup



Stelometer



Magnetic Stirrer



pH Meter



Vacuum Filtration



High precision digital micrometer



High pressure Vacuum pump



Bath Sonicator



Cobb60 tester